Study of Deposit Formation inside Diesel Injectors Nozzles

by

YinChun Wang

Submitted to the Department of Mechanical Engineering
in partial fulfillment of the requirements for the degree of

Doctor of Philosophy in Mechanical Engineering

at the

MASSACHUSETTS INSTITUTE OF TECHNOLOGY

February 2012

Author .....
Department of Mechanical Engineering
January 16, 2012

Certified by .....
Wai K. Cheng
Professor of Mechanical Engineering
Thesis Supervisor

Accepted by .....
David E. Hardt
Chairman, Department of Graduate Committee

Study of Deposit Formation inside Diesel Injectors Nozzles

by

YinChun Wang

Submitted to the Department of Mechanical Engineering
on January 16, 2012, in partial fulfillment of the
requirements for the degree of
Doctor of Philosophy in Mechanical Engineering

Abstract

Diesel engines are widely used in heavy duty transportation applications such as in trucks, buses and ships because of their reliability and high torque output. A key diesel technology is the injection system which is constantly improved to produce better spray quality and deeper spray penetration in the combustion chamber by using high injection pressure and improving the design of the nozzle holes. The hole size has been continuously reduced; future diameters less than 100 um are expected. Smaller nozzle holes are vulnerable to deposit formation, which will reduce the flow rate and affect the spray pattern.

The objective of this study is to understand the processes that would lead to deposit formation on the injector nozzle surfaces. In specific, a detailed mechanism is proposed after observing engine and injector simulation results. Models for the physical processes and chemical mechanisms responsible for the deposit formation are developed. These models are incorporated into a integrated software package to facilitate calculations of deposit formation rates under different conditions. A bench-scale test rig is also constructed to measure the deposit formation of different fuels and detergents. Experiments show that the test procedure can differentiate good detergents from ineffective ones; hence it can be used to pre-screen the detergents and fuels before engine tests. Thus the cost of testing could be reduced substantially.

This study is the first to develop a comprehensive quantitative model for injector nozzle deposit formation and a bench scale testing apparatus encompassing the key deposit formation processes of film formation, evaporation and washing.

Thesis Supervisor: Wai K. Cheng
Title: Professor of Mechanical Engineering

Acknowledgments

This research has been supported by ENI under the MIT Energy Initiative. The Technical direction of Dr. Riccardo Rausa is much appreciated.

Special thanks to my supervisor Professor Wai Cheng for his great guidance and support. His insights and knowledge always give me deeper understanding for the problem. Without his support this study could not have been done properly.

I would like to extend my thanks to Dr. Tian Tian who gave me support and helped me get through one of my worst times. I would also like to acknowledge Professor William Green, Dr. Richard West and Amrit Jalan in the Department of Chemical Engineering. They did great work for the chemical part of the work and also gave valuable advice along the way. Without their fantastic job, this study could not have been complete.

My appreciation also goes to members of MIT Sloan Automotive Lab for the opportunity to develop friendships and knowledge. In particular, I would like to thank Thane DeWitt and Raymond Phan. Without their help, the apparatus would not be finished promtply.

Finally, I also would like to thank my parents. Although I haven't seen them for almost four years, My love is always on their side.

Contents

List of Figures

List of Tables

Chapter 1

Introduction

Diesel fuel powers the global economy. It is used not only in heavy transport applications such as trucks,buses and ships, but also in the generation of electricity and farming thanks to the reliability, high torque output and fuel economy of diesel engines. In United States, the sales of on-road diesel fuel rose nearly three percent annually, from 32 billion gallons in 1999 to 37 billion gallons in 2004. In Europe and Asia, the amount of diesel fuel produced exceeded the production of gasoline by over 1.7 billion gallons due to the significant population of diesel-powered automobiles[30]. Despite all these advantages and developments, strict emission regulations bring many challenges to the fuel productions and engine designs.

Among the parts of diesel engines, the fuel injection equipment(FIE) has been improved to produce a better diesel spray quality and a deeper spray penetration in the combustion chamber by raising the injection pressure. The dimension of the injector spray channels has been correspondingly reduced to provide the appropriate fuel metering. While effective at resulting more complete combustion, the smaller nozzles are more vulnerable to the deposit coking, presenting considerable challenges to engine and diesel additive formulators.

In this chapter, diesel engines and FIE are introduced, followed by a detailed review of deposit study research available in the current literature. The project motivation and objectives are also discussed.

1.1 Diesel Engines

Diesel Engines distinguish themselves from gasoline engines with the absence of external ignition. This is achieved by inducting air alone into the cylinder and then injecting ignitable fuels into the highly compressed and hot air just before the combustion is required to start. Despite various advances in diesel engine research Since first invented by Rudolf Diesel in 1892, the operation of a typical four-stroke diesel engine has remained virtually unchanged. The four strokes are shown in Fig. 1-1. During intake stroke, air is inducted into the cylinder while the piston moves down from its highest position (TC) to its lowest position (BC). Then in compression stroke, the air is compressed to high pressures (4 MPa) and temperatures (800K) [37]. Near the end of the compression stroke, fuel is injected into the cylinder. After a short delay, spontaneous ignition initiates the combustion process. The hot gases produced by the combustion further increase the pressure in the cylinder and force the piston down. Finally, the exhaust valve opens when the piston is near BC so that when piston moves towards TC, most of the burned gases are forced out of the cylinder.

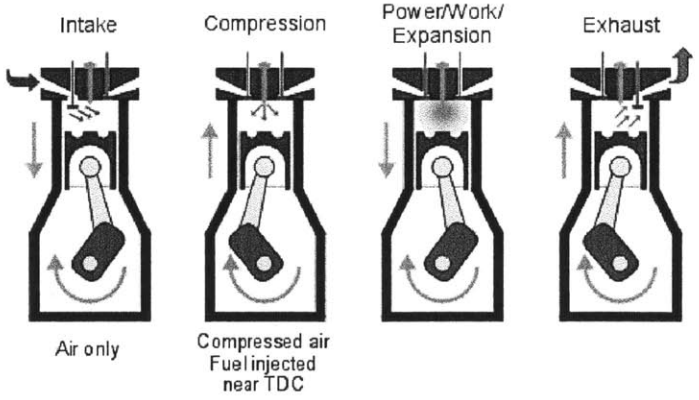

Figure 1-1: The Four-Stroke Diesel Engine Operation [46].

Mixture formation in diesel engine plays a import role in the combustion process and load control [66]. The absence of fuel in the combustion chamber during compression eliminates of uncontrolled autoignition or knock which is big problem limiting the compression ratio of conventional spark ignition engines. The compression of only

air enables the compression ratio of diesel engine to the range of 12 to 24 [37].

1.1.1 Diesel Engine Advantages

Compared with traditional SI engines, Diesel engines have a improved efficiency due to its higher compression ratio, low pumping loss with un-throttled operation. This high efficiency induces a 20-40% improvement in fuel economy for diesel-powered vehicles compared to gasoline-powered equivalents [70].

Because knock is not a limiting factor in diesel engine than in a SI engine, Diesel engines have high torque in the low speed range. The high pressure in the combustion chamber also requires better materials and robust construction which leads to an extension of the useful life to three or four times that of a comparable gasoline engine. The lack of any ignition system also greatly improves diesel engines' reliability.

The lean combustion in diesel engine results in extremely low carbon monoxide (CO) emissions. The presence of only air in the combustion chamber during the compression stroke also reduces the formation of hydrocarbon (HC) emissions from crevice volumes [37]. Moreover, maintenance and fuel costs for diesel engines are also typically lower than those of traditional SI engines.

1.1.2 Diesel Engine Disadvantages

For diesel engines, in addition to the emissions familiar from gasoline engines, i.e., CO2, NOx, HC and CO, particulate matter (PM) emissions, which includes diesel soot and aerosols such as ash particulates, metallic abrasion particles, sulfates, and silicates, have to be taken into consideration. The formation of PM is a complex process and is dependent on both fluid-dynamic and thermodynamic boundary conditions. Reducing the injection pressure or the oxygen concentration typically causes an increase in PM emissions [66].

The high local temperature of diesel combustion leads to high levels of NOx emissions from diesel engines. Moreover, the lean combustion of diesel combustion presents a challenge for NOx control through the use of exhaust after treatment systems, as

NOx reduction in an oxygen-rich environment cannot be easily achieved [70].

Although diesel engines have other disadvantages such as high noise and lower specific power output, reducing PM and NOx emissions simultaneously is perhaps the most difficult challenge facing diesel engine development especially when we are facing more and more tighter emission regulations as shown in Fig. 1-2. Things get more complex because reducing NOx generally lead to increased PM emissions and vice versa, often described as the PM-NOx trade-off. For example, the contribution to NOx emissions is almost insignificant at temperatures below 1700 K, while the PM will get increased out with lower temperatures [46].

In summary, current diesel powered vehicles are subject to increasingly stringent exhaust emission regulations, while at the same time having to meet end user requirements with respect to power, torque, fuel economy, good driveability and increasing levels of refinement. People have done a lot of research to advance the diesel engine technology. The most active ones include Diesel Particulate Filters (DPF), Homogeneous-charge compression Ignition (HCCI) and better fuel injection system. It is the latter that this paper is interested in.

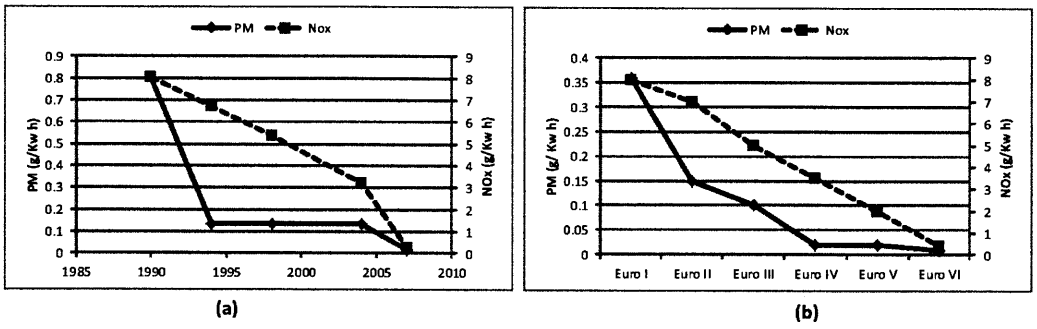

Figure 1-2: The Proposed emission standard for heavy duty trucks: (a) Federal EPA standard in US; (b) European Standard. (Data from [46].)

1.2 Diesel Fuel Injection Equipment

As described in the previous section, the performance and emission of diesel engines is heavily influenced by mixture formation which come from the injection system design. In fact, the most notable advances achieved in diesel engines resulted directly from superior fuel injection system designs. While the main purpose of the system is to deliver fuel to the cylinders of a diesel engine, it is how that fuel is delivered that makes the difference in engine performance, emissions, and noise characteristics [46].

When Diesel first invented the engine, he injected fuel with the assistance of compressed air, which atomized the fuel and forced it into the chamber through a nozzle. Although this air-blast injection gives the highest net power output and efficiency in all engines at that time, new injection systems are developed to meet drivers' needs. Diesel engines in service today have very high injection pressures using mechanical pumps and deliver it to the combustion chamber by pressure-activated injectors with precisely controlling the injection timing, fuel atomization, and other parameters. The diesel injection system has advanced from old mechanically-controlled pump-line-nozzle designs to the modern electronically-controlled unit injector and common rail designs.

1.2.1 Indirect and Direct Injection

In Indirect Injection (IDI) diesel engines, the fuel is injected into a small pre-chamber attached to the main cylinder chamber. The combination of rapidly swirling air in the prechamber and the jet-like expansion of combustion gases from the prechamber into the cylinder enhances the mixing and combustion of the fuel and air. Starting is aided by a high compression ratio (24-27) and a glow plug mounted in the pre-chamber. This design has the advantage of less noise and faster combustion, but typically suffers from poorer fuel economy.

In Direct-Injection (DI) diesel engines, the fuel is injected directly into the cylinder chamber. DI engines have two designs: a) High-swirl design, which have a deep bowl in the piston, a low number of holes in the injector and moderate injection pressures;

b) Low-swirl or quiescent design, which have a shallow bowl in the piston, a large number of holes in the injector and higher injection pressures. Smaller engines tend to be of the high-swirl type, while bigger engines tend to be of the quiescent type.

IDI engines are cheaper to build, but almost all in road-going vehicles most prefer the greater efficiency and better controlled emission levels of DI engines. IDI diesel engines can still be found in the many all-terrain vehicle (ATV) applications.

1.2.2 Common Rail FIE

Common Rail (CR) system is today the most commonly used fuel-injection system for modern passenger-car and commercial-vehicle diesel engines. It was invented by Bosch in late 1990s to address the increasing demands of higher pressures, faster switching times, and a variable rate-of-discharge curve on diesel engine fuel-injection systems [66].

The CR injections system consists of the following main components as shown in Fig. 1-3: the low-pressure system comprising the components of the fuel-supply system, the high-pressure system comprising the high pressure pump, the rail, the injectors, the high-pressure fuel lines and Electronic Control Model (ECM) [66, 48].

The key components of the CR injection system are the injectors connected to the rail. The structure of a solenoid valve injector is shown in Fig. 1-4. When the injector valve is closed, high pressure is supplied to the needle seat as well as a small chamber above the injector piston via a calibrated inlet port. The pressure forces balance with each other. When the solenoid is energized, the injector valve opens, high fuel pressure is relieved above the injector piston and returns to the fuel tank via the injector leak back ports. This creates a pressure difference above and below the piston and the needle is lifted. High fuel pressure drives the fuel out of the nozzles and now the fuel is injected to the cylinder. In 2003, Bosch unveiled the third generation of common rail injection featuring piezoelectric in-line injectors. The piezo injector offers quicker response time than solenoid-valve injector and could further reduce the diesel engine's fuel consumption and exhaust emissions, while also reducing the associated running noise [48].

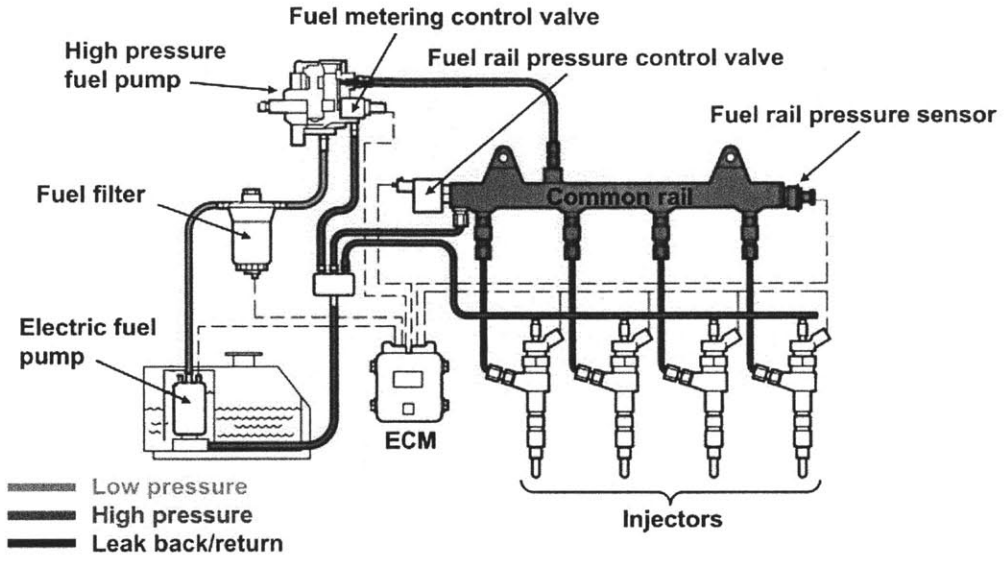

Figure 1-3: Common-Rail diesel fuel systems [48].

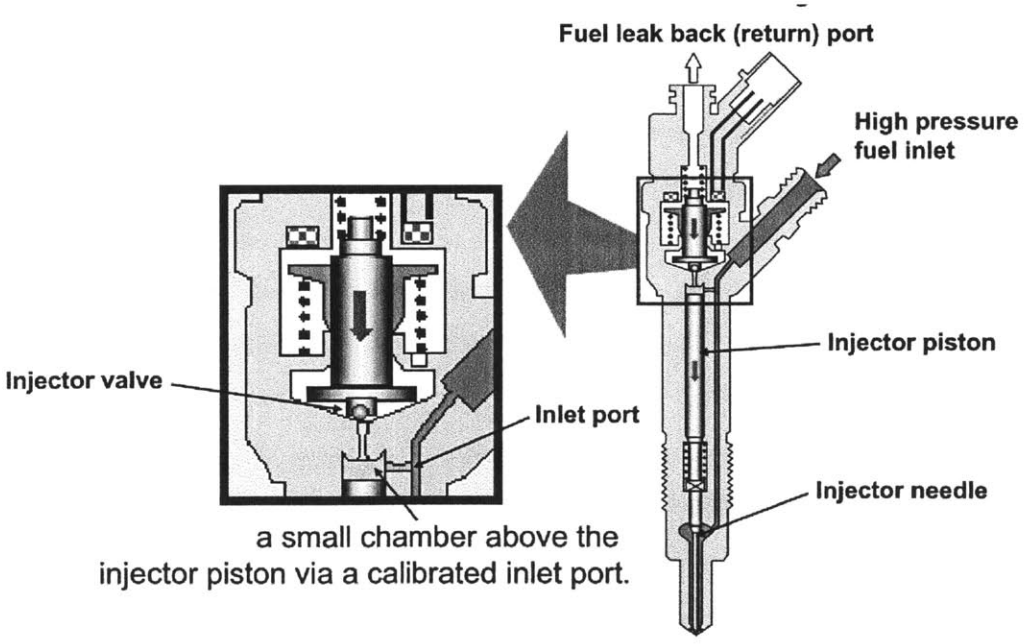

Figure 1-4: Main components of Solenoid-valve injector[48].

The main advantages of CR include [48]:

1. Fuel pressure is available on demand and could be adapted to the operating status.

2. A higher injection pressure could be achieved. Increased pressure allows the fuel to be injected into the cylinder through smaller nozzle orifices without lengthening the injection duration.

3. The injection pressure created is independent of engine speed. This was achieved by separating pressure generation (in the high-pressure pump) from the fuel-injection system (injectors) [66].

4. Multiple injections per cylinder combustion are possible.

With these advantages, CR injection system helps to raise specific power output, increase fuel economy, reduce noise emission and decrease pollutant emission in diesel engines.

Current developments target on higher injection pressure which allows the fuel to be injected into the cylinder through smaller nozzle orifices without lengthening the injection duration and fast response time which facilitates the multi-injection strategy. Fig. 1-5 shows the CR technology roadmap proposed by Bosch [21] and Fig. 1-6 shows the historical evolution in peak injection pressure. We can see an near exponential increase in injection pressure over the years to meet the regulation requirement.

The other active research area in the injection system is the nozzle design, especially the layout and the geometry of the spray holes. For a good emission performance, the injected fuel should be finely distributed into the combustion chamber to utilize all the provided air inside the combustion chamber [23]. The geometry of the holes favors the "'high efficiency"' nozzle, i.e. a nozzle with high degree of grinding at the spray hole inlet and conicity (CF) of the holes, which reduces cavitation, increases discharge coefficient and yields to a high hydraulic flow at small hole diameters[24].

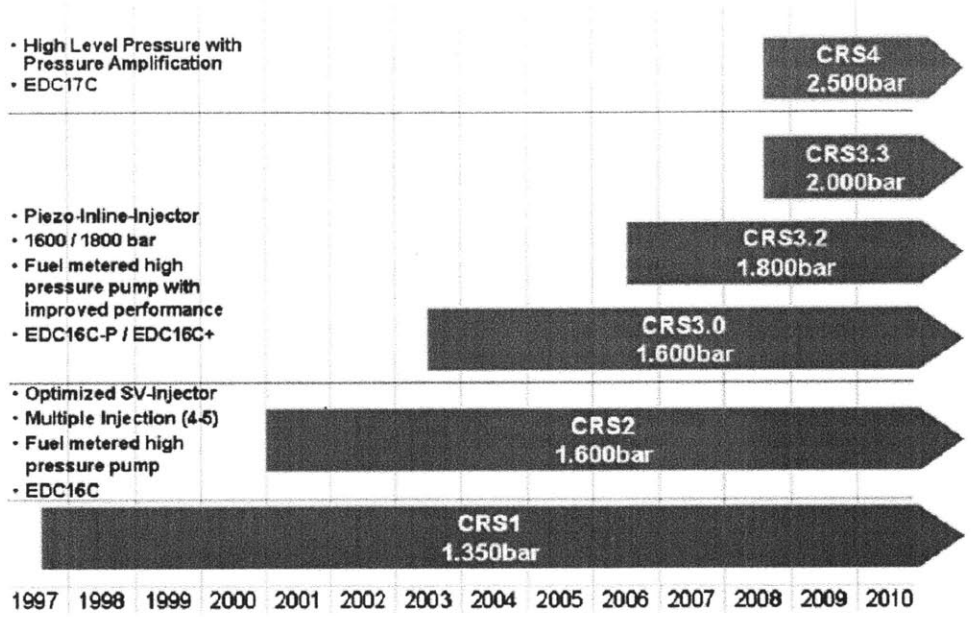

Figure 1-5: Roadmap of Bosch CR injection technology development [21].

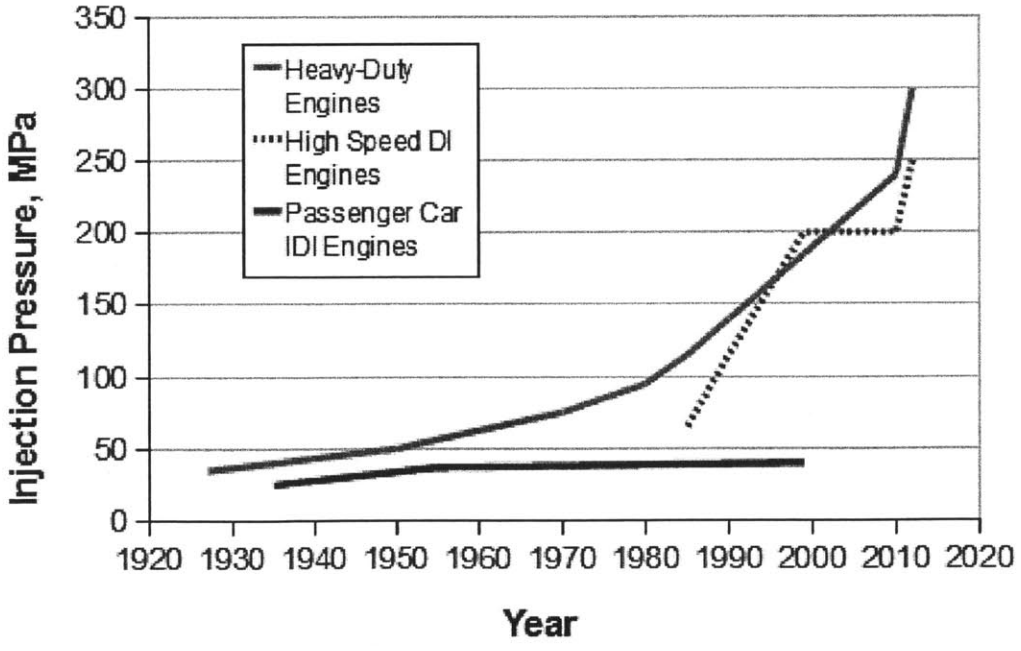

Figure 1-6: Peak Injection Pressure Versus Model Year[46].

1.2.3 Impact of deposits in nozzles

Deposit formation has been observed for many years in internal combustion engines. It regularly appears in both injection systems such as injector nozzles and engine parts in the combustion chamber such as the cylinder head, piston, intake and exhaust valves. Arifin reviewed deposit studies inside combustion chambers [10]. This paper focuses on the deposit formation inside diesel injector nozzles.

Deposits in injector nozzles influence the fuel injection resulting in a different mixture formation and combustion. Historically, It was more problematic in IDI engines operating with pintle type injector which could lead to increased acoustic [73] and pollutant emissions [36].

DI engines did not suffer to the same extent. But more recently, with the development in high pressure common rail injection system, the trend for smaller holes and high efficiency nozzles has resulted in many more instances of injector spray-hole deposits causing problems[69]. The reasons for the higher deposit damage include:

1. Smaller nozzle diameters. Future nozzle diameters could be less than 0.1 mm. This design trend dramatically increased the kinetic energy of the fuel jet, leading to smaller droplet size in the combustion chamber and then resulting in more complete combustion. However, smaller holes which for a given deposit level will result in a proportionately larger reduction in flow area and therefore larger flow rate reduction, resulting in loss of torque and power.

2. Reduction or elimination of cavitating flow within the nozzle as described at the end of Section 1.2.2. Fig. 1-7 (a) shows a relative comparison of emission results run in fossil diesel fuel of a nozzle with low discharge coefficient (75%) and a high discharge coefficient (83%). The nozzle with a lower discharge coefficient shows a significant increase of PM emissions compared with high efficiency nozzle. However, as shown in Fig. 1-7 (b), the nozzle with high discharge coefficient shows significantly increased power loss in the engine test compared with the nozzle with lower discharge coefficient which implies high deposit accumulation in the spray hole [24].

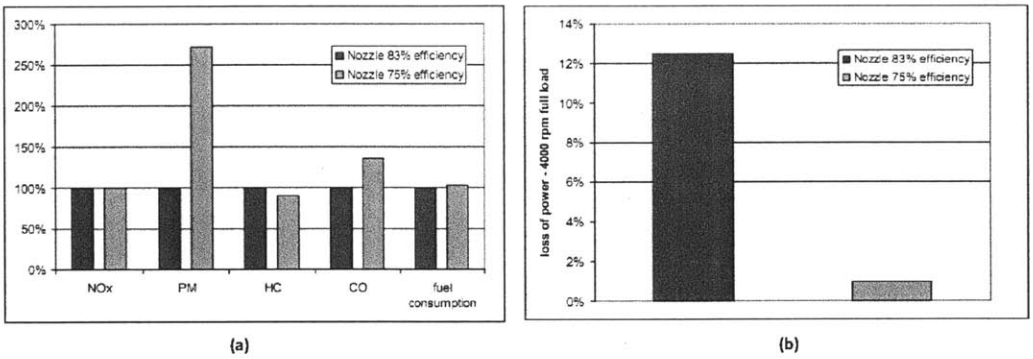

Figure 1-7: Relative comparison of 2 nozzle variations: (a) emission and fuel consumption (2280 rpm; 8.2 bar bmep); (b) loss of power from coking tests results[24].

3. Combustion and air management trends resulting in higher nozzle tip temperatures, which promote nozzle deposits. The trend towards downsized engines will tend to exacerbate this [69].

4. Complicated fuel delivery schemes which often involve multiple injections per cycle need precise metering of fuel and this further requires very tight tolerances within the injector. This tight tolerances made injectors more sensitive to fuel particulate contamination.

1.3 Injection Deposit Literature Review

1.3.1 Deposit Measurement Methods

Field Testing

Field testing is the most reliable yet expensive way to test the deposit formation. Usually several modern vehicles from different manufactures are filled with the fuel and run over 2-3 days using the whole tank of fuel. Then the tanks are refilled and the cycle is repeated. Metal contamination could be measured with regular time intervals. The final deposit could be also analyzed by taking the injectors out of the car. The deposit evolution, however, is not easy to be measured.

Engine Testing

Engine testing generally consists of a diesel engine which is connected to a dynamometer and run through a pre-defined drive cycle or protocol. Since deposit can not be measured directly, several metrics are used in these tests. The most basic metric is power loss when operating at fixed injection duration. Because the injection pattern and fuel flow rate are affected by the deposit formation, the loss of power is correlated with the deposit buildup. But it is difficult to relate the power loss to the deposit buildup rate.

Another testing metric commonly used is the pressure drop across the fuel injector. The pressure drop is calculated by measuring the fuel flow after stopping the engine. If the pressure drop increases significantly, we know deposit buildups have partially blocked the nozzles.

Different testing protocols are developed (see [12] for a latest review). Graupner et al. [56] proposed a detailed testing protocol as shown in Fig. 1-8. It is also used in [23] and [73].

Section	Name	Duration	Remarks
A	Test Preparation		installation of test fuel flushing of fuel system, feed and return lines engine start and warming up oil weighing and refill
B	Iso-speed measurement	approx. 1hr	variation of torque, smoke, cylinder pressure, specific fuel consumption & emissions as function of injector opening time
C	Nozzle coking cycle	8 hrs	deposit build up
D	Soak period	8 hrs	potential flaking off of labile deposits
E	Nozzle coking cycle	8 hrs	deposit build up
F	Iso-speed measurement	approx. 1hr	as for B
G	Disassembling of injectors		protection of deposits on injector tip
H	Injector inspection		photo documentation of deposits assessment of external deposit rating (not compulsory) hydraulic flow measurements (not compulsory)

Figure 1-8: Coking cycles proposed in [56].

Tang et al. [73] used a base cycle of 20 hours and an extended cycle of 34 hours with load evolution shown in Fig. 1-9.In comparison to Graupner's proposal, the duration of engine operation is longer and additionally, the soak time was shorter. The nozzle tip temperature is also higher.

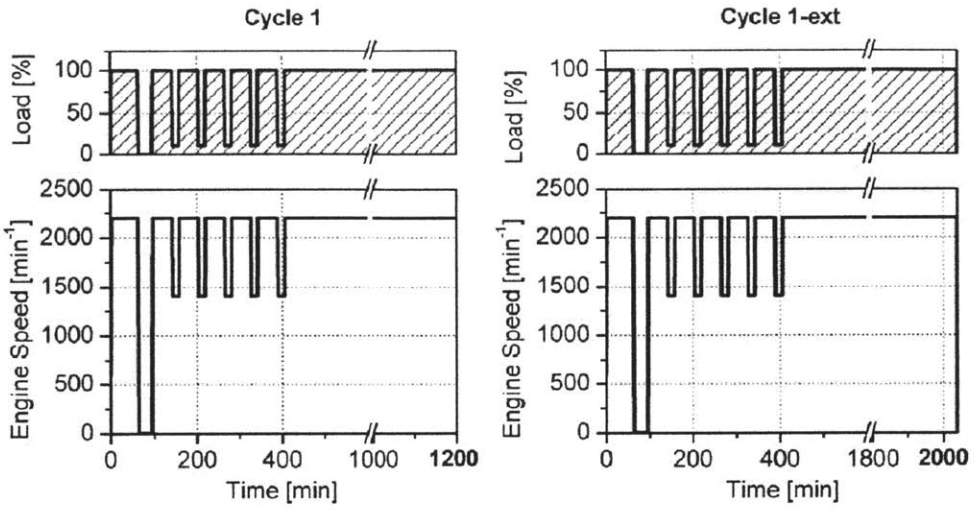

Figure 1-9: Coking cycles used in [73].

Engine tests are very time consuming and costly, but they are also necessary because the chemical reactions and deposit formation which take place inside the engines are sufficiently complex. A new detergency fuel which produces less deposit may have other side effects. Engine testing is possibly the only way to identify the possible adverse effects. On the other hand, because there are so many factors and uncertainties in engine testing, it is difficult to relate test condition to model development/validation. It is also hard to cut the injectors and analyze the deposit. Some authors [34, 25, 9] developed screening or accelerated tests based on engine testing with short running hours (6 hours), but they still embed the shortcomings of engine tests. Besides, only one fuel can be tested at a time and a new injector must be used for every test.

Screen testing

While engine testing should be conducted for a detergent before it enters the market, these tests are very expensive and time intensive and limit the ability of detergent developers to test a wide variety of potential detergent candidates in order to narrow

in on the best choice. A low cost screening method or apparatus could be used to test the deposit buildup in a system where most of the physical and chemical processes are preserved while other engine systems are eliminated.

To the best of the author's knowledge, people have designed the following testing methods to test the deposit formation before going to engine testing:

- Static Test. In static testing, usually fuels with additives or metals are blended and mixed in bottles, possibly heated. Then wait for several days or weeks, with regular sampling and analysis in regular intervals. Leedham et al. [50] put 20 g of metal into 800 g of fuel and then measured the metal concentration in the fuel every week. Ullmann et al. [44] mixed different additives together and found that the combination of a detergent of the family poly isobutylene succinimide (PIBSI) and Difatty acid was not stable and condensation/polymerisation was observed as shown in Fig. 1-10.

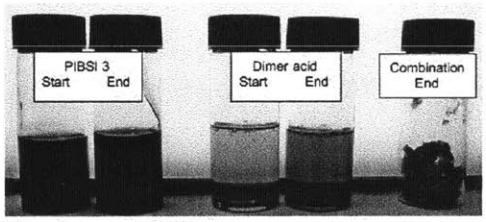

Figure 1-10: Static test with treatment at 180C for 6 hours [44].

- Fuel Coker. The coker was developed in the 1950s in US to test the thermal instability for aviation fuels. The coker combines two stress sections: a preheater assembly which is heated internally with an electric-powered cartridge heater and a test filter (as shown in Fig. 1-11). Fuel flows between an outer and inner tube and the inner tube is rated visually at the end of test for discoloration resulting from deposits plating onto the metal surface. The pressure drop across the filter is also recorded. In recent years, the test is replaced almost totally by JFTOT [35].

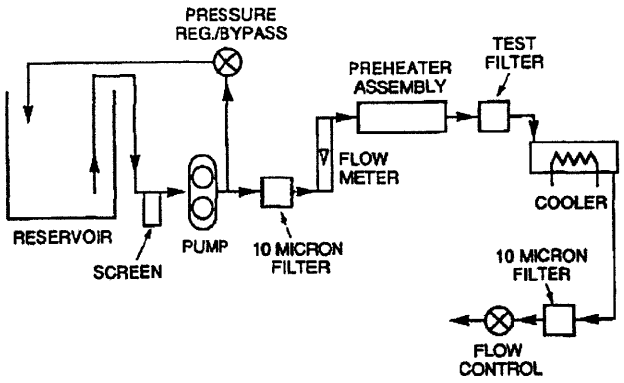

Figure 1-11: Diagram of the design of Fuel Coker [35].

- Jet Fuel Thermal Oxidization Tester (JFTOT). This method was introduced in the US in 1972 and the UK in 1973 [65]. The system has several different models as shown in Fig. 1-12. Some Models use a single fuel reservoir with a floating piston to separate the fresh fuel (in bottom) and spent fuel (on top) while others use two reservoirs, one for fresh fuel and one for spent. The heart of the test system is the tube-in-shell heat exchanger, or test section, which holds the test coupon and directs flow of fuel over it [1].

  The method passes pre-conditioned fuel over a heated tube and then through a filter to trap any filterable insolubles formed during the test. The fuel is rated partly by the extent of filter plugging, as indicated by a pressure drop across it, and by the visual appearance of the deposition on the heated tube which is compared to a standard color scale.

  The major deficiency of the JFTOT method is that it is qualitative and requires a subjective visual rating of thermal deposition. In order to improve the qualitative rating method and establish a quantitative method based on the JFTOT equipment, a number of instrumental rating techniques have been evaluated, including optical reflectance changes, interferometry, ellipsometry and dielectric breakdown measurements of deposit film thickness[28]. More recently, Rawson

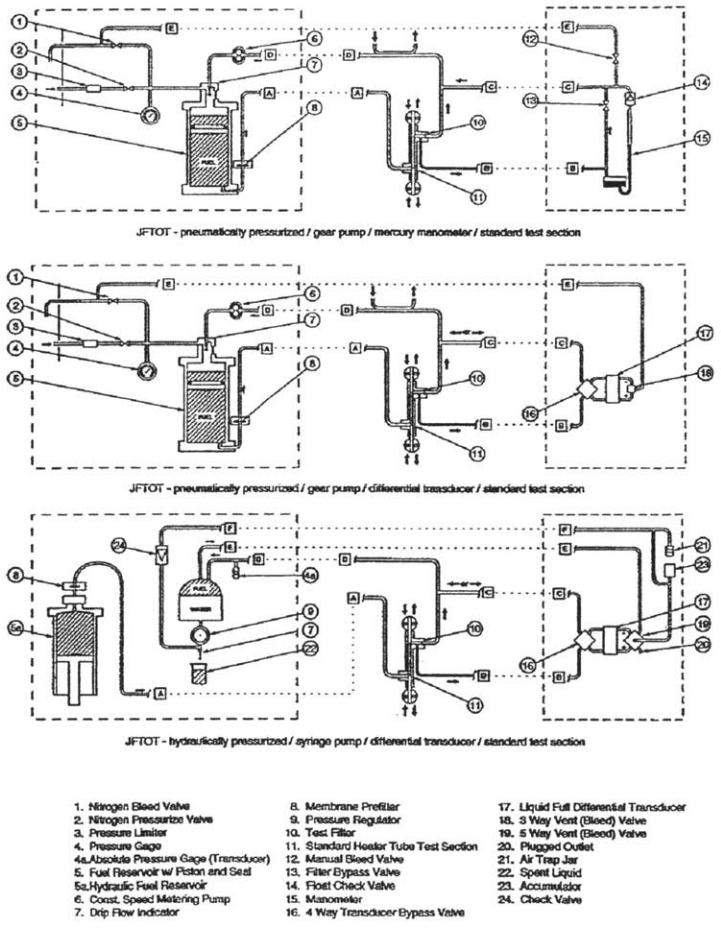

Figure 1-12: Fuel System Schematic in JFTOT [1].

adapted the JFTOT tube to metallic tube and made it operating in either Gravimetric JFTOT mode or U-Tube test section mode[65]. For our injection nozzle deposit testing purpose, the design do not have fuel film formation, evaporation or washing process.

- Flow Reactor. This reactor was designed by Venkataraman et al. ([77]) and is shown in Fig. 1-13. The reactor was heated to 470 C under flowing Argon at 34 atm (500 psig) before the fuel was introduced. The fuel was preheated to 250 C before entering the reactor. A uniform temperature profile along the heater was assumed due to the significantly larger dimensions of the heating block placed around the reactor. The start time for the experiment was noted after the fuel bulk temperature reached the wall temperature of 470 C. The fuel temperature and pressure were kept constant for the duration of the experiment. The fuel flow rate into the reactor was 4 mL/min. A single substrate foil was placed in an isothermal glass-lined stainless steel reactor measuring 200mm x 3mm.

  The advantage of this design is the feasibility to take out the foil with deposit for micro-structure analysis. It still lacks fuel film formation/evaporation/reaction process nor does it include washing effects.

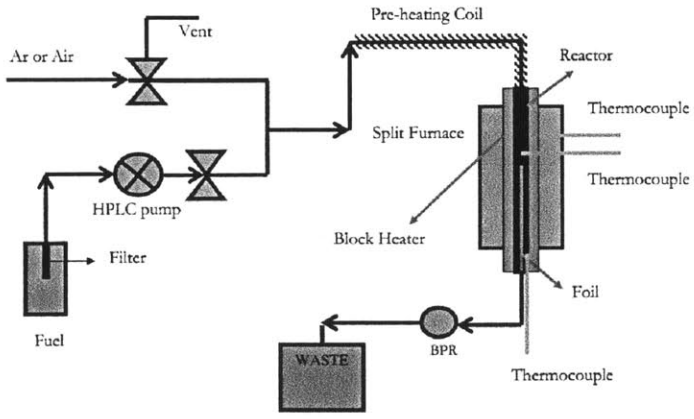

Figure 1-13: Schematic Representation of the flow reactor set-up [77].

- Hot surface deposit test. This apparatus was recently proposed by Yusmady et al [10]. A concave plate of aluminum alloy (JIS 2017S) was used as a hot surface plate. The plate was electrically heated and its surface temperature was controlled by a temperature controller. An infrared thermometer was also used to obtain a more accurate surface temperature. The needle tip is located 80 mm above the center of the hot surface to avoid pre-heating the test fuel and to minimize error caused by the splash loss of droplets mass at impingement. The impingement interval of droplets was controlled by adjusting the pinch cock. The number of droplets impinged was counted using an infrared laser detector and counting equipment [75]. The system is shown in Fig. 1-14.

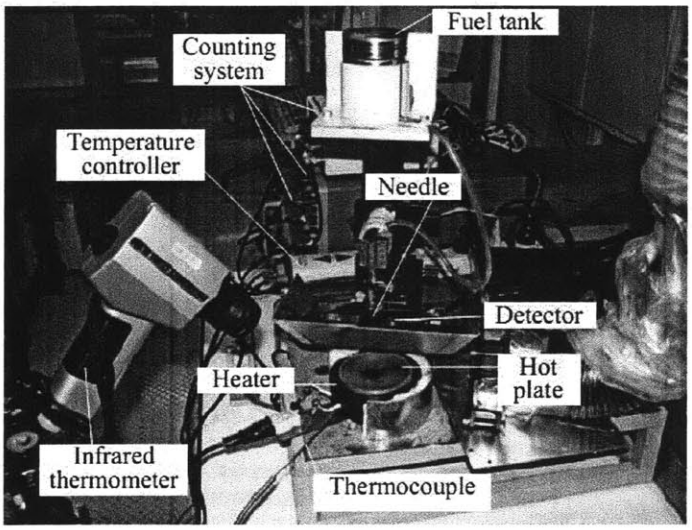

Figure 1-14: Photograph of hot surface deposition test bench [10].

- IID test apparatus. It is targeted to study Internal Injector Deposits (IID), i.e., within the injector body close to areas where fuel pressure is released either through normal fuel flow or internal leakage. The design is shown in Fig. 1-15. An electric motor driven fuel injection pump provides pressurized fuel to a common rail feeding a single fuel injector. The injected fuel is passed to a separate waste tank. The fuel injector is mounted in an electrically heated block, which replicates the heat flow to the injector tip from the combustion process in

engine operation. Nitrogen gas is used to prevent auto ignition within the heated block, which serves as a catchment vessel for the injected fuel [58]. The design recreates the engine environment, however, it can not be used to study nozzle-hole-deposit formation since the fuel comes through injector continuously.

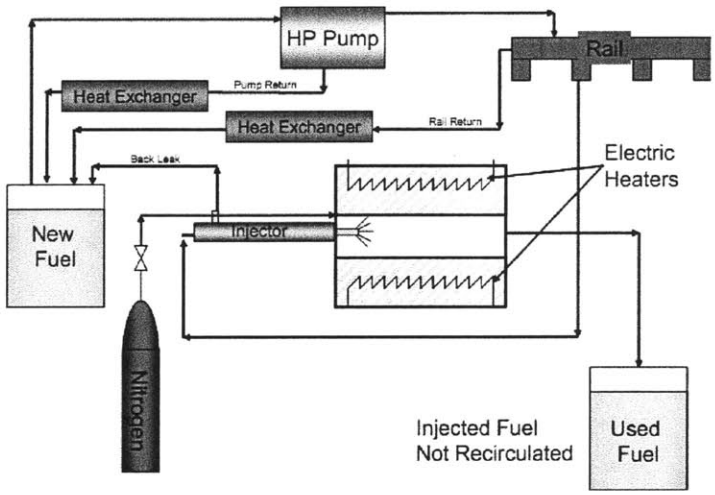

Figure 1-15: Schematic Diagram of Internal Injector Deposit (IID) Apparatus [58].

A ideal screening test should capture the most significant factors leading to deposit formation in real engines while at the same time remaining simple enough to easily extract desired data about the deposit formation mechanisms. In diesel engine injectors, the essential factors include evaporation, thin film formation, oxidation and deposit formation. All the above screening test designs address the oxidation only and that is why we developed a new test design in this work.

1.3.2 Experimental Results

Early in 1993, Caprotti et al. [63] demonstrated the injector deposit could affect the emissions and drivability over time. They also used engine test to study PM emissions and found out the PM were greatly increased when injector deposits were present (+45%) as shown in Fig. 1-16.

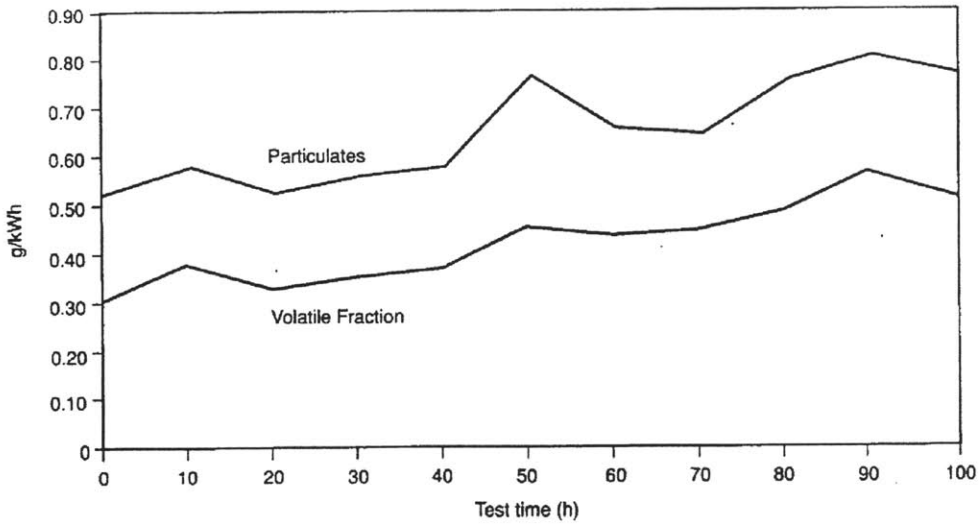

Figure 1-16: Particulate Emissions with time in nozzle fouling test [63].

Kinoshita et al. [47] studied the deposit formation in the direct injection gasoline engine injectors using engine tests. They cooled the nozzle with water and compared the deposit formation in nozzles with different temperatures. They found that When the nozzle temperature is lower than the 90 vol. % distillation temperature, deposit precursors in the fuel are easily washed away by fuel injections, because the residual fuel is kept in a liquid state and the deposit precursors disperse. On the other hand, when the nozzle temperature is higher than the 90 vol. % distillation temperature, it is hard for the deposit precursors to be washed away from the nozzle hole by fuel injections, because the deposit precursors cohere each other and adhere to the wall.

Leedham et al. [50] used Engine Test, Laboratory Test and Field Test to investigate the deposit formation of European diesel in injector tips and nozzle holes. For engine test, the test length was 24 hours. He found no obvious torque loss for base fuel and around 10 percent torque loss for fuel contaminated with 1 ppm Zinc. For lab emersion test, they put 20 g of metal into 800 g of fuel and then measured the metal concentration in the fuel every week. They found that among Mg, Fe, Al, Cu, Pb and Zn, Pb and Zn were absorbed into the fuel while the other metals were not detected in the fuel. They further found good detergency could decrease the metal

concentration in the fuel. For field test, they filled the tanks of different cars and consumed the fuel over 2-3 days. The metal concentration was measured from fuels sampled from a full, half and almost empty tank. They found larger Zn and Pb contamination when acid lubricity agents were present.

Caprotti et al. [23] found out that the type and composition of the deposit appears to be independent from both the test length and the level of metal added to fuel. They also used a modern 2 Liter 4 cylinder diesel engine to test the torque loss. Their results are shown in Fig. 1-17. For Zinc-dopped fuels, the results are more repeatable, however, for base diesel, in the double-length run, the engine torque recovered from previous loss.

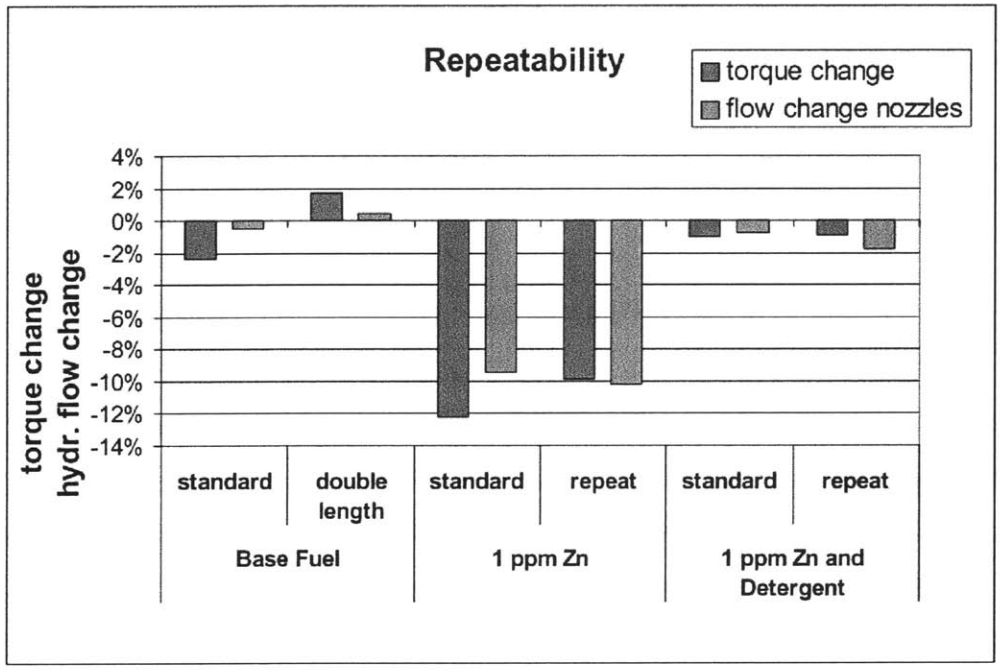

Figure 1-17: Repeatability of Test Protocol [23].

Caprotti et al. [24] used engine tests to investigate deposit formation with fuels with Fatty Acid Methyl Esters (FAME) and Rapeseed Methyl Ester (RME). The results indicate that RME can generate a higher level of deposits in the indirect injection engines with swirl chamber and with future Euro V type common rail injection

systems. They also found large variability in the torque loss for a same RME fuel as shown in Fig. 1-18. One RME batch showed some deposit formation at 16 hours while the other has a completely different profile.

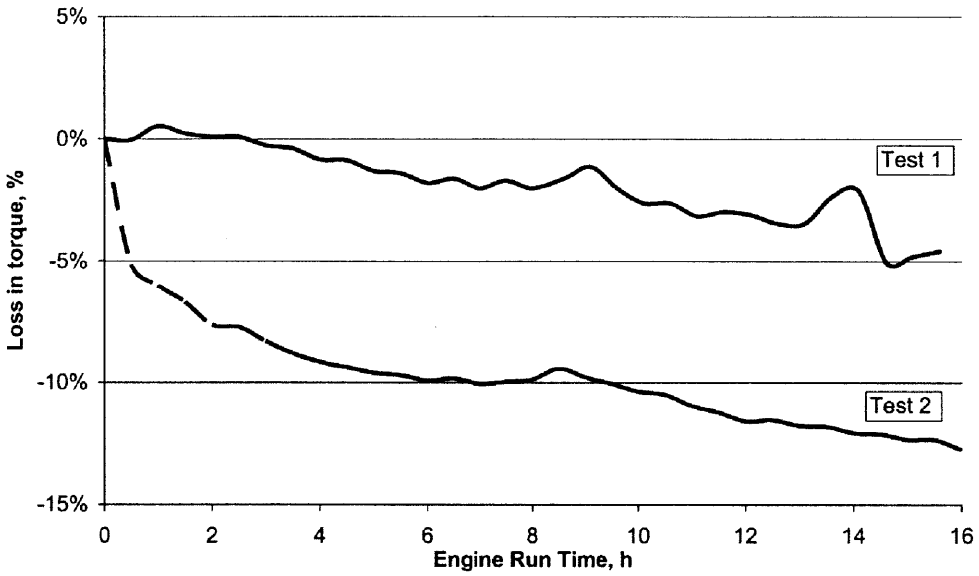

Figure 1-18: Results with different Batches of B5 RME[24].

Argueyrolles et al. [19] studied the influence of nozzle injector geometry and cavitation on deposit formation using engine tests. They studied two geometric parameters in specific: C_f (Hole Conicity) Factor and He (Hole Hydro Grinding Level) and the results are shown in Fig. 1-19. For the hydro grinding, although high He nozzle leads to a high coking level, reducing He level does not guarantee an decreased deposit formation. For hole conicity, for all the nozzles tested, fuel flow losses increase as the conicity level increases. Thus, nozzle coking seems to be directly linked to the nozzle conicity while coking phenomenon cannot be directly linked with hydro-grinding level.

Tang et al. [73] used medium-duty truck engine OM906 to test deposit formation in three different sac-hole nozzles: 1) cylindrical, no rounding; 2)cylindrical, high rounding; 3)conical, high rounding (ks nozzles). They found a critical Zinc concen-

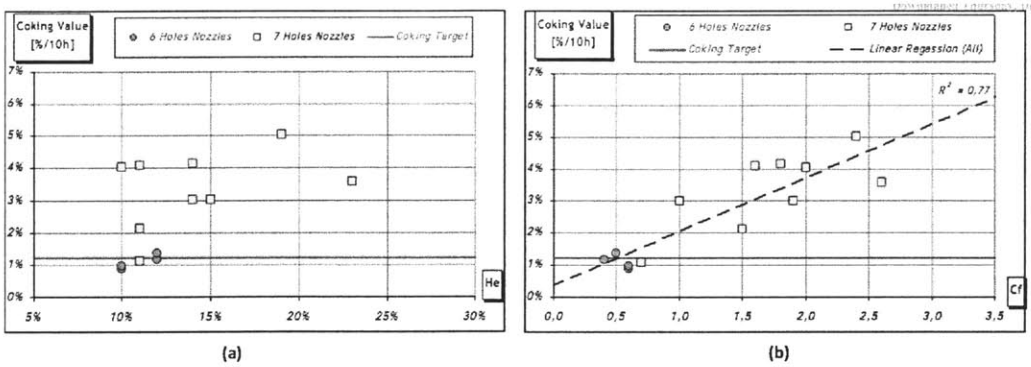

Figure 1-19: Effects of different nozzle geometry parameters on coking: (a) hydro grinding; (b) nozzle conicity [19].

tration of around 0.6 - 1ppm was required in their operation to develop reasonable fouling. They also concluded that partially zinc-derived deposits could be washed away using zinc-free fuels as shown in Fig. 1-20. Temperature increased deposit formation in their study. They then studied deposit formation in nozzles with different geometries and type 2 geometry reduced in power output by more than six percent while type 1 nozzles indicated no significant coking level. The reason, they believed, was because type 2 nozzle utilized a hydro-grinded (rounded) spray hole inlet to reduce cavitation in the nozzle orifice.

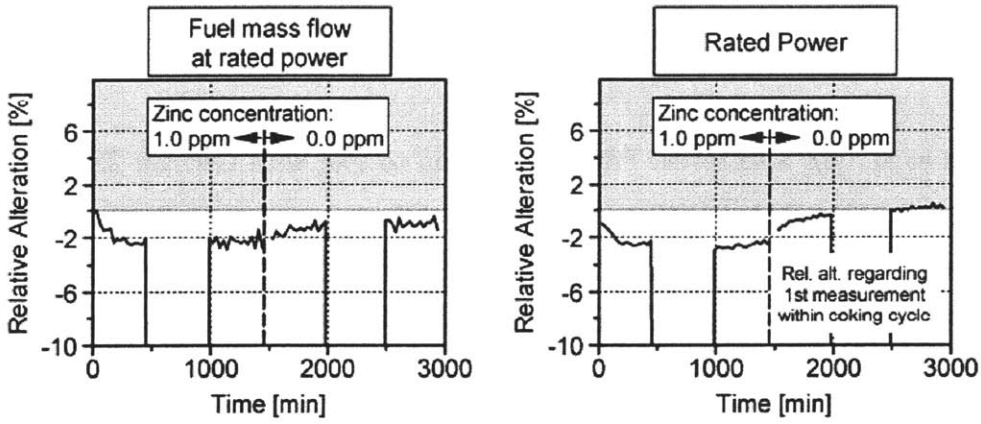

Figure 1-20: Reversibility of zinc-derived nozzle fouling [73].

Tang et al. [73] also studied micro-structure of deposits using EDX and SEM. They found out the size of deposit particles correlated with the position in nozzle. The closer the spray hole outlet was, the smaller were the grains. One explanation was due to the reduced zinc concentration in flow direction, the other was the effect of higher temperature close to the outlet. Distributions of C, O and Zinc were analyzed. While the amount of C was constant, the primary deposit layer exhibited a high concentration of zinc in comparison to the rest of the deposits. The investigation with SAD revealed that no crystalline structures were detected. Therefore, the deposits are most probably amorphous.

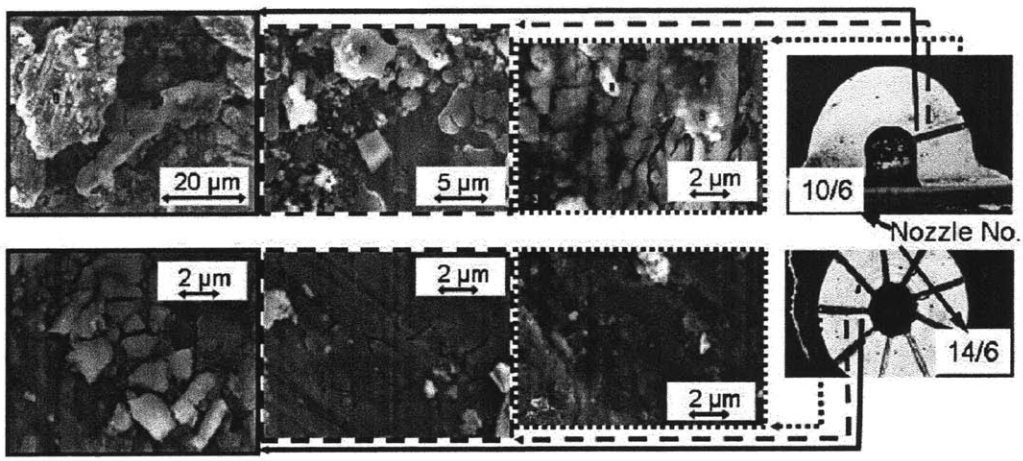

Figure 1-21: Reduction of size of zinc agglomerates in direction of the fuel flow in the nozzle orifice [73].

Uitz et al. [67] also tested FAME diesel (up to 7%) with German ZSD (B0) as a base fuel using PSA DW10 engine. They evaluated power, Brake Specific Fuel Consumption (BSFC) and black smoke data and found that no measurable injector nozzle fouling occurred with any of the B10 or the B0 ZSD fuels without adding zinc. Li et al. [38] studied another bio-fuel - rapeseed oil on fuel injector deposit control and found the emissions of CO increased significantly with deposit build up.

More recently, people started to study the deposit inside injectors, the so called internal injector deposit (IID). A recent component analysis of a number of High

pressure CR injectors showing symptoms of needle and/or command plunger sticking from the field or from OEM test stands shows that the bulk of these deposits were comprised of sodium salts of alkenyl (hexadecenyl or dodecenyl) succinic acids [71]. Sodium can enter the fuel distribution system from salt driers and caustic water used at refineries, storage tank water bottoms and seawater used as ship ballast. Alkenyl succinic acids are widely used as pipeline corrosion inhibitors and in additive packages. Once formed, these salts are insoluble in ULSD fuel and can exist as very fine particulates that can pass through vehicle fuel filters, eventually depositing on the internal surfaces of an injector. The deposit components were also confirmed by Schwab [71] using engine tests.

For the clean up actions of detergency fuels, Aradi et al. [8] studied the clean-up action of detergents in direct injection gasoline engine using engine tests. When using higher than normal dose EM-1 additive, up to 70% flow loss could be recovered as shown in Fig. 1-22. The clean up actions are more interesting in diesel engines.

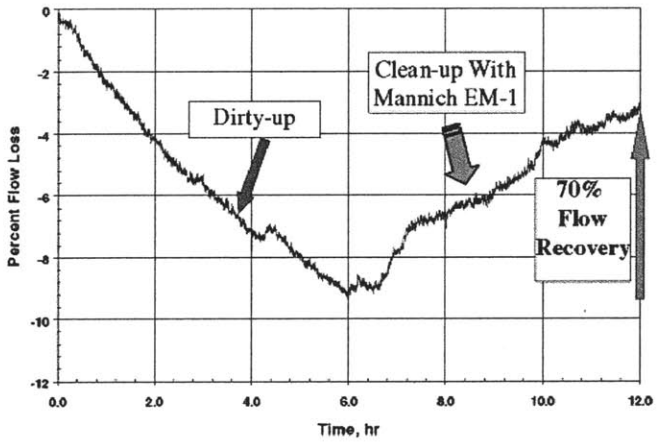

Figure 1-22: DIG injectors dirty-up for 6 hours followed by a clean-up with base fuel additized at a higher than regular dose for 6 hours. [8].

Caprotti et al. tested the clean-up action for B7 base fuel with detergency fuels and found that the vast majority of the deposit is removed in the first hour, approximately 70%, which corresponds to 2% absolute power loss. There was a sudden recovery

in the power loss immediately after the clean-up started as shown in 1-23. The phenomenon may be related to the ultra-high injection pressure in CR diesel engines.

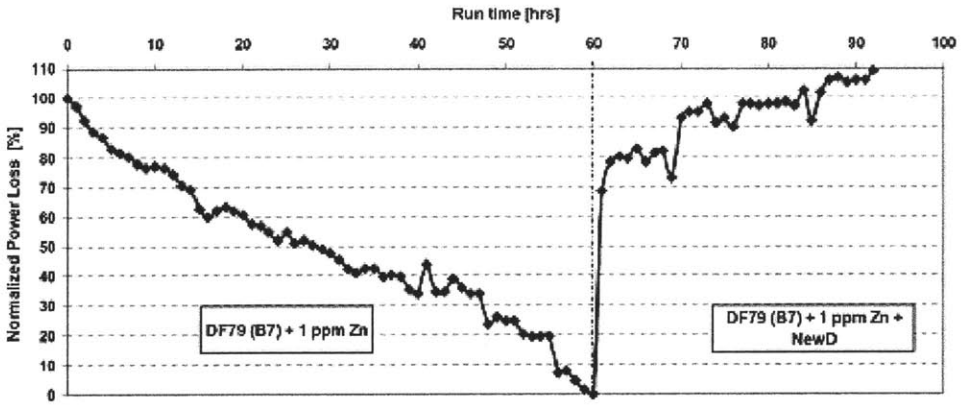

Figure 1-23: Normalized power loss- DW10 clean up performance. [69].

1.3.3 Deposit Mechanisms

Lepperhoff and Houben [51] explained the formation and removal of deposits in internal combustion engines by means of basic mechanisms which is shown in Fig. 1-24. These mechanisms are applicable to the combustion chamber and nozzle tip. But inside injection nozzles, the deposit is continuous and the soot and gas may not be as important in formating the deposit.

In a review of deposit formation in the holes of diesel injector nozzles giving by Birgel et al. [3], they discussed possible physical mechanism of the deposit formation at nozzle tip as shown in Fig. 1-25. After closing of the nozzle in the high pressure part of the combustion process, liquid fuel is stored in the injector holes. This fuel expands during the expansion stroke due to temperature increase of the injector body. Therefore a liquid film is formed outside the holes at the nozzle tip. The high surface temperature at this location increases at the same time the evaporation of fuel components and degradation processes, leading to sticky deposits. Soot and high boiling

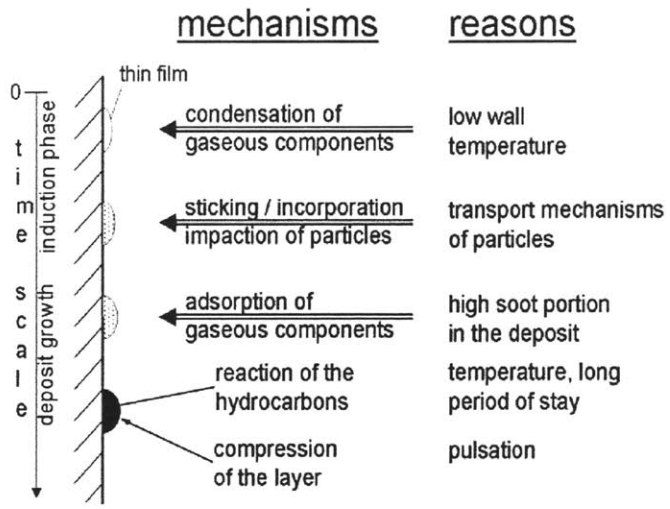

Figure 1-24: Mechanism of Deposit Formation[51].

hydrocarbons formed during combustion as well as lubricant components accumulate at the deposit interface (absorption, condensation, or physical compacting) increasing the rate of deposit formation. Further fuel expanding out of the nozzle holes is adsorbed in this sooty deposit and reacts to further increase deposit formation rate.

More recently, Barker et al. listed possible causes of internal injector deposit (IID) formation as shown in Fig. 1-26. They then tried to get some insights by studying the characterization of deposits in the fuel injectors. Deposits found within different parts of the injector were analyzed using, Gas Chromatography with Mass Spectrometry detection (GC/MS), Fourier Transform Infra-red analysis (FTIR), Inductively Coupled Plasma spectroscopy (ICP), Nuclear Magnetic Resonance spectroscopy (NMR) and elemental analysis. Regarding the metal concentrations in the fuels analyzed it was found that: a)Only one of the fuels contained a measurable amount of zinc, this fuel was known to have a propensity to form deposits; b)the presence of a measurable amount of metal is not a prerequisite for deposit formation; c)An ion associated with a C19 carboxylic salt was identified as being more abundant in the fuel without the deposit forming tendency; d)The more heavily fouled injector deposits contained substantial amounts of sodium but that it was not present as a carboxylate [13].

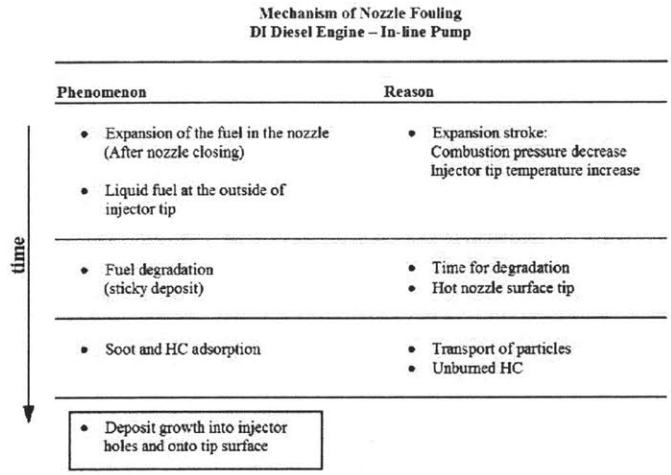

Figure 1-25: Mechanism of Nozzle Fouling, DI Diesel Engine[63].

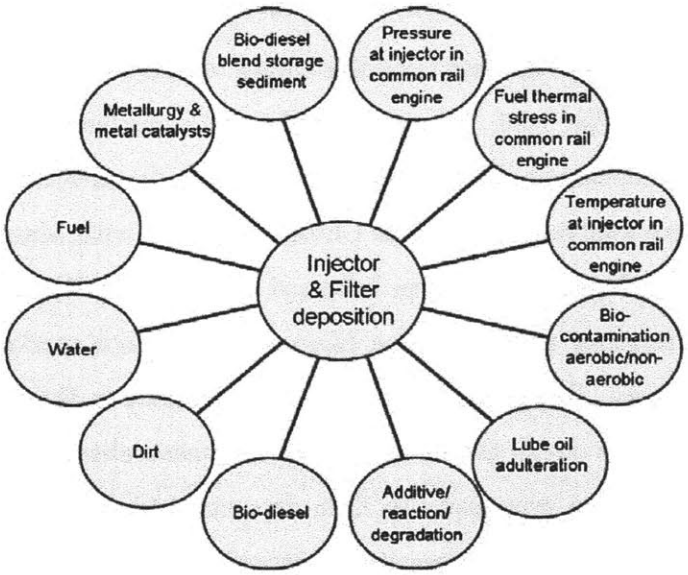

Figure 1-26: Possible causes of fuel system deposits[13].

A mechanism of the deposit formation on the nozzle hole wall was proposed by Kinoshita [53] and is shown in Fig. 1-27. After a fuel injection a small amount of fuel remains on the nozzle hole wall. The deposit precursors disperse in the fuel which remains on the wall (Fig. 1-27a). After time, the fuel will evaporate, and cohesion of the deposit precursors will progress in the fuel. When the nozzle temperature is lower than 90% distillation temperature of the fuel, some fuel evaporates, and most of the fuel remains in a liquid state. Thus, the deposit precursors maintain a state of dispersion in the fuel (Fig. 1-27b). In such a state, the deposit precursors are washed away from the nozzle hole by future fuel injections. However, when the nozzle temperature is higher than the 90% distillation temperature of the fuel, most of the fuel evaporates and the deposit precursors cohere on the nozzle hole wall (Fig. 1-27c). The deposit precursors in this state are not easily washed away by the fuel injections, and the deposit precursors remain in the nozzle hole. The deposit formation thus progresses in the nozzle hole. This mechanism is quite similar with our underlying idea [79], but it did not say how the precursors formate deposit and it also assumed all reaction products were washed away which may not be true.

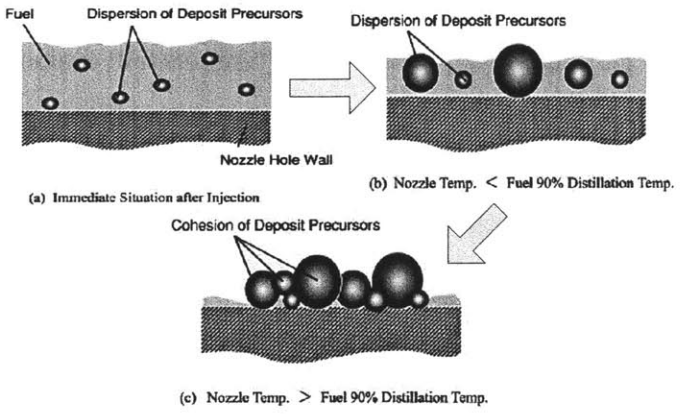

Figure 1-27: Mechanism of Deposit Formation[53].

1.3.4 Modeling Results

Flow in nozzles

Collicott and Li [27] visualized the internal flow in diesel injectors. They found that the abundance of what is likely roughness-induced cavitation, especially at high pressures means that roughness, cavitation, and boundary layer interactions are likely important to droplet production.

A lot of efforts are put to study the flow and cavitation behaviors inside the nozzles(see [16, 72] for a review). Bunnell simulated unsteady cavitation flows inside injectors [20]. Argueyrolles et al. [19] did 3D CFD simulation of flows in nozzles with different geometries. They found out low levels of conicity generate cavitation and the deposit formation is reduced with implosions of cavitation pockets occurring closer to the exit.

Nozzle Temperature

Leuthel and his collegues [52] studied Thermal-Fluid-Interaction in a diesel fuel injector using numerical simulation. In their simulation, coupled fluid-thermal analysis for a Diesel fuel injector was performed using a 3D-CFD-Code for both the solid structures and the fluid domain with temperature boundary conditions given by physical measurements. In particular, they obtained the temperature evolution over two working cycles as shown in Fig. 1-28. They also compared the flow in cylindrical and ks nozzles. The sharp edged cylindrical nozzle shows distinctive cavitation zones (shaded areas within the nozzle) over the whole nozzle length whereas in the ks-nozzle no vaporous zones arise leading to a very homogeneous and less turbulent flow pattern at nozzle exit.

Chemical Reaction

Liquid phase fuel oxidizations have been studied by several groups [43, 80, 22, 45, 5, 55, 77, 57], mostly for the liquid-phase autoxidation and deposition of jet fuels (see KATTA1998 for a review). Zabarnick et al. [80] found out the RO2 radical is the

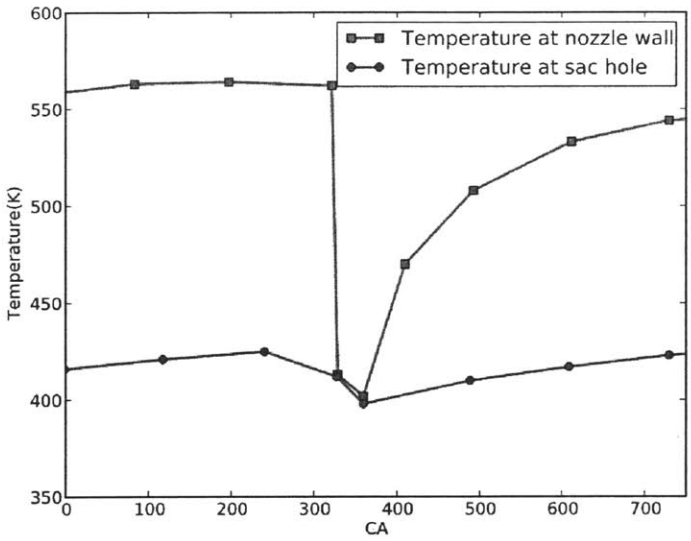

Figure 1-28: Temperature variation of the fuel in the injector over two working cycles (Data extracted from [52]).

chain carrier while oxygen is present in the fuel. They also stressed the importance of hydroperoxides in the oxidation process. Wang et al. [22] studied deposit formation in lubricant film using a simple model shown in Fig. 1-29. Chemically, the original lubricant molecules A, react with the dissolved oxygen to form primary oxidation products. These primary oxidation products then react to form polymers P, and finally, the polymers can result in insoluble deposit D. The model is easy to use, but many import mechanisms are missing.

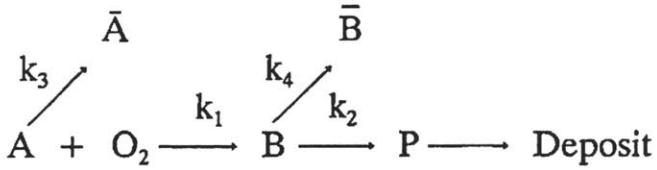

Figure 1-29: Reaction model for lubricant degradation and evaporation[22].

1.4 Project Objectives

While previous research have studied the effects of injector nozzle deposits, few of them provide quantitative information to describe the underlying fundamental mechanisms responsible for the observed deposit formation, such as the models about physical processes, chemical reaction kinetics and the deposit phase separation models. Due to the complex environment in diesel engines, it is not practicable if possible to identify all factors in the deposit formation quantitatively. Nevertheless, simple quantitative models for essential physical and chemical processes in the injector nozzle deposit formation will deepen the understanding of mechanisms involved, help to predict deposit formation for new fuels and make the comparisons between models and experiments possible.

Most of the injector nozzle research rely on engine testing. Although we think engine testing is necessary for any formal development. Testing every idea using engines is very costly and time consuming. Bench-scale apparatus is important in screening tests to check ideas quickly and efficiently. However, current screening testing equipments are either based on engine tests hence inherit their shortcomings or unable to cover the essential physical and chemical processes in the deposit formation. A well designed bench-scale apparatus could also help to extract information about the deposit formation mechanism and hence benefit the modeling developments.

The objective of the project is to fill in the gap and help to better understand the deposit formation and abatement processes in diesel injector nozzles. It is achieved through four tasks:

1. Modeling of the fuel film physical processes into which the deposit/abatement chemistry is embedded. Our goal is not to study every process happened in the deposit formation, but to develop quantitative models for the most important ones. Then the model could be used to help design better injection equipments that make deposit formation more difficult.

2. Modeling of the deposit formation chemistry and detergent action. With the great work from the Green group in MIT chemical engineering department,

we are able to have a fairly complete chemical kinetic mechanisms for liquid phase reactions. Although the models still need more experimental data to calibrate, this is a first step in the literature so far to a complete understanding of the chemical reaction, phase separation and detergent action. This would be extremely useful for the design of new detergent additives.

3. With commercial engine and simulation software packages, combined with our physical and chemical models, We are able to build a quantitative modeling framework for simulating engine injector deposit formation and abatement under different operating conditions. Note that it is a first nozzle deposit simulation framework in the community and we believe it will also be useful to injector and chamber deposit in general.

4. Measurement of deposit formation rate with fuel and fuel/detergent mixtures in a bench scale apparatus. The procedure would provide data for confirmation of the chemistry model, and serve as a screening test for detergents. The goal is to keep the design as simple as possible, while covering the essential processes in the injector nozzle deposit formation. As of our best knowledge, the resulting test rig is a first in his kind to best resemble what happened in real engine testing such as film formation, evaporation, diffusion, oxidization and washing.

Chapter 2

Engine and Injector Simulations

Without knowing the environment in the injector nozzle such as the temperature, pressure etc., It would be impossible to modeling the deposit formation and abatement process, nor could we design bench scale tests to resemble the environment. Besides, we know the engine environment is complex, ever-changing and the deposit formation mechanism is sophisticated. It would be intractable nor necessary to study every aspects of the deposit formation processes. With a better understanding of the engine and injector environment, we can make assumptions to simplify our model development as well as experiment design.

In this chapter, we used engine simulation to calculate pressure and temperature evolution inside combustion chamber. Then we simulated the flow inside the spray hole for a Siemens DW10 injector. Finally, combining the simulation results and experimental data, we proposed a general picture for deposit formation/abatement as well as assumptions for our model development. A surrogate model for the diesel fuel is also presented.

2.1 Engine Simulation

Modern diesel engines usually have multiple injection events. However, in our simulation, we will only consider the main injection to make it simpler. In Fig. 2-1, a single cylinder diesel engine was modeled using GT-Power. The pressure and temperature

evolution were shown in Fig. 2-2. We can see in most of the cycle, the pressure is close to atmospheric pressure while the temperature is quite high.

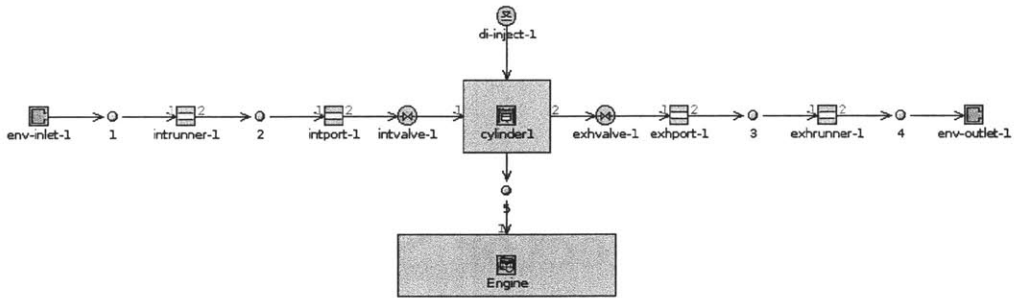

Figure 2-1: A single cylinder diesel engine model in GT-Power.

2.2 Common Rail FIE Modeling

As described in Chapter 1, the common rail fuel injections system is the most advanced injection system which could provide high injection pressure and flexible electronic event control. Sophisticated hydraulic models are required to model the fuel behavior in the system. However, if the rail pressure of the injector nozzle can be estimated or measured and assume the flow in each nozzle is quasi-steady, incompressible and 1D, we have a simple relationship between the mass flow rate and the injection pressure [37]

$$\dot{m}_f = C_D A_n \sqrt{2\rho_f \Delta p} \tag{2.1}$$

where A_n is the nozzle minimum area, C_D is the discharge coefficient and Δp is the pressure drop across the nozzle.

But what we are interested in are more than the fluid velocity in nozzle. Our goal is to figure out the fluid column configuration after the injection. Before constructing the model for residue fuel column, the commercial diesel injector simulation package, GT-Fuel, from Gama Technology, was used to compute the fuel pressure and needle motion using a lumped parameter model for the injector components, see Fig. 2-3.

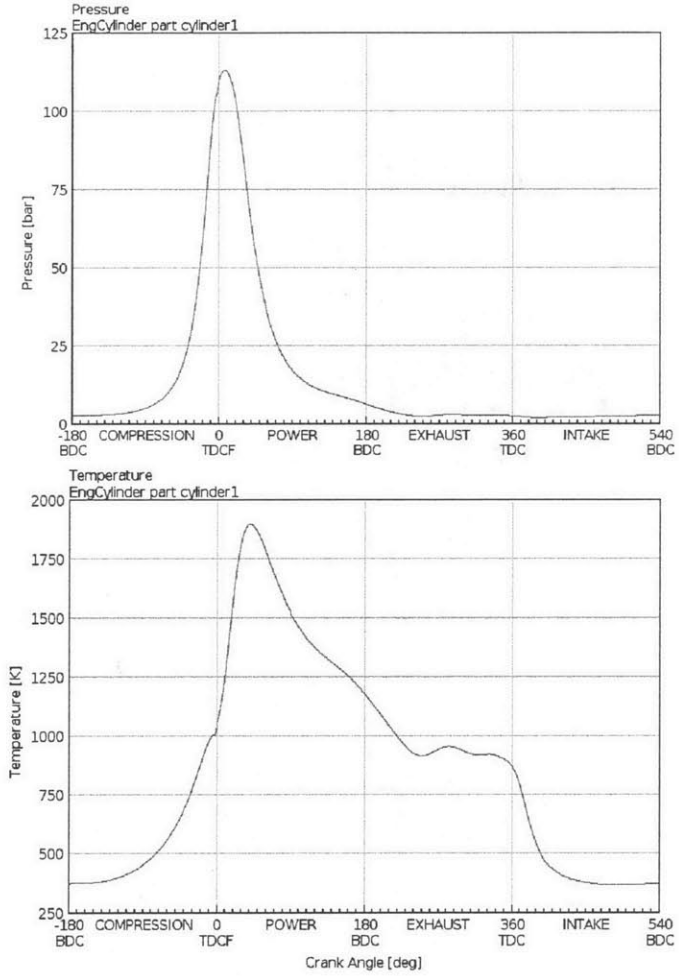

Figure 2-2: Pressure and Temperature evolution in a diesel Cycle.

The injection pressure used is 2000 bar. The specifications of the injector components modeled were based on a modern common rail diesel injector (Siemens DW10 prototype injector) which is shown in Appendix A.

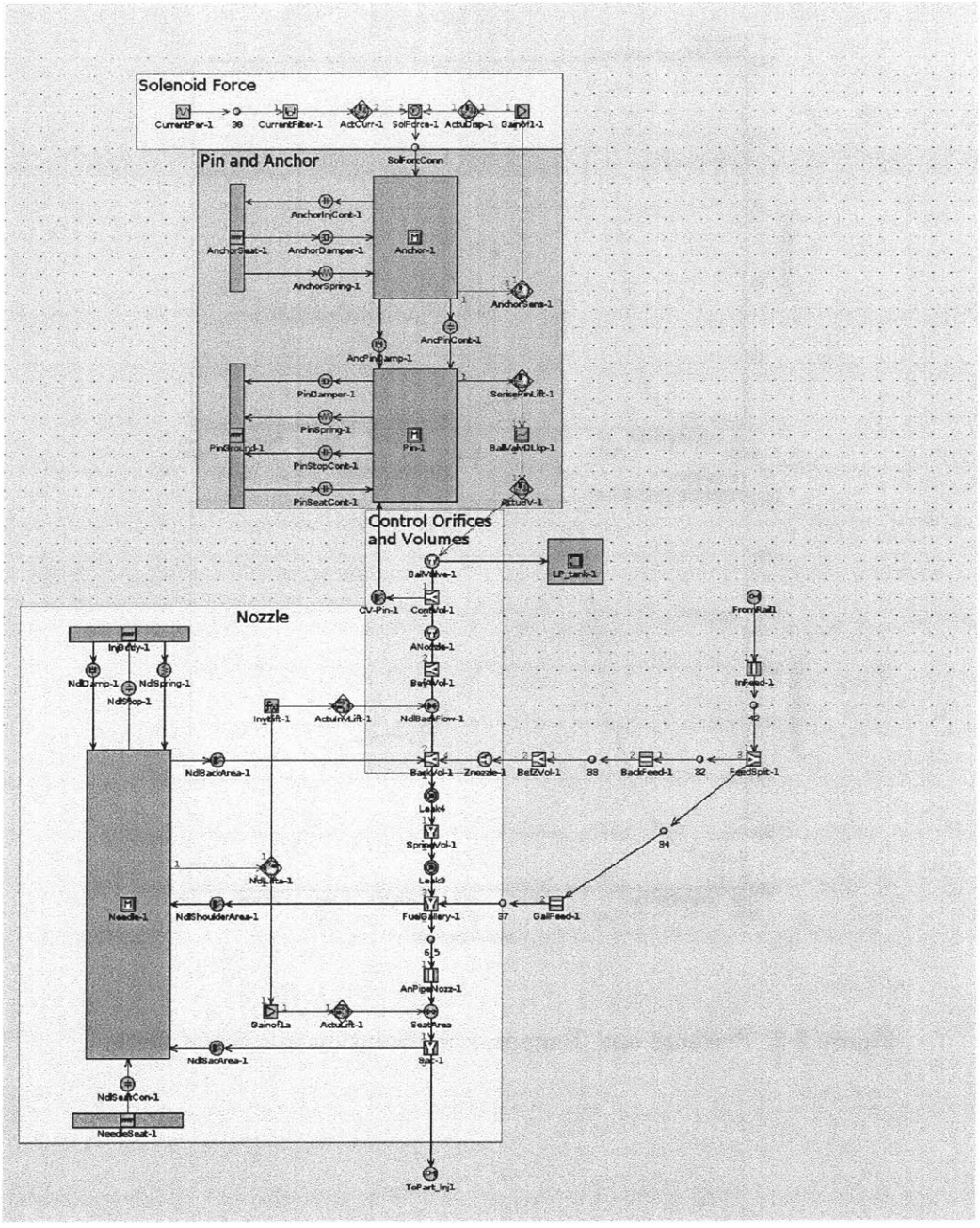

Figure 2-3: Siemens DW10 injector model in GT-Fuel.

The gallery pressure from the simulation is shown in Fig. 2-4. Because in a common rail injector, the needle motion is governed by the differential fuel pressure force acting on the needle, the fuel gallery pressure does not change appreciably in the needle closing process which is also noted in [32]. Thus the details of the injector do not substantially affect the process that governs how much residual fuel is retained in the nozzle at the end of injection, and the velocity of the fuel in the nozzle remains high (hundreds of m/s) up to the seating of the needle; see Fig. 2-5.

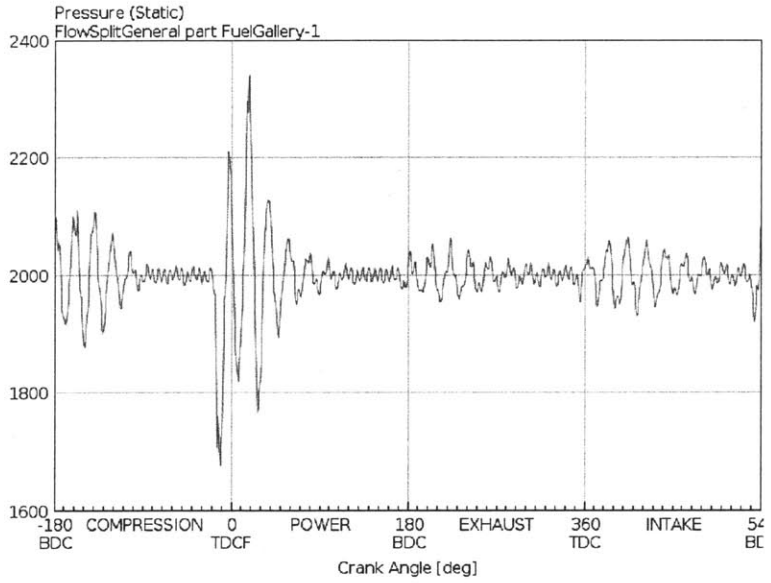

Figure 2-4: Injector gallery pressure in a cycle.

The fuel behavior at the last moment of the needle seating process can be divided into four sub-processes:

1. Because of the high velocity of the fluid in the nozzle, at some point in the seating process, the fuel feed from the sac through the limited gap between the needle and the orifice could not keep up with the motion of the nozzle fluid. The latter, because of inertia, does not slow down much. The fuel will cavitate at the end close to the needle seat.

2. While there is cavitation close to the needle seat, most of the nozzle fluid empties out of the nozzle due to inertia, leaving thin boundary layer fluid on the nozzle wall, see Fig. 2-6 (a).

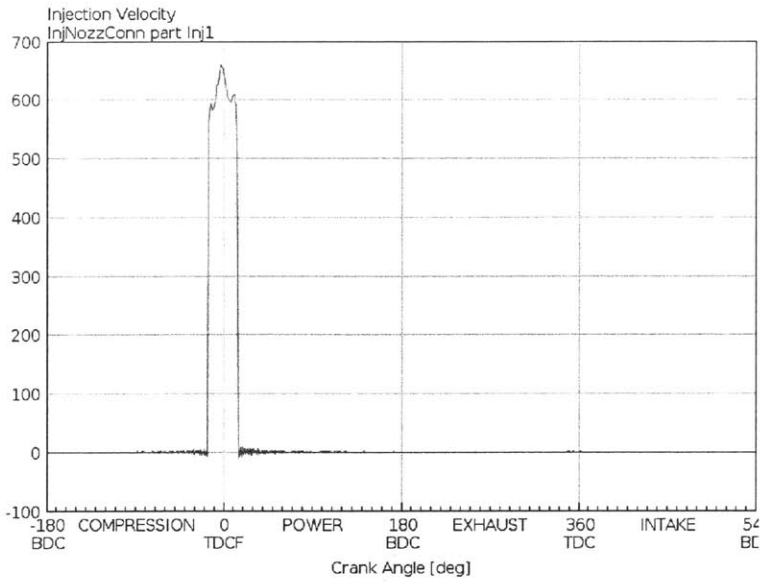

Figure 2-5: Injector nozzle velocity in a cycle.

3. Due to the events in combustion chamber, the nozzle passage is refilled by combustion gases.

4. Then in the last few microns of the needle lift, because of the significant fuel pressure, there would be still be a substantial amount of fuel leakage into the nozzle passage. This leakage would constitute the residual fuel in the nozzle after fuel injection, see Fig. 2-6 (b).

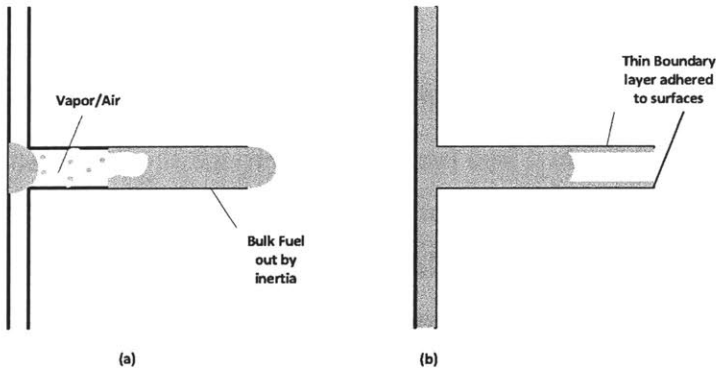

Figure 2-6: Schematics of residual fuel formation process in nozzle: (a) emptying of nozzle fluid by inertia; (b) residual fuel formed from leakage of fuel in the last few microns of needle lift.

To quantify the amount of residual fuel in the nozzle, a model of the flow in the needle seating process was used [78]. Fig. 2-4 shows the fuel gallery pressure approximately constant during a cycle, thus besides geometric details and fuel properties, the only dynamic parameter relevant to determining the flow inside the spray hole in the needle closing process is the needle seating velocity. The velocity is modeled using GT-Fuel and is shown in Fig. 2-7.

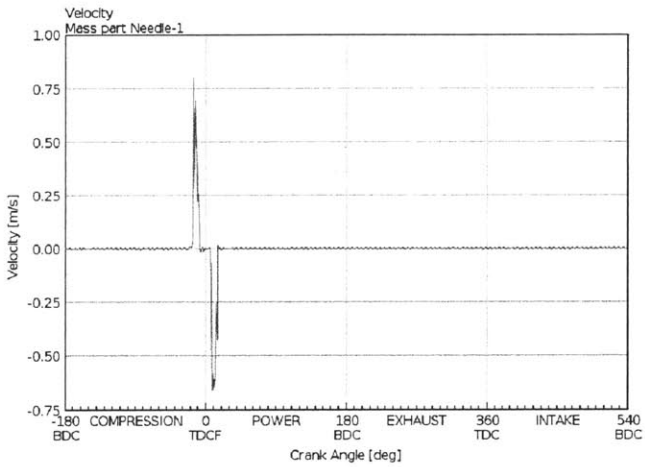

Figure 2-7: Injector needle seating velocity in a cycle.

Our focus is the final approach of the seating process. The gap size, h, is of the order of microns to tens of microns. It will be justified post-priori that the flow velocity in the gap is much larger than the seating velocity (which will be of the order of 1 m/s); thus the flow in the gap and nozzle may be considered as quasi-steady. Because of the conical geometry of the needle, the flow velocity U in the gap increases with x (see Fig. 2-8 for coordinate), and is given by:

$$U(x)d(x) = U_0 d_0 \tag{2.2}$$

where $d(x) = d_0 - x\sin(\theta)$. And subscript 0 denotes the quantities at x=0. The

pressure drop in the gap is obtained from U by integrating the pressure gradient:

$$\Delta p_g = \int_0^a \frac{1}{2}\rho U^2 f \frac{dx}{h} \tag{2.3}$$

where f is the friction factor. For turbulent flows, Moody chart or correlations need to be used and the expression for Δp has to be calculated numerically. For laminar flows, f=64/Re based on hydraulic diameter of the gap. We get

$$\Delta p_g = 32 \ln\left(\frac{d_0}{d_a}\right) \frac{\mu a U_0}{h^2} \tag{2.4}$$

In a same logic, the pressure drop in the nozzle hole is

$$\Delta p_n = \frac{1}{2}\rho V^2 f \frac{L}{\delta} \tag{2.5}$$

where V is the fluid velocity in the nozzle. V and U are related through continuity. For N spray holes, we have

$$VN\frac{\pi\delta^2}{4} = U_a \pi h d_a \tag{2.6}$$

The last equation we need is the injection pressure equity:

$$\Delta p = \Delta p_g + \Delta p_n \tag{2.7}$$

For laminar flows in both the gap and the nozzle, analytical solution may be obtained. For turbulent flow, the system of equations, which is implicit, since the friction factor f depends on velocity through the Reynolds number, has to be numerically solved. The solution from GT-Fuel is shown in Fig. 2-9. The fluid velocity U in the gap until the gap is almost closed (1 μm clearance) is of the order of tens of meters per second, which is large compared to the seating velocity. Thus the quasi-steady assumption is valid.

Note also that the solution, being quasi-static, is independent of the seating velocity. The only place that velocity is used is to translate the needle lift position into

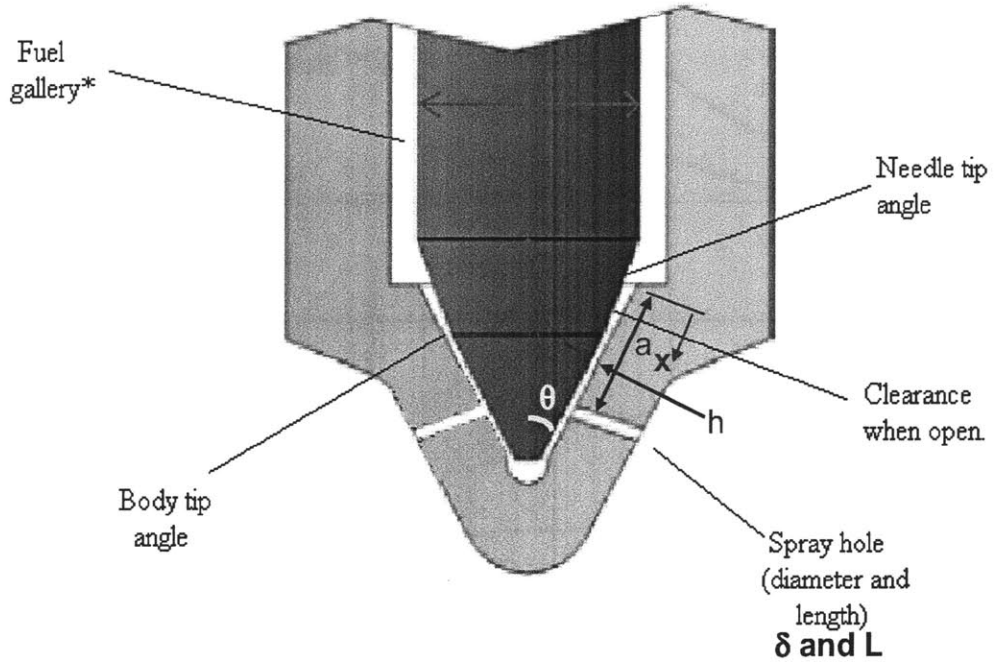

Figure 2-8: Injector needle and spray hole geometry for nozzle flow residual fuel modeling.

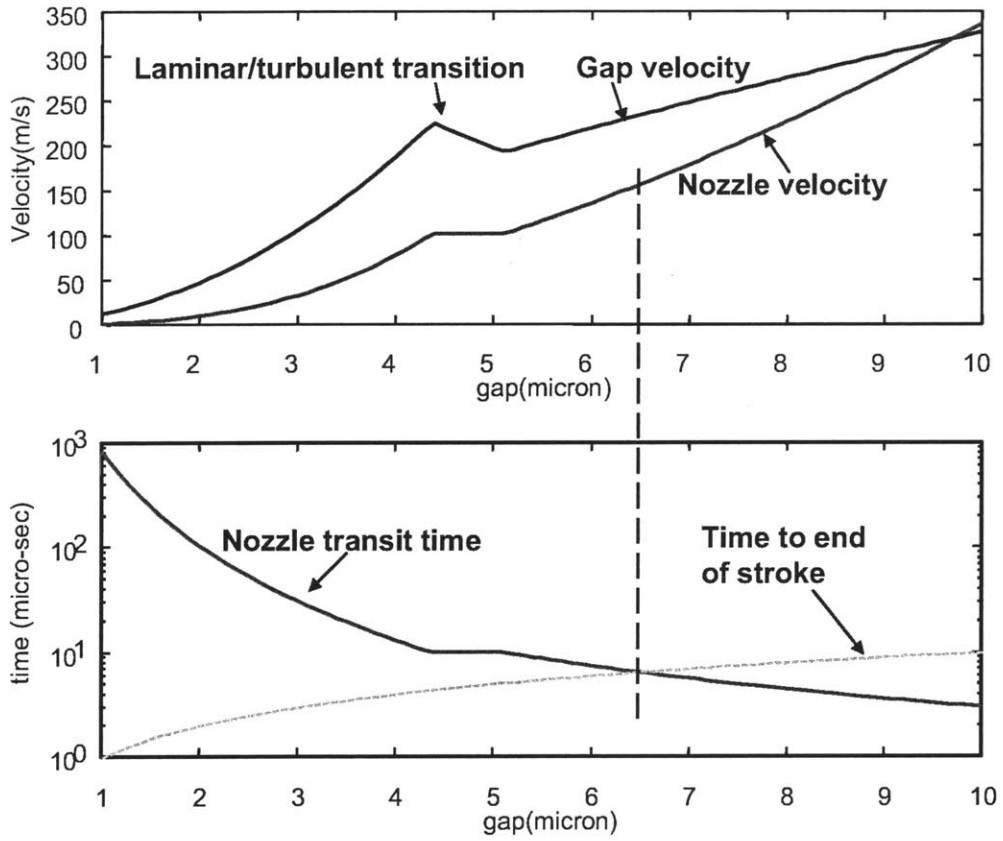

Figure 2-9: As function of the gap size between the needle and the injector wall: top - fluid velocity in gap and nozzle; bottom - transit time of fluid in nozzle and time to when the needle seats on the orifice. Needle closing velocity at 1 m/s. Nozzle passage length at 1 mm. Fuel pressure at 1500 bar.

the time-to-end-of stroke. A seating velocity of 1 m/s is used in Fig. 2-9. For other seating velocities, the result could be easily scaled.

The results in Fig. 2-9 may be interpreted as follows. As the injector needle closes (moving from right to left in Fig. 2-9), The fluid velocity in the nozzle decreases due to the frictional pressure drop of the clearance between the needle and the seat (the gap). However, the magnitude of the nozzle velocity is still substantial (more than 100m/s). The time for this fluid to clear the nozzle is shown as the nozzle transit time in the lower graph. If this time is faster than the time to end of stroke of the needle, the nozzle fluid could still clear the nozzle as a continuous stream. If not (at 6.5 μm gap in Fig. 2-9), however, cavitation would occur and the liquid column would break off. The leakage flow after this break off would constitute the residual fuel. Thus the amount of residual fuel is equal to the cumulative fuel that leaks through the orifice in the last few micron of the seating process. In this example, the fuel would fill 40% of the nozzle passageway as shown in Fig. 2-10.

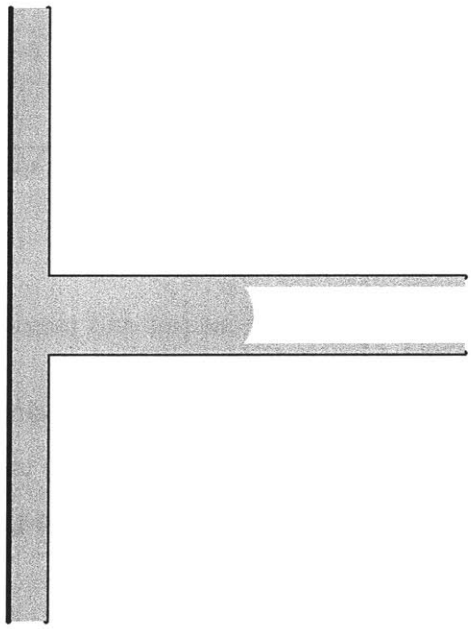

Figure 2-10: Final fuel distribution inside the nozzle: around 40% fuel column and the other 60% covered by thin fuel film.

2.3 Deposit Formation and Detergent Action

Now We have the information about the fluid distribution inside the nozzle (from the injector simulation, see 2-10) and the pressure inside the nozzle in one cycle (from the engine simulation, see top graph in Fig. 2-2). We still need the temperature evolution of the nozzle wall. To get the temperature, either measurement or CFD simulation have to be conducted. Here, we use the results from the literature. Tang et al. [73] measured the relationship between nozzle tip temperatures and engine power output, which is shown in Fig. 2-11. Leuthel et al. did a CFD simulation with their result

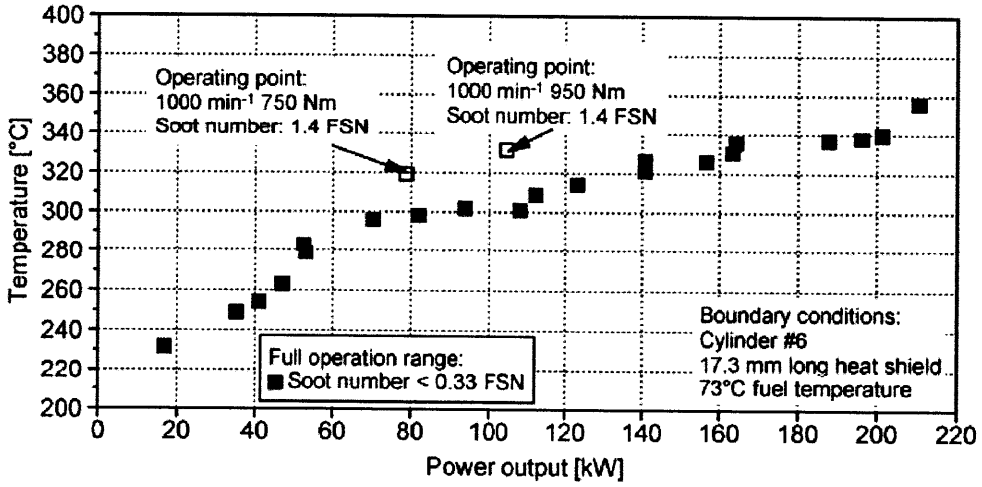

Figure 2-11: Correlation of engine power out put and nozzle tip temperature [73].

shown in Fig. 1-28. From the measurement as well the simulation, we can see the nozzle wall temperature is generally around 550 K (300 C) until the injection ejected, when the temperature drops to around 400 K (150 C). In the expansion stroke, the nozzle wall temperature recovers back to around 550 K.

With all these results, we are set to think about the deposit formation mechanism. For a typical four-stroke diesel engine, we have

1. Intake stroke. The pressure is approximately 1 bar, the nozzle wall temperature is high, oxygen gets diffused into the fuel film in the nozzle wall and chemical

species reacts with each other and form deposits.

2. Compression stroke. The pressure goes up, wall temperature is still high. But in the same time, high pressure limits evaporation (due to high partial pressure and lower diffusivity of the vapor). The diffusion coefficient is [29]:

$$D_{AB} \sim p^{-1} \tag{2.8}$$

   The compression process puts more oxygen into the nozzle hole and increases the oxygen concentration.

3. Expansion stroke. Towards the end of the compression stroke, we have fuel injection. With fuel velocity as high as 500 m/s, some deposit is washed away while some get sticked with the wall. In the same time, fresh diesel fuel film is formed on the nozzle wall. After the injection, the temperature of the nozzle wall decreases substantially which is due to the fuel cooling effect, and then recovers due to the heat transfer from the hot burned gas in the cylinder, see Fig. 1-28. The comparatively lower temperature of the stroke reduces the fuel film oxidation. The deposit formation process is not as significant as in the other periods of the cycle.

4. Exhaust stroke. We have the same case as intake stroke, i.e., high temperature and low pressure, although the oxygen concentration is lower.

We argue that the deposit formation mainly occurs inside the liquid film close to the chamber instead of the residual fuel column. The argument is based on the following points:

- Since the inner part of the nozzle was covered by the liquid column, the deposit precursors there are washed out by the next injection. Hence small deposit accumulation.

- The oxygen readily diffuses into the thin film, while less oxygen could diffuse across the fuel column.

- The temperature of the metal is higher towards the combustion chamber (the thermal skin depth in the metal is of the order of 500 m.) Hence accelerating the deposit formation.

In summary, although the pressure and temperature in the nozzle are changing all the time, the heavy deposit is accumulated mainly in intake and exhaust stroke and we will make the following assumptions for our model development:

- The pressure in the nozzle is constant atmospheric pressure.
- The temperature of the nozzle wall is constant at 573.15 K(300 C).

Then the deposit formation process can be shown in Fig. 2-12 [68]. The deposit formation starts with fresh diesel film (on the left of figure), the species inside the film reacts with oxygen and the diesel is partially oxidized (on the top of figure), then due to the polar nature, some reaction products are separated from the diesel solvent and the insoluble oxygenates accumulate on the wall (on the right of figure). The next injection comes in, some deposit pre-cursors are washed away and we have a mixture of fresh and partially washed diesel and the cycle repeats. Across cycles, the oxygenates may go through secondary oxidization and react with the metal wall. But those secondary reaction mechanisms are not discussed in this paper.

2.4 Diesel Surrogate

Real diesel fuel is complex and it comprises hundreds of compounds with a substantial range of physical and chemical properties. To develop our physics and chemistry models, we need to somehow represent the fuel by a surrogate consisting of a few compounds to reduce the fuel properties to a manageable set of chemical and physical properties. In choosing the components for the fuel surrogate, we have limited the classes of organic compounds to normal and iso-paraffins, and aromatics. The number of C atoms in each would be chosen to match roughly the distillation curve of the real fuel. In addition, the surrogate components have to be readily available in the

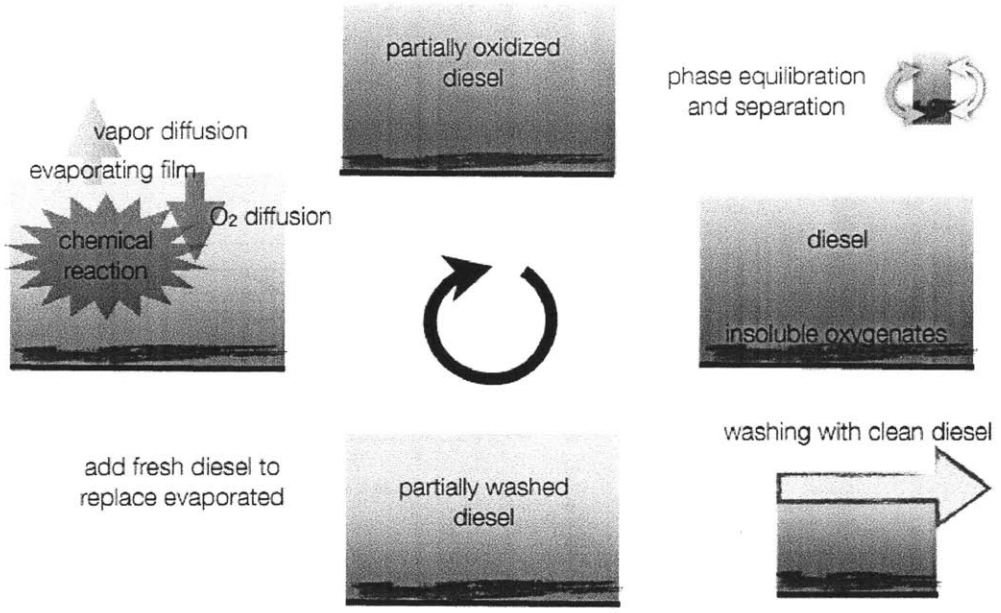

Figure 2-12: Diesel injector nozzle deposit formation illustration.

market so that they could be used in the laboratory experiment for deposit formation rate measurements.

There are currently significant activities in selecting diesel fuel surrogate components and the tabulation of the chemistry and physical properties of these components by an ad-hoc Diesel Fuel Surrogate Working Group[39]. Here, we used a surrogate development method proposed by Cheng et al. [78].

The Normal Boiling Point (NBP) of hydrocarbons is approximately only a function of the number of C atoms in the molecule (see Fig. 2-13). Thus the C numbers are used to match up the distillation curves for the diesel fuel. The first step is to use a collection of n-alkanes to produce the distillation curve as shown in Fig. 2-14, in which the NBP for alkanes with C10 to C22 are shown on the left, and then the NBP for the selected components are shown on the right. The quantity of each component corresponds to the amount distilled at the individual NBP values.

The next step was to add the aromatics. A 1-ring compound, decylbenzene with NBP at 300 C and a 2-ring compound, 1-methyl naphthalene (C11H10), with NBP

Normal boiling points		
Compound	**C**	**NBP(C)**
Normal Paraffins		
nC5	5	36.1
nC6	6	68.7
nC7	7	98.4
nC8	8	125.7
nC10	10	174
nC12	12	216.3
nC16	16	286
nC18	18	316
nC20	20	344
Iso Paraffins		
223 TMB	7	89
224 TMP	8	99
Olefins		
1-pentene	5	30
1-heptene	7	93
Aromatics		
Benzene	6	80
toluene	7	110
Ethyl Benzene	8	136
Meta Xylene	8	139
n-propyl Benzene	9	159
iso-propyl Benzene (cumene)	9	152

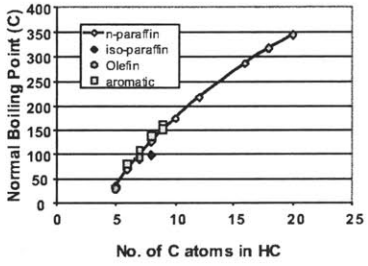

Figure 2-13: Relationship of NBP and number of carbon atoms in the hydrocarbons.

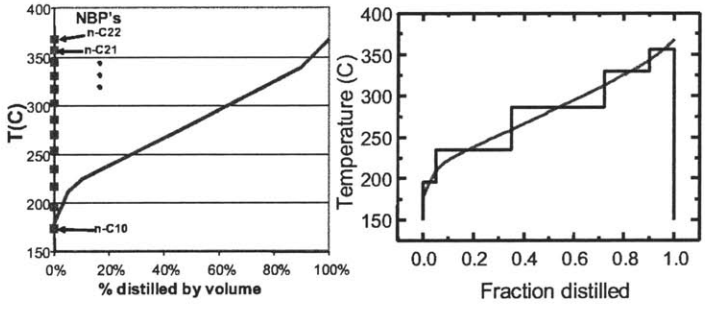

Figure 2-14: Selection of n-alkanes to represent the distillation curve.

at 241 C were added. Both compounds were readily available in the market, and they were recommended species as surrogate components by the Diesel Fuel Surrogate Working Group. The total aromatics to saturates ratio was adjusted to be 77:23, same as the value in the properties of diesel fuel (see Appendix B). The ratio of decylbenzene to 1-methyl naphthalene was adjusted , the value for the 1-ring to 2-ring aromatics ratio in the diesel fuel. The final composition for the diesel fuel surrogate and the corresponding distillation curve are shown in Fig. 2-15.

nbp (deg C)	fraction by volume	cum % in surrogate	name	cas number	C	H	Type
195.6	5.00%	5.00%	n-undecane	1120-21-4	11	24	n-paraffin
235.0	19.00%	24.00%	n-tridecane	1029-50-5	13	28	n-paraffin
241.0	11.00%	35.00%	1M-naphthalene	90-12-0	11	10	2-ring aromatics
286.0	25.00%	60.00%	n-hexadecane	544-76-3	16	34	n-paraffin
300.0	12.00%	72.00%	n-Decyl Benzene	104-72-3	16	26	1-ring aromatics
329.5	18.00%	90.00%	n-nonadecane	629-92-5	19	40	n-paraffin
356.3	10.00%	100.00%	n-heneicosane	629-94-7%	21	44	n-paraffin

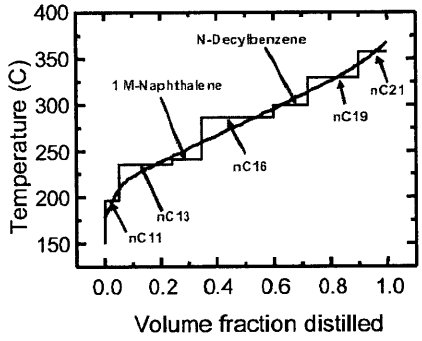

Figure 2-15: Fuel surrogate components and corresponding distillation curve.

Chapter 3

Deposit Formation Physics

From the mechanisms discussed in last chapter, four essential physical processes have to be modeled: film formation, evaporation, oxygen diffusion and washing.

3.1 Estimation of residual film thickness

Fluid coating, which is the operation of forcing a fluid to coat a solid by a movement, has been studied since Landau [49]. They are very important in the Fibre industry. Quere et al. [62] reviewed the latest research of fluid fibre or wire coating, and Aussillous [11] further studied the deposition of fluid on a wall of a tube. Here we will extend their results to the liquid thin film formation in injector nozzles as well as in vertical tubes.

Imagine the needle in the injector is closed, the last fuel column is pushed out by inertia and vapor is behind the fuel column (see Fig. 3-1). The problem is the knowledge of the amount of liquid remaining on the wall. In this thesis, we will not employ computational fluid dynamics to solve for the thickness h, instead, scale analysis is used to develop a model and then experimental data are calibrated with the model.

For Newtonian fluid, depending on the velocity of the liquid and the relative magnitudes of surface tension, viscous force and inertia force, three regimes could happen with the film formation: visco-capillary deposition, visco-inertia deposition

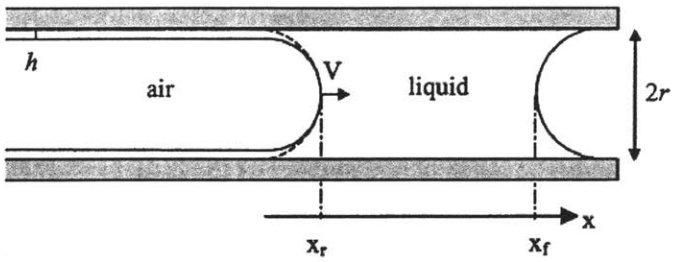

Figure 3-1: A drop of a wetting liquid moved in capillary nozzle leaves behind a thin film. The thickness h of this film generally depends on the fluid velocity V. x_f and x_r are the time-dependent front and rear positions of the last fluid droplet and the nozzle radius is noted r. [11]

and viscous boundary layer deposition.

3.1.1 visco-capillary deposition

When the fluid velocity is not large, the deposition of a film is due to the viscosity η and the boundary condition at the solid-liquid interface. The static meniscus at the liquid-air interface (dotted line in Fig. 3-1), which is hemispherical for small tubes, is deformed by the fluid motion. A non-dimensional number called capillary number could be used here as the ratio of the viscous and capillary forces:

$$Ca = \frac{\eta V}{\gamma} \tag{3.1}$$

where γ is the surface tension. The visco-capillary regime is where the film thickness only depends on capillary number Ca. The regime is what Taylor studied back in 1961 [74].

For thin films, the film forms in the dynamic meniscus of thickness of order h and length λ. By balancing the viscous force with the pressure force across the dynamic

meniscus, we have

$$\eta \frac{\partial^2 V}{\partial y^2} \sim \frac{\partial P}{\partial x}$$
$$\frac{\eta V}{h^2} \sim \frac{\gamma}{\lambda r} \tag{3.2}$$

To derive the second equation, the pressure is given by the Young-Laplace equation. Now we still need to know λ. It is calculated by matching the static and the dynamic meniscus: one caused by the curvature of the nozzle (tube) and one relative to the second derivative (curvature) of the profile. The balance of the Laplace pressures could be written as :

$$\frac{\gamma}{r} \sim \frac{\gamma h}{\lambda^2} \tag{3.3}$$

Thus we have $\lambda \sim \sqrt{hr}$, from which the classical Bretherton law can be deduced [17]:

$$\frac{h}{r} \sim Ca^{2/3} \tag{3.4}$$

As Ca increases, r need to be replaced by (r-h) in Equations 3.2 and 3.3, so that the thickness scaling law becomes:

$$\frac{h}{r} \sim \frac{Ca^{2/3}}{1 + Ca^{2/3}} \tag{3.5}$$

Both results agree with the experimental data obtained by Taylor [74] with different viscous oils. A fit of form (3.5) can found as:

$$\frac{h}{r} = 1.34 \frac{Ca^{2/3}}{1 + 1.34 \times 2.5 Ca^{2/3}} \tag{3.6}$$

3.1.2 Visco-inertial regime

When the fluid flows at high speed, the film becomes thicker and the Taylor's law is not valid when Ca is larger than a critical number Ca^*. The effect could be understood by modifying the scaling law (3.2,3.3) to include inertia. We have the

scaling navier-stokes equation:

$$\frac{\eta V}{h^2} \sim \frac{\gamma}{\lambda(r-h)} - \frac{1}{\lambda}\rho V^2 \tag{3.7}$$

where ρ is the fluid density. Similarly, we can derive the equation for λ:

$$-\frac{\gamma}{r-h} + \rho V^2 \sim -\frac{\gamma h}{\lambda^2} \tag{3.8}$$

Combining the two equation, we have a scaling law:

$$\frac{h}{r} \sim \frac{Ca^{2/3}}{1 + Ca^{2/3} - We} \tag{3.9}$$

where the We is a non-dimensional number comparing the inertia with capillary force:

$$We = \frac{\rho V^2 (r-h)}{\gamma} \tag{3.10}$$

It is also observed by Aussillous that the nozzle or tube radius has an effect on the critical Ca number: the larger the tube, the smaller the critical Ca number and the higher the deviation toward Taylor's law. For a radius of 0.78 mm, the critical Ca is around 0.02. Also notice that in Equation 3.9, if We is very large, the h will go negative which is not valid anymore, that's for our last regime.

3.1.3 Viscous boundary layer regime

The previous two regimes implicitly suppose that the viscous boundary layer is well developed in the dynamic meniscus. However, for very high fluid velocity, this assumption is not necessarily satisfied. With high fluid velocity, the thickness of the deposited film can be limited by the viscous boundary layer and its thickness d is simply given by balancing inertia and viscosity, which yields the classical Prandtl law:

$$\delta \sim \left(\frac{\eta L}{\rho V}\right) \tag{3.11}$$

Injection pressure	Nozzle length	Diameter	density	viscosity
2000 bar	700 μm	140μm	820 kg/m^3	3.5mm^2/s

Table 3.1: Values for film thickness estimation

And correspondingly, for turbulent flow, we have

$$\delta \sim \frac{0.16}{(Re_x)^{1/7}} x \tag{3.12}$$

$$Re_x = \frac{\rho V x}{\eta} \tag{3.13}$$

3.1.4 Film thickness Calculation

In diesel fuel injectors, the flow velocity could be as high as 600 m/s (see Fig. 2-5). Hence it would be in the viscous boundary layer regime. To estimate the boundary layer thickness, the following values were used.

Thus at the end of the nozzle (x=L), the boundary layer thickness is around 16 μm. The residual fuel film thickness maybe estimated as half of the boundary layer thickness i.e., a coefficient of 0.5 in Equation 3.12. Hence h(L) = 10 μm. Since the boundary layer thickness scales approximately linearly in x, and the final residual film occupies half of the nozzle, a reasonable estimate of the average film thickness is $h = (5 + 10)/2 \approx 7\mu m$.

During the combustion, the residual fuel film is exposed to the shock wave and the subsequent reflected shock. However, the shocks pass quickly ($\Delta t = L/u_{shock} \sim 1\mu s$, the inertia of the liquid would keep the film static. For a 700 μm length layer run over by the entering shock wave with a pressure difference of 50 bar across the wave, the induced velocity is (from mass conservation)

$$\Delta V = \frac{\Delta p \Delta t}{\rho L} \sim 9.0 m/s \tag{3.14}$$

Assume the velocity is persistent, the fluid would have moved a distance of around 5 μm which is about 1/10 of the nozzle length. However, the reflected shock quickly negated the induced velocity. The back-forth gas dynamics may take several cycles

Pressure drop	Length	Diameter	density	viscosity
51.3 KPa	76.2 mm	1.08 mm	800 kg/m^3	$3.5mm^2/s$

Table 3.2: Values for tube film thickness estimation

Pressure (KPa)	Mass of Film (mg)	Thickness(μm)
18.2	3.49	16.5
34.7	2.73	12.9
51.3	2.26	10.7

Table 3.3: Tube Film Thickness Measurement

(a few μs) to settle, but the net effect would be the film stays put with the thickness unaffected. In summary, during time between injection (tens of milliseconds), the residual fuel on the nozzle wall is essentially a stationary film of liquid with a thickness approximately equal to 6 μm under conditions of Table 3.1.

To model our bench scale apparatus (to be discussed in Chapter 6), we also want to calculate the film thickness of a vertical tube after fuel blows through. In laminar pipe flows, we have

$$\Delta p = \left(\frac{64}{Re} \frac{L}{D} + K \right) \frac{1}{2} \rho V^2 \tag{3.15}$$

Where K is the minor losses (K=2 is used in our case). The parameters for the tube in our experimental settings are shown in Table 3.2.

For a driven pressure difference of 51.3 KPa (7.44 psi), the average velocity in pipe is around 5 m/s and the Reynolds number is around 1600. The We number in this case is 456. Hence we are in the viscous boundary layer regime again. Unlike engine nozzle case, here we can measure the film thickness by assuming a uniform thickness distribution and weighing the tube before and after one injection. Three pressures are used and the resulting tube mass increments are shown in Table 3.3. We can see that the film thickness decreases with higher pressure and high velocity, which also excludes the other two regimes. The experimental data are plotted against the results from Equation 3.11 as shown in Fig. 3-2. The scaling law from model seems matching the experimental data very well.

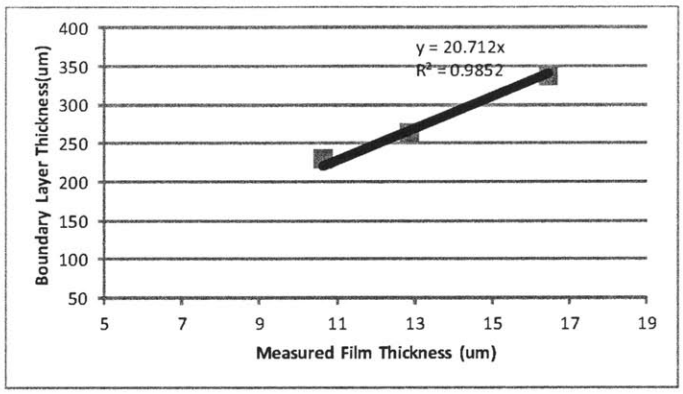

Figure 3-2: Comparison of measured film thickness verus modeling results in the tube.

3.2 Evaporation Modeling

After obtaining the film thickness, we can start on the evaporation modeling. In this section, the evaporation of the thin fuel film is simulated via a 1D model first with some assumptions and then a 2D model simulaiton is conducted to validate the assumptions.

3.2.1 Lumped liquid film Evaporation model

Before the modeling, let's look at the diffusion scale in the liquid, assume the film thickness is 5 um and the diffusivity is $5 \times 10^{-8} m^2/s$:

$$t = \frac{L^2}{4D} = \frac{25 \times 10^{-12}}{20 \times 10^{-8}} = 0.12ms$$

which is comparable to the radial vapor diffusion, but far smaller than the diffusion in the axial direction. So we neglect the diffusion in the liquid film and the concentrations are uniform.

Consider the liquid film as a control volume as shown in Fig. 3-3, if we assume the liquid film has uniform thickness in the axial direction, we can write the thickness

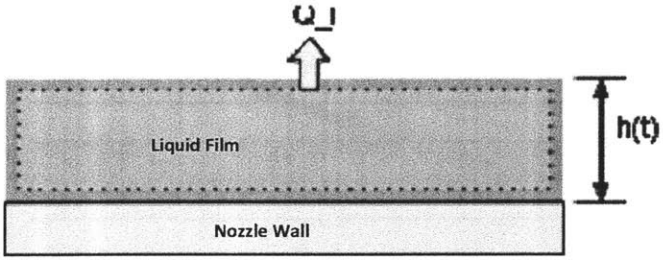

Figure 3-3: Lumped Liquid film diagram.

profile as $h(t)$ and we have mass conservation for each component:

$$\frac{\partial \rho_{l,i}}{\partial t} = -\frac{A_l}{V_l}\left(Q_{v,i} + \rho_{l,i}\frac{dh}{dt}\right) \tag{3.16}$$

where $\rho_{l,i}$ is the partial mass density of component i and $Q_{v,i}$ is the evaporation flux of component i to the vapor. A and V are the surface area and volume respectively.

For the liquid film as a whole, we also have mass conservation:

$$A_l \sum_i Q_{v,i} + A_l \rho_l \frac{dh}{dt} + \frac{d\rho_l}{dt} V_l = 0 \tag{3.17}$$

where the ρ_l is the total mass density of fuel. If dissolve effect is negligible, we can say the total density of fuel does not change with time. So the above equation can be simplified:

$$\frac{dh}{dt} = -\frac{1}{\rho_l}\sum_i Q_{v,i} \tag{3.18}$$

Since the fuel vapor concentrations in the combustion chamber are much more dilute than those in the nozzle, the evaporation process is assumed to be limited by the diffusion of the vapor from the nozzle exit to the chamber as shown in Fig. 3-4. Also the fuel film area is assumed to be large compared to the end-face area of the leaked fuel column. The diffusion out of the nozzle is approximated by a diffusion flux in a hemisphere of the nozzle diameter. Then the boundary condition at the film

surface for the 1D film evaporation becomes:

$$Q_{v,i} = \left[D_{v,i} \frac{\rho_{s,i}}{d} \frac{\pi d^2}{4} \right] \frac{1}{\pi d L_f} = \frac{1}{4 L_f} D_{v,i} \rho_{s,i} \tag{3.19}$$

where d is the nozzle diameter, L_f is the axial length of the film and $\rho_{s,i}$ is the vapor density of component i at the film surface. The final equation needed to complete the set is the Roult's law which is used to determine the surface vapor concentration of an ideal liquid.

$$\begin{aligned} p_{v,i} &= p_{sat,i}(T) y_i \\ \rho_{s,i} &= \frac{p_{sat,i}}{RT} y_i \end{aligned} \tag{3.20}$$

where $p_{sat,i}$ is the saturation vapor pressure at temperature T for component i and y_i is the mole fraction of species i in the liquid phase. If necessary, this implementation will be improved by considering the fugacity of the species. Now we can we can solve the ODEs for the liquid film thickness h.

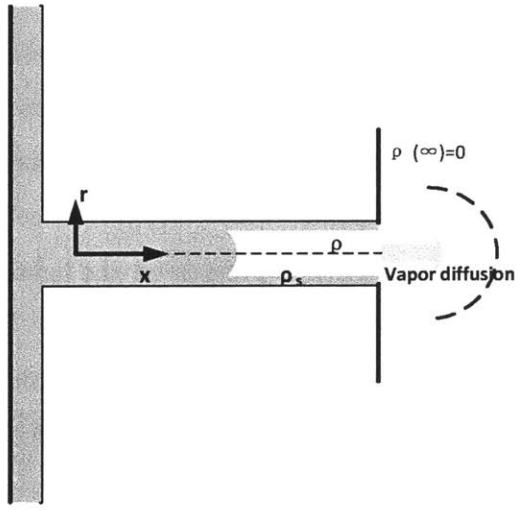

Figure 3-4: Fuel vapor diffusion from the nozzle passage to the combustion chamber.

The time for drying the nozzle fuel film (complete evaporation) as a function of wall temperature and initial film thickness using the fuel surrogates and the chemistry

model as described in Chapter 4 is shown in Fig. 3-5. Also marked on the figure are the time between injection at 1000 and 3000 rpm. Thus for a film of 5 μm initial thickness or more, there are residual liquid when the next injection comes along.

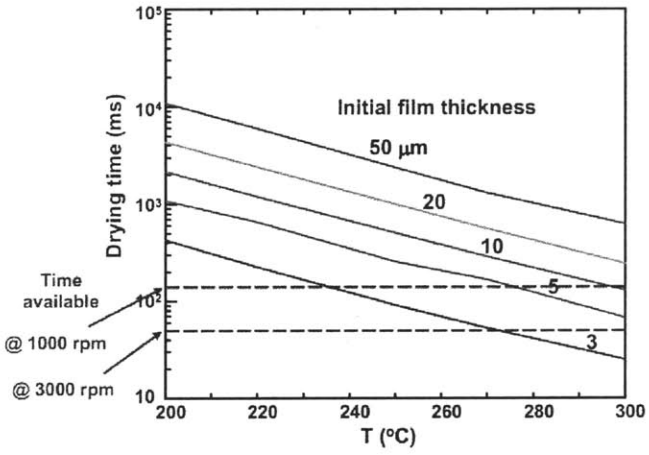

Figure 3-5: Time for complete evaporation of the fuel film as a function of wall temperature and initial film thickness. The time between injection at 1000 and 3000 rpm are also shown.

For a 5 μm film at 250 C, the concentrations of the 7 fuel surrogate species for the diesel fuel as a function of the film thickness as the film evaporates are shown in Fig. 3-6. It should be noted that the mass diffusion time for a 5μm layer is very fast (0.36 ms) compared to the evaporation time. Therefore, the concentrations are essentially uniform across the layer. As evaporation progresses, the lighter components diminish and the heavier components are made more concentrate. The amount of deposit concentration is very small until the layer is 30% of its initial thickness. The film thickness at elapsed time of 40 ms is also marked on the plot.

3.2.2 Two-dimensional Evaporation Model

To evaluate the effect of the finite domain on the axial distribution of evaporation characteristics along the nozzle, a 2D evaporation model has been formulated and solved numerically. The diffusion equation in cylindrical coordinates is shown in

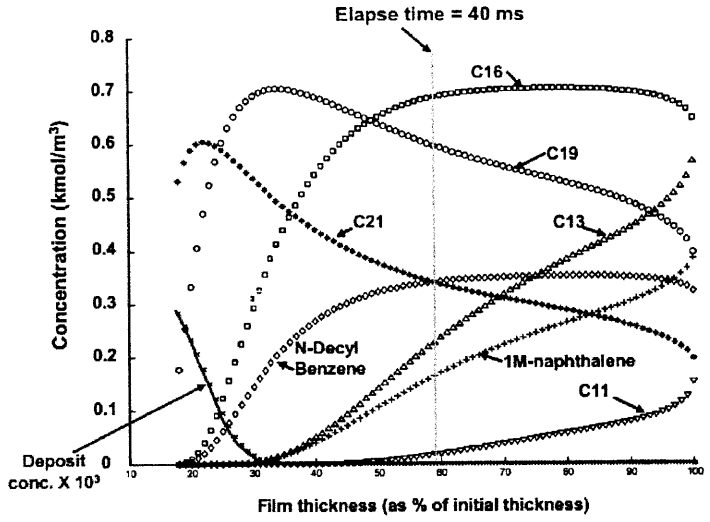

Figure 3-6: Concentrations of the 7 fuel surrogate species as a function of film thickness. Initial film was 5 μm thick; temperature at 250 C.

Equation 3.21 and the numerical grid set up is shown in Fig. 3-7. The domain of computation comprises the fuel nozzle of diameter d and length L, and the combustion chamber region at the nozzle exit in an axis-symmetric geometry. The domain in the combustion chamber is a cylindrical region of radius 10d and length 10d so that the boundary condition far away from the nozzle has approximately zero fuel concentration. The nozzle radial wall is covered with a fuel film of initial thickness h_0, and the nozzle end (away from the combustion chamber) is assumed to be the surface of the residual fuel column. The 7-component surrogate fuel described in section 2.4 was used. The temperature of the fuel is assumed to be constant and equal to the wall temperature, since the thermal diffusion time through the film thickness and in the fuel column are fast compared to the cycle time. In the trial calculation, the numerical values are L = 500 um; d = 140 um; h_0 = 3 um, and nozzle wall temperature

is 250 C.

$$\frac{\partial \rho_{v,i}}{\partial t} = D_{v,i}\nabla^2 \rho_{v,i}$$
$$\frac{\partial \rho_{v,i}}{\partial t} = \frac{1}{r}\frac{\partial}{\partial r}\left(r\frac{\partial \rho_{v,i}}{\partial r}\right) + r^2\frac{\partial^2 \rho_{v,i}}{\partial \theta^2} + \frac{\partial^2 \rho_{v,i}}{\partial z^2} \tag{3.21}$$

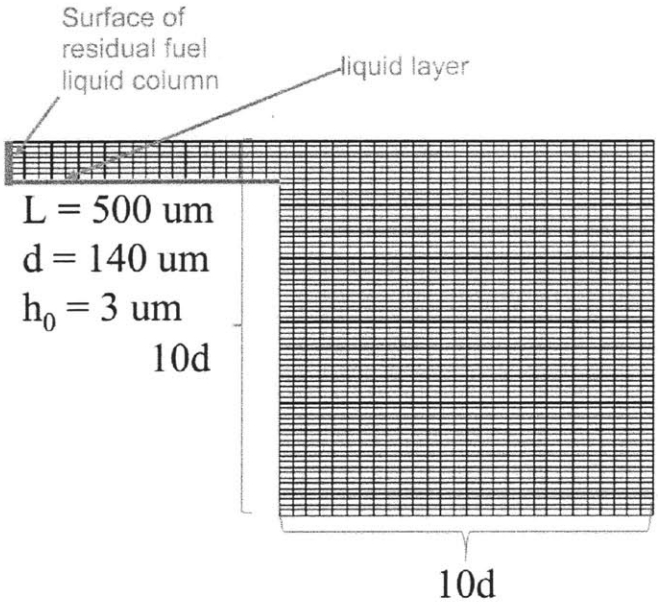

Figure 3-7: Computation domain for 2D evaporation model.

Initial and Boundary Conditions

If we choose a initial condition as zero vapor concentration inside and outside the nozzle, the discontinuity of variable need a very small time step and may cause unstableness.

Hence when $t = 0$, we give the nozzle saturated vapor densities and give the combustion chamber a gradually changing initial condition to smooth out the jumps. Thus if z_0 is the position of the nozzle exit, and r_0(=d/2) the nozzle radius, the initial

vapor concentration n_i for each species :

$$
\begin{aligned}
n(r, z, t = 0) &= f(z)M(z_0, r) \\
f(z) &= \begin{cases} \dfrac{1 + \cos\left(\frac{\pi(z - z_0)}{r_0}\right)}{2} & z_0 < z < z_0 + r_0 \\ 0 & z > z_0 + r_0 \end{cases} \\
M(z_0, r) &= \begin{cases} M_S & 0 < r < r_0 \\ \dfrac{M_S\left[1 - \cos\left(\frac{\pi r}{r_0}\right)\right]}{2} & r_0 < r < 2r_0 \\ 0 & r > 2r_0 \end{cases}
\end{aligned}
\tag{3.22}
$$

where M_S is the saturated vapor partial density, z_0 is the start z coordinate of combustion chamber and r_0 is the radius of the nozzle.

The boundary conditions are as following: at the film surface, vapor density values are given by Roult's law according to the fuel temperature and fuel composition; far from the nozzle exit in the combustion chamber, the vapor density is zero; on external surfaces of chamber, the gradient of vapor density is zero. The initial and boundary conditions are shown in Fig. 3-8.

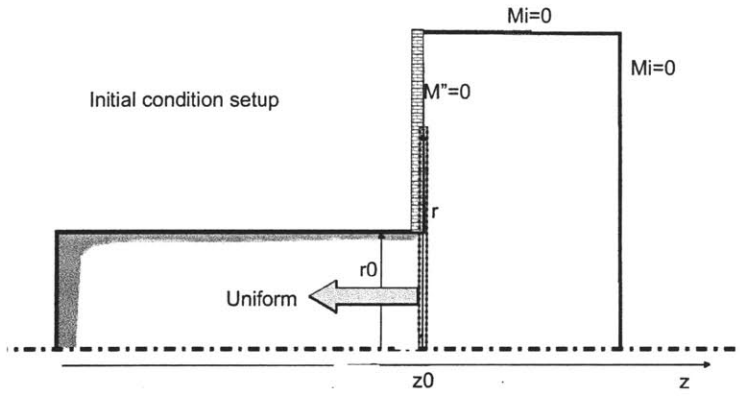

Figure 3-8: Initial and Boundary conditions for the 2D evaporation model.

Thickness Profile

The fuel film thickness as a function of time and distance from nozzle exit is shown in Fig. 3-9. The profile of the film thickness as a function of time is again shown in Fig. 3-10 to illustrate the progressive drying out of the film at the vicinity of the nozzle exit. The thickness of the fuel film as a function of time at different axial locations is shown in Fig. 3-11.

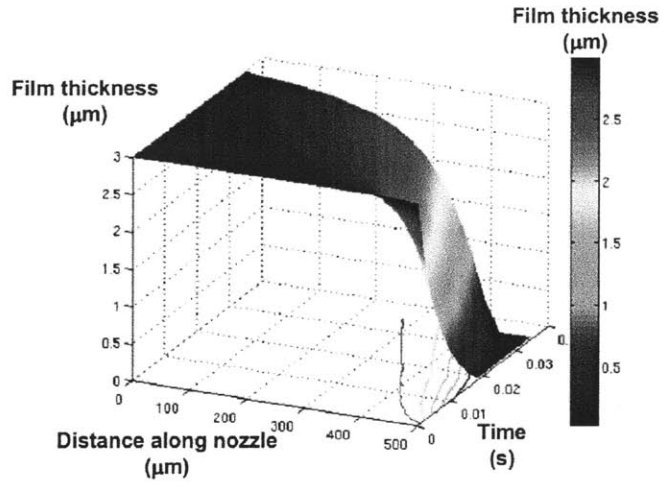

Figure 3-9: Fuel film thickness inside nozzle as a function of time. Initial thickness is 3 um; temperature is 250 C.

The drying out of the fuel film at the nozzle exit described in the above is the most important result of the 2D simulation. The process implies that there is a substantial change in the concentrations of the various species within the film in this region. Since radial diffusion in the film is fast (diffusion time of the order of 0.1 ms), the species concentration is uniform across the film. However, because the light components evaporate much faster than the heavy ones, the concentrations of the heavy components will be much higher. Also oxygen is more available to this region. These factors enhance deposit production in the nozzle exit region.

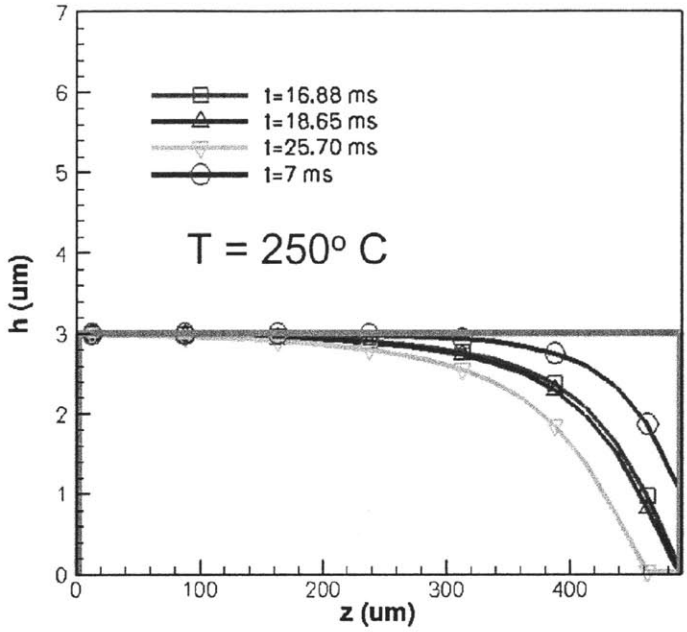

Figure 3-10: Film thickness profile as a function of time. Note that when the film dries out, the boundary condition is replaced by that of a solid wall.

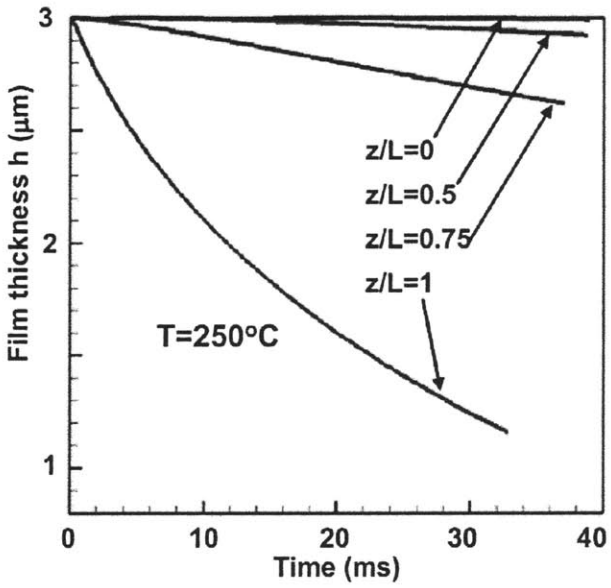

Figure 3-11: Film thickness as a function of time at various locations along nozzle.

Limited diffusion approximation

To studied the validity of the limited diffusion approximation used in the lumped liquid model, vapor diffusion profile at a time snapshot (t=16.88 ms)along the z and r axis is shown in Fig. 3-12. We can see that the vapor densities gradually reduced to zero in the combustion chamber and our assumption of uniform vapor density across the radial axis employed in the lumped liquid model is actually accurate.

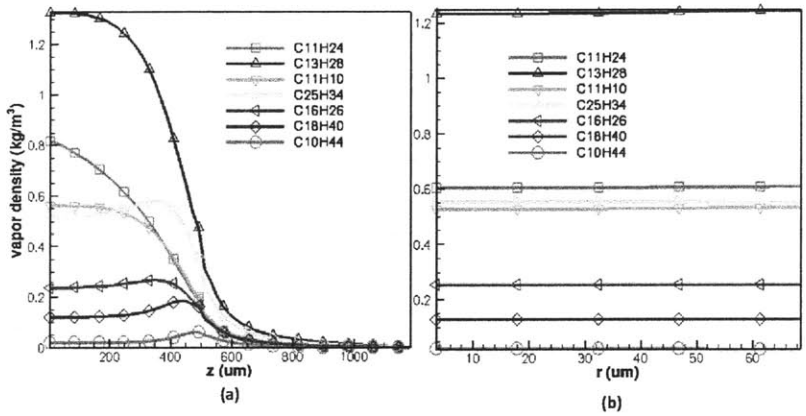

Figure 3-12: Vapor densities profile of diesel surrogate components at t=16.88 ms: (a) along axial direction; (b) along radial direction at z/L=0.5.

Then we calculated the vapor flux out of the nozzle and compared it with the limited diffusion approximation we used in the lumped liquid model. The result is shown in Fig. 3-13. We can see that the approximation is fairly accurate, except some small discrepancies for the very light components.

Effect of residule fuel column

In the lumped liquid model, we did not make adjustments for the leaked fuel column. To see the effect of the fuel column, simulation with the column and without the column were conducted and the results are shown in Fig. 3-14. As you can see, one can hardly distinguish the two set of lines and the approximation is quite accurate and the diffusion of the inner column is very slow.

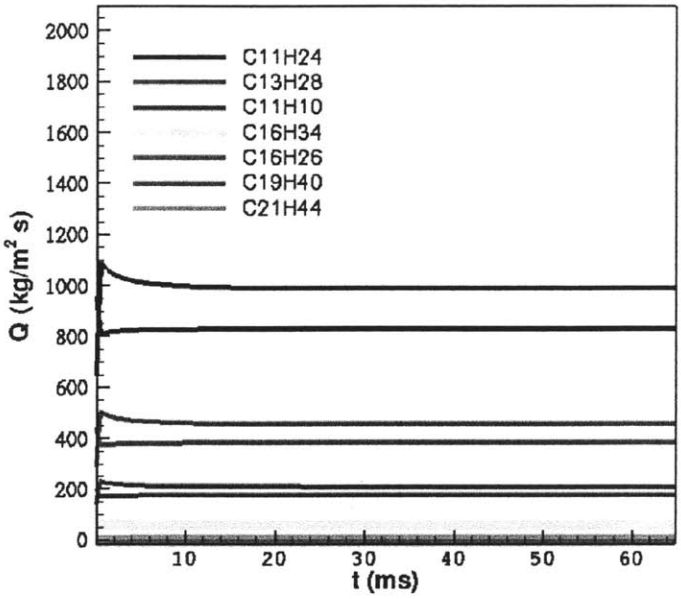

Figure 3-13: Comparison of vapor flux out of nozzle exit.

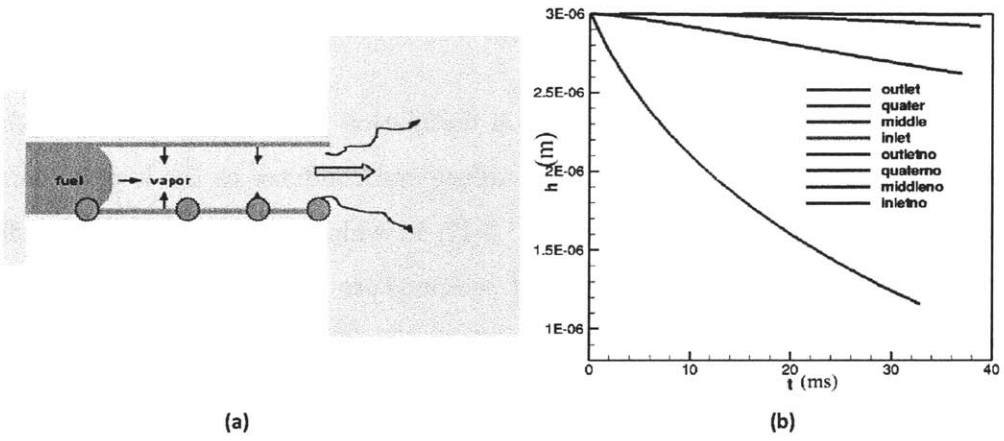

Figure 3-14: Study of the effect of fuel column: (a) Four locations of the readings; (b) Thickness evolution with time at various locations. The red lines which include the liquid column was covered by blue lines and could not be seen.

Non-uniform temperature distribution

To assess the effect of a non-uniform temperature distribution along the nozzle, calculation has been done with a linear temperature profile which rises from 200 C to 300 C towards the nozzle exit as shown in Fig. 3-15. The dry times under constant temperature and linear temperature distribution are shown in Fig. 3-16. Under 2D model, the dry time is not constant anymore and layers of deposit are expected in the nozzle wall.

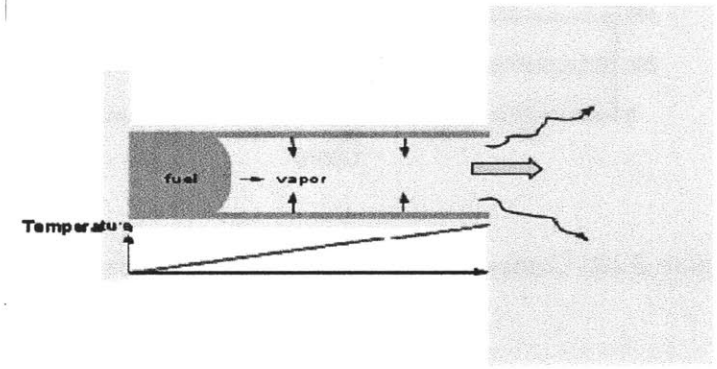

Figure 3-15: Non-uniform temperature distribution file used in the simulation.

The temperature gradient produces a distillation process - that the evaporated fuel at the high temperature end could diffuse and condense at the low temperature end. This process is illustrated in Fig. 3-17, in which the film thickness profile at elapsed time of 3.6 ms for the constant temperature case at 200 C is compared to that for the case with the linear temperature distribution. For the latter, the film thickness at the cold end of the nozzle is larger than the initial thickness of 3 um. The film thickness as a function of time at various axial locations for the linear axial temperature profile is shown in Fig. 3-18. The mechanism for the condensation could be seen more clearly from Fig. 3-19 where the vapor density contour is plotted. We can see with a non-uniform temperature distribution, the high vapor density close to the nozzle exit induces diffusion not only to the combustion chamber, but also to the

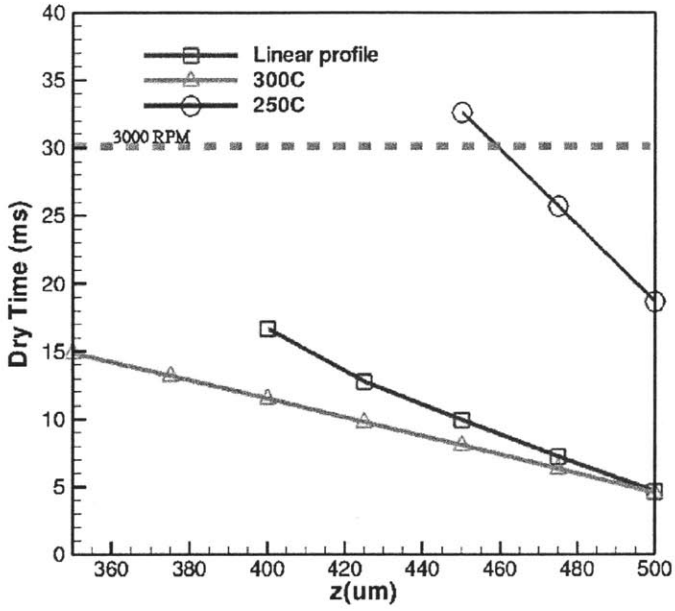

Figure 3-16: Dry time comparison for different temperature distributions.

liquid fuel column. The cold temperature close the needle end further increases the condensation.

3.3 Oxygen solubility and diffusion

Oxygen plays a major role in the oxidation of the species in the fuel film to form deposit precursors, and in the secondary oxidation of the deposit that is already formed on the nozzle wall. The oxygen from the combustion chamber has to diffuse through the gas phase components in the nozzle hole to reach the fuel film. Thus the fuel film in the vicinity of the nozzle exit has a higher exposure to oxygen than that in the region upstream of the exit.

The oxygen concentration diffusion problem is governed by the same set of equations which governs the fuel species diffusion in the configuration as shown in Equation 3.21. The concentration far away from the nozzle exit is assumed to be that of air. At the film surface, oxygen flux into the liquid is equal to the local integrated (over film

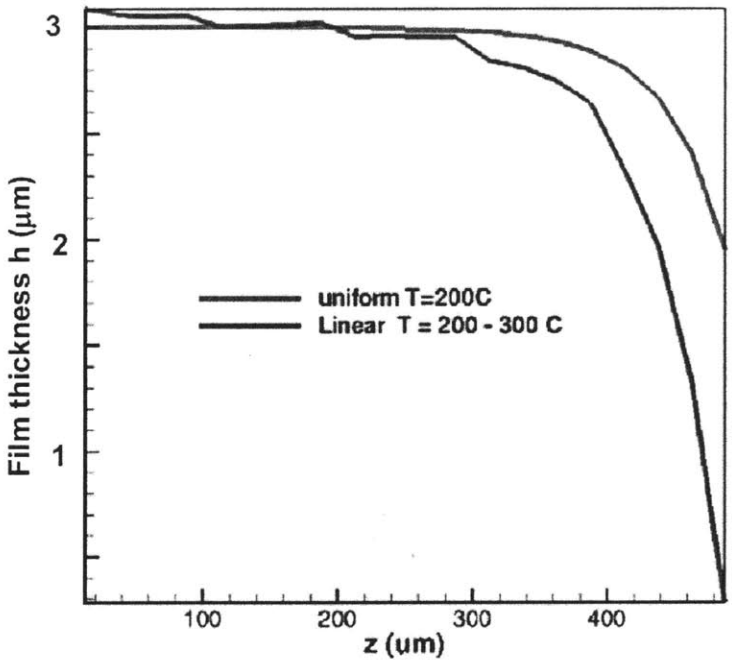

Figure 3-17: Film thickness profile at 3.6 ms elapsed time.

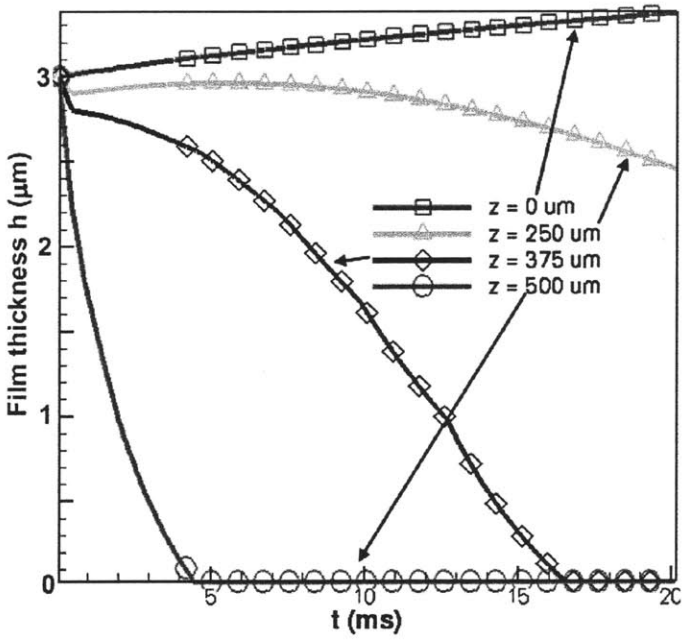

Figure 3-18: Film thickness as function of time at various axial locations; linear axial temperature profile from 200 to 300 C.

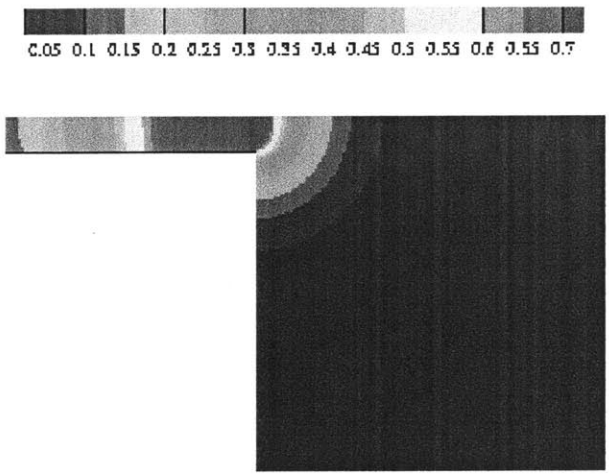

Figure 3-19: Contour plot of vapor density with a linear axial temperature profile from 200 to 300 C.

thickness) oxygen consumption rate per unit area of the film. Since the deposit formation chemistry is much slower than the gas phase transport processes, the surface oxygen flux is assume to be approximately zero; thus the physical transport processes are decoupled from the chemistry.

In chemistry, we can estimate the dissolved gas in liquid using Henry's Law:
At a constant temperature, the amount of a given gas dissolved in a given type and volume of liquid is directly proportional to the partial pressure of that gas in equilibrium with that liquid.
In equations, Henry's law is

$$p = k_h(T)x \tag{3.23}$$

where p is the partial pressure of gas above the solution and x is the mole fraction of gas dissolved in solution.

The oxygen concentration in the liquid phase is assumed to be in equilibrium with that in the gas phase. To simplify the calculation, the liquid/gas phase equilibrium

T(K)	1,3 Dimethyl benzene	1,4 Dimethyl benzene	Methyl-cyclo-hexane	n-Decane
298.15	11.96	11.69	15.82	21.78
303.15	-	11.67	15.92	21.74
313.15	-	11.65	16.12	21.67
323.15	-	11.63	-	-
333.15	-	11.61	-	-
343.15	-	11.59	-	-
353.15	-	11.57	-	-

Table 3.4: Equilibrium mole fractions ($\times 10^{-4}$) of oxygen in single component hydrocarbons as a function of temperature. Partial pressure of oxygen in the gas phase is 1.013 KPa; data from Battino et al[14].

is assumed to be that of an ideal mixture so that Henry's law applies, although in reality, the fugacity of the non-ideal multi-species mixture has to be considered.

The Henry's law constant $k_H(T)$ may be obtained by measurements of p and x for a mixture in phase equilibrium at temperature T. The functional dependence of x on T is usually expressed as

$$\ln(x) = \ln\left(\frac{p}{k_H(T)}\right) = A_0 + \frac{A_1}{\tau} + A_2\ln(\tau) + A_3\tau + A_4\tau^2 \tag{3.24}$$

where $\tau = T(K)/100$. Data of oxygen solubility in single component aromatics and paraffins are shown in Table 3.4 and Fig. 3-20 [14]. Since the temperature dependence is weak, the value of $k_H^{O2}(T)$ for oxygen is assumed to be independent of temperature, and its value for the mixture is to be governed by the following weighted sum:

$$\frac{1}{k^{O2}_{H_{diesel}}} = 0.8\frac{1}{k^{O2}_{H_{n-decane}}} + 0.2\frac{1}{k^{O2}_{H_{1,4dimethylbenzene}}} = 19.7\times 10^{-4} atmosphere^{-1} \tag{3.25}$$

N-decane and 1,4 dimethyl benzene are used as surrogates for paraffins and aromatics. The weighting factor reflects roughly the proportion of paraffin to aromatic molar ratio.

To complete the model, the transport of nitrogen has to be considered in a similar manner. The data from Battino et al [15] are used for the Henry's law correlation. N-hexadecane and benzene are used as surrogates for the paraffins and aromatics in the

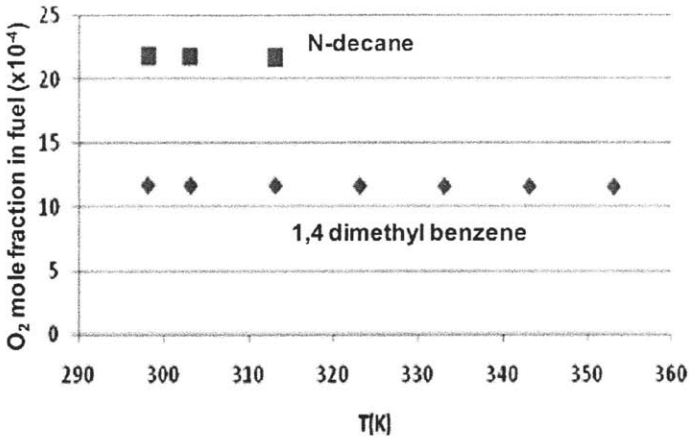

Figure 3-20: Equilibrium mole fraction of oxygen in n-decane and 1,4 dimethyl benzene as a function of temperature. Gas phase oxygen partial pressure is at 1 atmosphere.

diesel fuel. There is temperature dependence in k_H^{N2}; see Fig. 3-21. The dependence may be fit by the first two terms of Equation 3.24. Thus, with $\tau = T(K)/100$, the correlations are:

$$\frac{1}{k^{N2}_{H_{n-hexadecane}}} = \exp\left(-6.8288 - \frac{0.3404}{\tau}\right) atmosphere^{-1} \tag{3.26}$$

$$\frac{1}{k^{N2}_{H_{benzene}}} = \exp\left(-6.05445 - \frac{4.95673}{\tau}\right) atmosphere^{-1} \tag{3.27}$$

The Henry's law constant of nitrogen for the diesel mixture is then

$$\frac{1}{k^{N2}_{H_{diesel}}} = 0.8\frac{1}{k^{N2}_{H_{n-hexadecane}}} + 0.2\frac{1}{k^{N2}_{H_{benzene}}} \tag{3.28}$$

The 2D simulation of the diffusion of oxygen and nitrogen are carried out at a pressure of 1 atmosphere and temperature of 250 C. The initial vapor distribution is given by Equation 3.22. The distribution of oxygen and nitrogen in the nozzle and combustion chamber at 30.2 ms are shown in Fig. 3-22. Because of the presence of vapor, there is a significant reduction of oxygen towards the rear of the nozzle.

The mole fractions of the oxygen and nitrogen in the fuel film are shown in Fig.

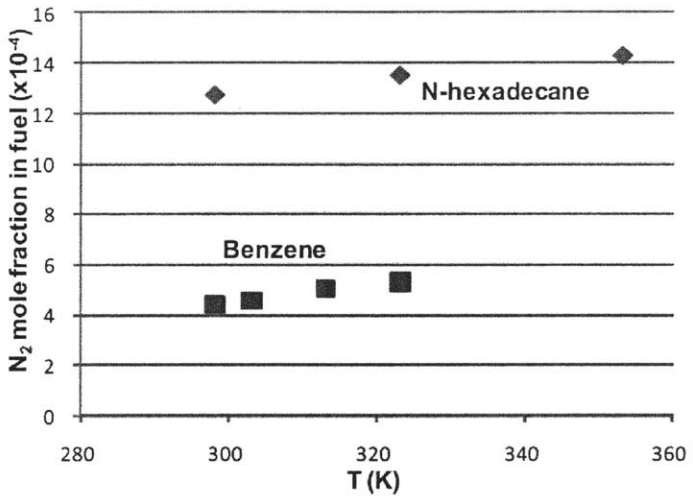

Figure 3-21: Equilibrium mole fraction of nitrogen in n-hexadecane and benzene as a function of temperature. Gas phase oxygen partial pressure is at 1 atmosphere.

3-23 for different elapsed time in the simulation. As time progresses, oxygen diffuses through the fuel vapor and gets absorbed in the liquid fuel film. Because of the diffusion time, there is a significant oxygen gradient along the fuel film. The oxygen deficiency at the rear of the nozzle and that the oxygen is readily available towards the nozzle exit have substantial effects on the oxidation process and the rate of deposit formation along the nozzle.

3.4 Washing Models

In engine injector nozzles, after a fresh injection, some of the deposit pre-cursors will be washed away. The washing was also designed into the bench-scale lab test. How much of the pre-cursors are transported to the flow and washed out has a big effect on the final deposit formation.

In this section, convective mass transfer models for laminar and turbulent pipe flows are used to model the mass transfer. The local mass flux of species from the

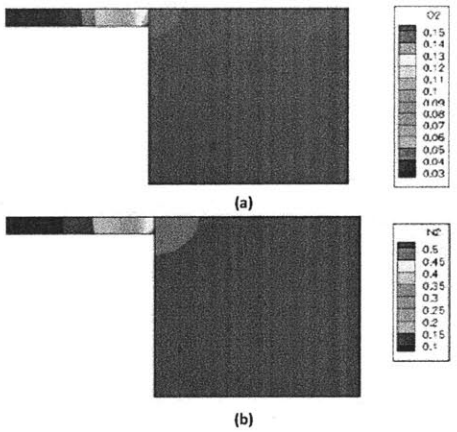

Figure 3-22: Oxygen and nitrogen partial density at 30.19 ms: (a) Oxygen; (b) Nitrogen.

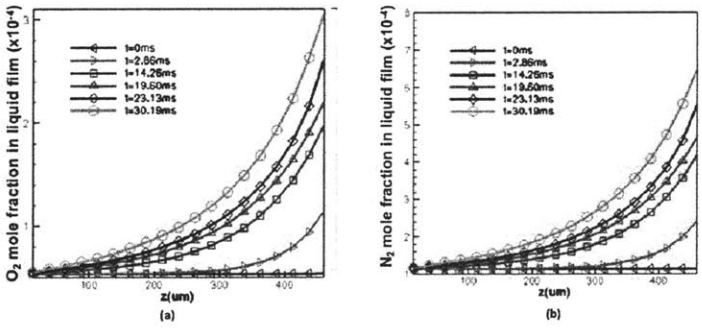

Figure 3-23: Mole fraction of O2 and N2 in fuel film at different time: (a) Oxygen; (b) Nitrogen.

film may be computed of the form

$$n_i'' = h_m(\rho_{i,film} - \rho_{i,flow}) \tag{3.29}$$

then the total rate of species transfer for a pipe of surface area A_s can be expressed as

$$n_i = h_m A_s \Delta\rho_{i,lm} \tag{3.30}$$

$$\Delta\rho_{i,lm} = \frac{\Delta\rho_{i,o} - \Delta\rho_{i,i}}{\ln(\Delta\rho_{i,o}/\Delta\rho_{i,i})} \tag{3.31}$$

where the $\Delta\rho_{i,lm}$ is the log mean concentration difference. If we know the convection mass transfer coefficient h_m we can solve for the amount of transfer.

The non-dimensional numbers in mass transfer are the Sherwood number (or mass Nusselt number) defined as $Sh_D = h_m D/D_{ij}$ and Schmidt number defined as $Sc = \mu/\rho D_{ij}$. Then with a uniform vapor density at the surface of a circular duct and fully developed laminar flow through the duct, we have

$$Sh_D = 3.66 \tag{3.32}$$

For fully developed turbulent flow, we have [31]

$$Sh_D = 0.023 Re_D^{4/5} Sc^{0.4} \tag{3.33}$$

Except the above Sherwood number correlation, the concentration difference and the injection interval are also the main factors for the intensity of washing.

3.5 Parameters Estimation

3.5.1 Saturated Vapor pressures

The saturation pressure for each component of the surrogate is obtained using the Antoine equation. It is a vapor pressure equation that describes the relation of the

Compound	Formula	A	B	C
n-undecane	C11H24	6.97220	1569.570	187.700
n-tridecane	C13H28	7.00756	1690.670	174.220
1M-naphthalene	C11H10	7.03592	1826.948	195.002
n-hexadecane	C16H34	7.02867	1830.510	154.450
n-decylbenzene	C16H26	7.81480	2396.800	199.574
n-nonadecane	C19H40	7.01530	1932.800	137.600
n-heneicosane	C21H44	7.08420	2054.000	120.100

Table 3.5: Antoine Constants for diesel surrogate components

saturated vapor pressure and the temperature for pure components. It is derived from the Clausius-Clapeyron relation. The equation is:

$$\log_{10} P = A - \frac{B}{C+T} \tag{3.34}$$

where T is the temperature of the vapor, and A,B and C are constants that are characteristic of the constituent. The values for these constants can be obtained from standardized tables and list in Table 3.5.

However, not every reaction intermediate products have Antonie coefficients documented. For those species, the partition coefficient model was used, see Section 4.2.

3.5.2 Diffusivity

One of the most common equations used in predicting binary gas diffusivities is the Hirschfelder-Bird-Spotz equation. A more recent empirical correlation has been developed by Fuller, the so called Fuller, Schettler, and Giddings Correlation []. The correlation is shown in Equation 3.35.

$$D_{ij} = \frac{10^{-3} T^{1}.75 \left(\frac{1}{M_i} + \frac{1}{M_j}\right)^{1/2}}{P\left[(\sum V_i)^{1/3} + (\sum V_j)^{1/3}\right]^2} \tag{3.35}$$

where P is the total pressure, M_i is the molecular weight and $\sum V_i$ is the sum of diffusion volume for component i.

For diffusivities in the liquid, Stokes-Einstein diffusion equation was used. The diffusivity is a function of solute radius and solvent viscosity, see Section 4.3.

3.5.3 Molecular Properties

The radius and molar density are calculated using the UNIFAC group additivity scheme which is included in RMG [4]. The UNIFAC scheme allows one to calculate the solute volume based on the volumes of the individual fragments (functional groups) making up the molecule. Once the volume has been estimated an effective radius can be estimated assuming the molecule to be spherical.

Chapter 4

Deposit Formation Chemistry

The study of physical models gives a clear idea of the film formation, the evaporation profile and the oxygen content in the film. In order to understand and predict the effects of fuel detergents on deposit formation in diesel injector nozzles, a detailed model describing chemical processes involved in the deposit formation is necessary. The aim here is to understand the chemical changes that occur in the fuel surrogate at the existing conditions within the injector nozzle, during the time scale set by evaporation. The chemical models include solvation, diffusion and detailed liquid phase kinetics. These models were developed by MIT Green Group [64, 4] and will be used in the integrated deposit formation model trying to reproduce quantitatively the results observed in the bench scale experiments and to predict the engine injector nozzle deposit behaviors.

4.1 Reaction Mechanism Generator (RMG)

Many practical reaction systems have very complicated chemistry. The autoxidation of hydrocarbons is one of them. The reaction has complicated radical reaction pathways[59]. These reaction networks may contain thousands of reactions and species. Reacting systems such as this may also have complicated temperature dependencies, where the dominant reaction pathway may change at different temperatures leading to a change in reaction order.

The typical way to model these systems was to choose a simple chemistry model such as shown in Fig. 4-1 based on our understanding of the system. The reaction

$$\mathrm{A} + \mathrm{B} \leftrightharpoons \mathrm{C} + \mathrm{D}$$

Figure 4-1: A simple reversible chemical reaction.

rate can be written as

$$r = k_f[A][B] - k_r[C][D] \tag{4.1}$$

And k_f can be expressed using Arrhenius form:

$$k_f = A \exp\left(\frac{-E_a}{RT}\right) \tag{4.2}$$

where E_a is the activation energy. The reverse reaction rate k_r could be calculated using equilibrium constant:

$$\frac{k_f}{k_r} = K_{eq} = \exp\left(\frac{-\Delta G}{RT}\right) \tag{4.3}$$

$$\Delta G = \Delta H - T\Delta S \tag{4.4}$$

Usually the coefficients and thermodynamic properties are estimated by fitting experimental data. These models have been used to check and refine our understanding of the chemistry: if we cannot make the model match the experiment, then our theory behind the model needs revising. However, even if the model can be made to fit the data, this does not prove the underlying understanding is correct; the fitted parameters may not be physically meaningful. Additionally, these models are not reliably predictive for conditions outside the range covered by experimental data, due to the possibility of complex temperature-dependency mentioned above. There are actually numerous other species and reactions, typically involving competing catalytic cycles, and these complicated reaction networks cannot be described with a sequential linear kinetics model except in a very narrow range of conditions. Fortunately we are able

to perform experiments in the same temperature range as that of a slowly cooling diesel engine, so temperature extrapolation is not necessary in this case. However, if we wish to extend our model to include detergency effects, oxidation and degradation of detergent, and other attempts to mitigate deposit formation, then a physically meaningful understanding of reaction pathways and intermediate species will be important; a simple fuel intermediate deposit model with parameters tuned to fit our flat plate experiments may not be sufficient.

A detailed kinetic model consists of two parts: a list of species, and a list of reactions. For each species there must be thermochemical data for all temperatures covered by the model; the standard enthalpy of formation, standard entropy, and heat capacity as a function of temperature are sufficient to calculate all other thermodynamic properties. For each reaction there must be a forward rate coefficient for all temperatures (the reverse rate is calculated from the chemical equilibrium constant, derived from the thermochemistry); for elementary reactions this is usually given as a function of temperature in Arrhenius form.

Because complex kinetic models may contain thousands of species and reactions, creating them manually is tedious and error-prone. Automatic generation of kinetic models would allow a chemical engineer to model arbitrarily complicated chemistry systems without years of effort by chemists. Several research groups are working on computational tools to automate the process [61, 33, 18]. All these tools have common requirements: (1) a method for representing molecules in the computer memory, and of uniquely identifying the molecules and recognizing equivalents; (2) a method for creating reactions and their product species; (3) a method for predicting thermochemical and kinetic parameters for each of the species and reactions.

RMG (Reaction Mechanism Generator) is an automatic reaction mechanism generator [40, 76]. Molecules are represented as graphs, with atoms as nodes and bonds as edges connecting the nodes. Standard graph-theory methods are used to identify equivalent graphs and ensure uniqueness. RMG uses "'reaction families"' to generate all the possible reactions that a species can undergo in the presence of the other species in the chemical mechanism. Every reaction family represents a particular

type of elementary chemical reaction, such as bond breaking, or radical addition to a double bond. Each reaction family has a recipe for mutating the graph, and a library of rate expressions for different functional groups. There are currently over 30 primary reaction families in RMG. Because the model can contain thousands of species and rates, the estimation of thermochemical and kinetic parameters must be very fast. As with most mechanism generating tools, RMG uses a database of known values wherever possible to find thermochemical data for species, but usually it estimates parameters using a group contribution method. The functional groups are recognized using a graph-theory matching algorithm. A similar method is used to estimate the rate coefficients for the reactions. RMG uses a rate-based termination criterion; the reaction network is expanded until the rates of all reactions going to species not included in the network fall below a certain threshold.

Unfortunately, the original RMG only support gas phases, we could model the liquid chemistry as gas phase chemistry with the pressure adjusted so that the species concentrations match the liquid phase values. But this approach neglects the liquid phase effects such as solvent cage and diffusion limits.

4.2 Solvation Thermochemistry

Solvation is the process of attraction and association of molecules of a solvent with molecules or ions of a solute. As solute dissolve in a solvent they spread out and become surrounded by solvent molecules. It is widely appreciated that changing the solvent can dramatically change reaction rates, and many cases are known where the gas-phase and solution-phase rate coefficients differ by several orders of magnitude [26, 41]. Thus to properly model solution phase chemistry, we must estimate the changes in the thermo-chemical properties of a species going from the gas phase to the solvent phase.

There are two ways in which solvents can affect the reaction rates of liquid chemical reactions: through static or equilibrium solvent effects or through dynamic or frictional solvent effects. In this thesis, we will focus on the first approach. Based on

a [41], the thermodynamics of solvation are best modeled using the idea of partition coefficients.

The partition coefficient of a species is defined as "'the ratio of the concentration of the species in the solvent phase to that in the gas phase at equilibrium":

$$K = \frac{c_{solvant,eq}}{c_{gas,eq}} \tag{4.5}$$

Then the change in the Gibbs free energy of a species in going from the gas phase to the solvent phase may be written as

$$\Delta G^0_{i,solvant} = -RT \ln \frac{c_{i,solvant,eq}}{c_{i,gas,eq}} = -RT \ln K_i = -2.303RT \log_{10} K_i \tag{4.6}$$

where the superscript '0' represents the standard state. Hence, if we can develop a model for the partition coefficient, we can solve for the free energy of solvation.

After identifying the partition coefficient as a potential route to the estimation of solvation thermodynamic properties, Our logic would be to use a model for K to calculate ΔG, then we use another model for ΔH, together, we can solve for ΔS and finish the solvation thermodynamic modeling.

4.2.1 Estimation of Partition Coefficient

Partition coefficients have been a subject of interest mainly in the chromatography and separations communities. Several workers have made attempts at understanding the molecular origin of chromatography by in turn trying to understand the fundamental nature of solute-solvent interactions that govern the solvation process. These efforts have given rise to a very intense area of research popularly known as Linear Solvation Energy Relationships (LSERs). The Abraham model is the current state of the art in the formalism. It models solute-solvent interactions using molecular descriptors for each type of interaction and allows one to predict the partition coefficient of a species in a large number of solvents. The Abraham model has been used widely in the 15 years since its inception and continues to evolve today. Several modifications

to the model have been proposed to suit specific needs. For our purposes however, the basic formulation is adequate.

The Abraham model is an empirical model in that it relies on experimental partition coefficient data to estimate the parameters that go into the model. The governing equation of the model is:

$$\log_{10} K = c + aA + bB + cC + sS + eE + lL \tag{4.7}$$

where the capital case parameters A, B, E, S and L are properties of the solute, i.e. the species going from the gas phase to the solution phase, while the lower case letters c, s, a, b, e and l are properties of the solvent. Because $log_{10}K$ is directly proportional to the Gibbs free energy change, each term on the right hand side can be viewed as accounting for the free energy change due to different solute-solvent interactions. In the Abraham model each solute-solvent interaction is modeled as the product of a solute descriptor (uppercase parameters) and a solvent descriptor (lowercase parameter). We can now describe the wide variety of solute-solvent interactions that the Abraham model accounts for:

1. aA & bB: Account for the energy change associated with the formation of hydrogen bonds between the solute and the solvent.

2. sS & eE: Account for the energy change associated with intermolecular interactions like dipole-dipole, dipole-induced dipole etc.

3. lL: Accounts for the free energy change associated with the cavity formation process.

4. c: May be treated as a correction factor accounting for any additional interactions between the solute and the solvent. It should be noted that 'c' is a solvent descriptor and has no contribution from the solute.

The solvent parameters c, e, s, a, b, l are obtained using multiple linear regression techniques on partition coefficient data of several solutes in the solvent of interest. As a result these parameters are fixed once the solvent has been fixed.

The technique used to obtain the solute parameters A, B, S, E, L for a compound for which experimental data is available is similar to the method used for the solvent parameters, but in order to use the model in a predictive fashion one needs to determine these numbers for solutes without experimental data. Hence the main challenge lies in estimating these parameters using just molecular structure as the input.

Jalan et al. [4] utilized a Group Additivity based scheme proposed by Platts et al. [60] for the estimation of Abraham solute parameters. They chose n-decane to be a model solvent because it is a relatively heavy alkane with characteristics close to those of diesel. Then they built the models to RMG and compared the solvation energies from the simulation against the Minnesota Solvation Database, a collection of over 2000 experimental solvation free energies (comprising neutral species and ions, with around 800 points for species containing only C, H and O in solvents).

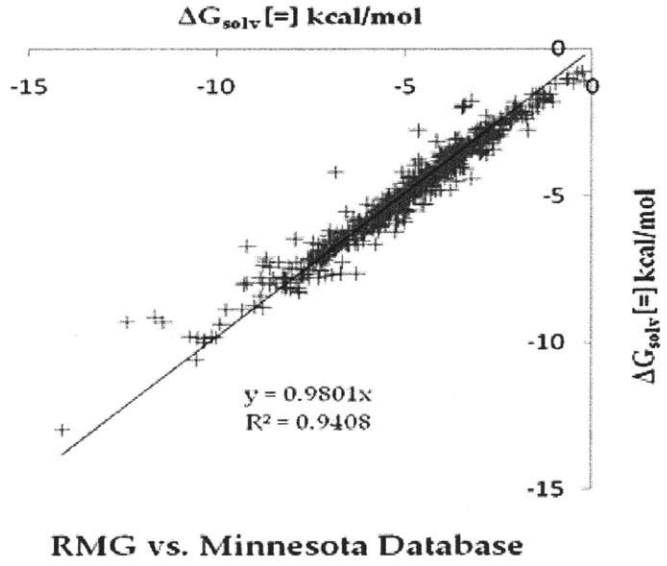

Figure 4-2: Comparison of solvation energy obtained from the RMG and the values from the Minnesota Database.

Figure 4-2 (around 725 solute/solvent pairs) shows that the predictions from RMG are in very good agreement with those from the Minnesota database: the Mean Average Deviation (MAD) of the RMG predictions was 0.273 kcal/mol. The extent of agreement can also be gauged by fitting a linear trend line to the data and looking

at the deviation of the slope from 1.0. The slope for the RMG vs. Minnesota was 0.98 with an R2 value of 0.94 quantifying the robustness of the fit.

The plots above clearly indicate that the Abraham model works well as a predictive model for the free energies of solvation of small to medium molecules.

4.2.2 Estimation for Enthalpy of Solvation

Mintz et al. [54] have developed mathematical correlation equations for predicting the enthalpies of the solvation of gaseous solutes in the linear alkane solvents, pentane through hexadecane. The Mintz correlations are very similar to the Abraham model, in their approach, Mintz et al. have collected and organized experimental enthalpy of solvation data (at 298 K) for a large number of solute-solvent pairs. These experimental values have been obtained from a variety of sources including but not limited to direct calorimetric measurements, calculations based on the temperature dependence of the infinite dilution activity coefficient, etc. The basic idea of the Mintz approach is to use the experimental ΔH_{solv} values to develop correlations of the following form:

$$\Delta H_{solv} = c^{'} + a^{'}A + b^{'}B + s^{'}S + e^{'}E + l^{'}L \tag{4.8}$$

where A,B,E,S and L are the same solute descriptors used in the Abraham model for the estimation of ΔG_{solv}. The lowercase coefficients c', a', b', e', s', l' characterize the solvent and are obtained by regression to experimental data similar to that employed in the development of the Abraham correlations. Mintz correlations have been proposed for several solvents including alkanes, alcohols, tetrachloromethane, aromatic solvents like benzene and toluene, etc. The performance of these correlations for the hexane test case mentioned earlier is shown in Fig. 4-3.

4.3 Diffusion Limits

In liquid phase reactions, after the solutes are dissolved in solvants (discussed in the previous section), diffusive processes can limit the rate at which species hit each other

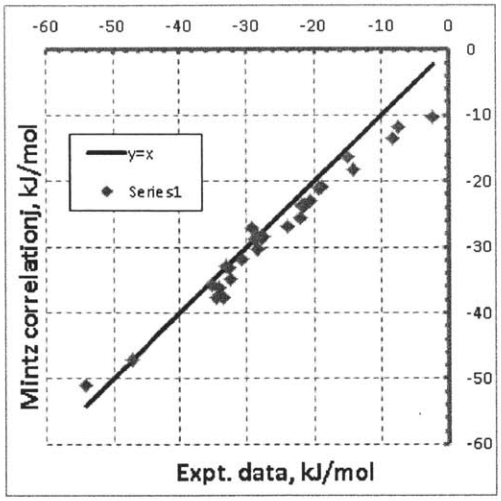

Figure 4-3: Comparison of solvation enthalpy obtained from the Mintz correlation and the experimental data.

in solution hence adding the possibility of another rate limiting step in the process. The steps to solute reactions are shown in Fig. 4-4.

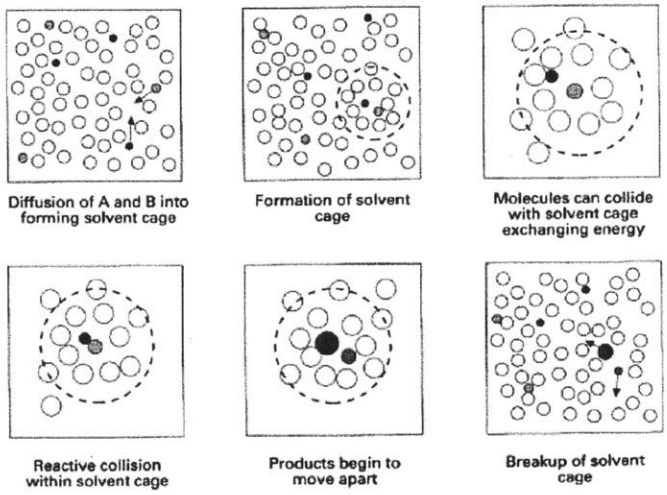

Figure 4-4: Sequence of steps leading to reaction in the presence of diffusion[4].

The processes shown in the figure contribute to what is known as the "'diffusive limit"' for reactions in solution and occurs in the case of bimolecular reactions only. It signifies the fact that even though intrinsically a reaction may be very fast, the

process of diffusion slows down the net rate of reaction. The effects of diffusion may be summed up in the expression for the effective rate of a reaction in solution [4]:

$$k_{eff} = \frac{k_r k_d}{k_r + k_d} \tag{4.9}$$

where k_r is the intrinsic rate of reaction and k_d is the diffusion-limited rate of reaction. One can see there are two limiting cases:

1. $k_r >> k_d$: This implies a very fast intrinsic reaction and $k_{eff} \sim k_d$, i.e. the reaction is diffusion limited.

2. $k_r << k_d$: This implies a very slow intrinsic reaction and $k_{eff} \sim k_r$, i.e. the reaction is activation limited.

Not all cases are at these extremes, and the effects of diffusion can slow down reaction rates by factors varying from ~ 1 to ~ 1000. Diffusive limits directly impact reactive fluxes so one expects that they would also affect the final mechanism. As a result, any reaction network in the solution phase would be incomplete without incorporating diffusive effects.

The simplest expression for the effective reaction rate for the bimolecular reaction A+B -¿ Products is the one obtained assuming equilibrium between diffusive and reactive processes ($t \to \infty$)[4]:

$$k_{eff} = \frac{4\pi D_{A,B} r_{A,B} k_r}{k_r + 4\pi D_{A,B} r_{A,B} k_r} \tag{4.10}$$

where D_{AB} is the relative diffusivity of B towards A and r_{AB} may be treated as the distance between A and B when reaction occurs. The typical values for D_{AB} and r_{AB} are calculated using Equation 4.13 and Stokes-Einstein equation is used to estimate

n-decylbenzene	n-undecane	n-tridecane	naphthalene
1.11	0.22	0.89	0.44
n-hexadecane	O2	n-nonadecane	n-heneicosane
1.11	0.0022	0.89	0.44

Table 4.1: Initial concentration in reactor simulation

species diffusivity:

$$D_{A,B} = D_A + D_B \tag{4.11}$$

$$r_{A,B} = \frac{r_A + r_B}{2} \tag{4.12}$$

$$D_i = \frac{k_B r}{6\pi\eta(T) r_i} \tag{4.13}$$

where k_B is Boltzmann's constant, T is temperature, η is the viscosity of the solvent and r_i is the radius of the diffusing species.

Jalan et al [4] used UNIFAC scheme for estimating the species radius. And for viscosity of the solvent, they assumed that the viscosity (η) was independent of temperature and was the same as the model solvent n-decane. The value of the viscosity used is 4.72E-4 Pa-s.

To test the liquid phase effects (salvation and diffusion), computation was carried out with a batch reactor containing the 7 component surrogate fuel [4]. The temperature was fixed at 500 K and the total molar density was fixed at 5.1 mol/L. The initial concentrations of species (mol/L) were shown in Table 4.1. The concentration of O2 was maintained as constant.

The progressions of the N-decyl benzene concentration using the three simulations are shown in Fig. 4-5. One of the most noticeable differences between the three simulations is the final conversions of n-decyl benzene (t=900 sec). While the gas phase simulation (A) returned a conversion of 75%, the conversions were significantly lower in the solution phase (18% and with diffusion off and 25% with diffusion on). The low solution phase conversions may be entirely due to shifts in reaction equilibria, which is due to the solvation thermodynamics. We also notice that in these simulations, switching diffusion 'on' resulted in higher conversions of the most reactive

component n-decylbenzene (a jump of about 7%). The most probable reason for this observation could be that diffusion increases the average lifetime of free radicals since it slows down the bimolecular radical-radical termination reactions.

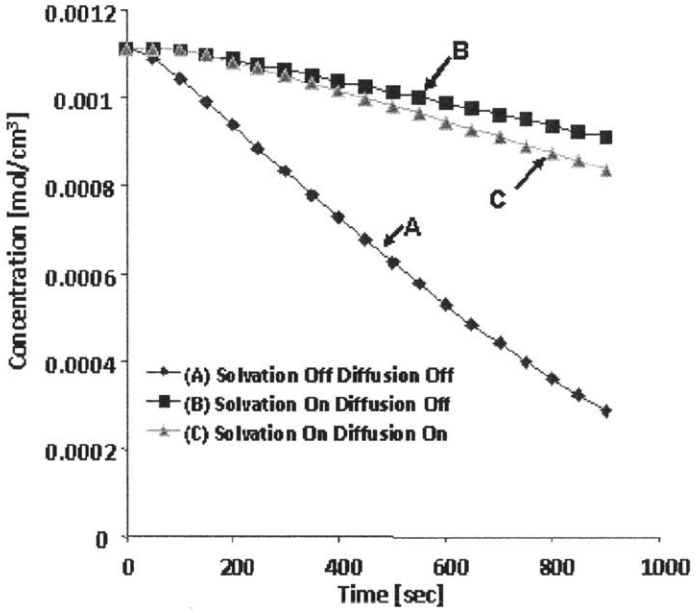

Figure 4-5: Progressions of n-decyl benzene concentrations with the three different simulation schemes[4].

4.4 Liquid Phase Oxidation Chemistry

Automatic mechanism generation is based on the principle of exploring all possible pathways for a given set of species and expanding the size of the model using only the most important species and reactions. And softwares such as RMG could not help if major pathways are missing in their reactions database. Hence, after combining solvation thermochemistry estimation and diffusive limits estimation presented in the previous sections into RMG, the resulting mechanisms have to be validated with experimental data to make sure most of the major reactions pathways are not missing.

Jalan et al. [4] surveyed the major pathways in Liquid phase autoxidation of alkanes as shown in Fig. 4-6. After putting all major pathways to RMG database,

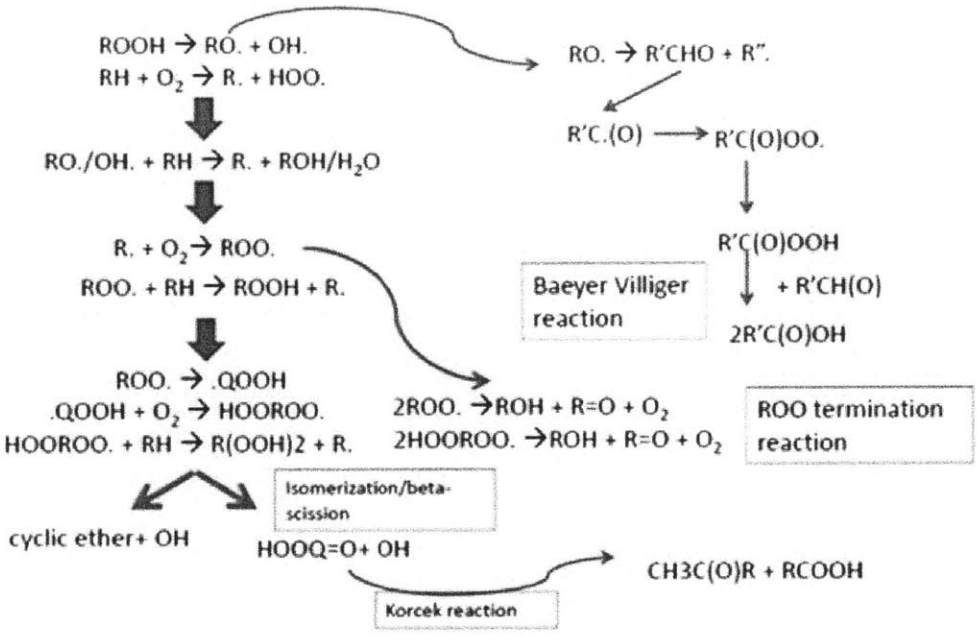

Figure 4-6: Major pathways involved in liquid phase oxidation of hydrocarbons[4].

the new reaction rates, diffusive limits, RMG features and the improved methods to model temperature dependence of solvation thermochemistry were brought together to model the liquid phase oxidation of octane which has experimental data collected by Korcek [42]. The oxygen concentration was obtained from estimates of the Henry's law constant in hexadecane and the partial pressure reported by Korcek [42]. The concentration of octane was kept the same as that of pure hexadecane (also reported by Korcek[42]). In addition, the initial species mix was seeded with small amounts of the corresponding ROOH species to initiate the oxidation process. Estimates of the ROOH concentration to be used were obtained from the first measurement reported by Korcek (at time 43 sec [ROOH] = 1.45x10-6 mol/cm3). The resulting species profiles for the primary and cleavage oxidation products are shown in Fig. 4-7.

The generated model successfully predicts the qualitative trend in the species profiles of all primary oxidation products. The quantities of different species reported in the model are within a factor of 4 compared with experimental data. The deviations were a little larger than those usually observed with gas-phase predictive kinetic

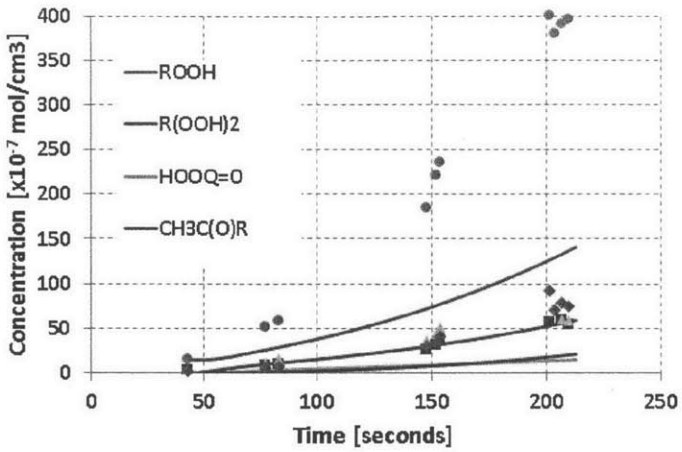

Figure 4-7: Model predictions from RMG compared with experimental data from Korcek et al.[4].

models. This validation shows that the chemical modeling approach is fairly accurate, at least for alkane fuels and can be extended to model the diesel surrogate oxidation.

Chapter 5

Simulation of Deposit formation

After modeling the essential physical and chemical processes, We need a procedure to couple them together. To use the integrated model to simulate deposit formation, we also need to define the "'deposit"', two possible definitions are used. Finally, some modeling efforts for detergent effects are discussed.

5.1 Coupled Solver

As stated before, since the liquid film is thin, the transport across it is fast and the concentration is uniform. Liquid phase transport can be neglected. The other assumption we made here to make the problem approachable is to assume that the gas/liquid interface is at equilibrium at the surface. Then the gas phase transport and the liquid phase chemistry can be solved with minimal interdependence.

The simulation framework is shown in Fig. 5-1. The steps within this framework could be shown as following:

- The reaction mechanisms are produced by RMG and fed to the liquid chemistry solver. And the initial liquid phase concentrations are given.

- The concentration of each species in the gas phase at equilibrium with the liquid is found using the gas/solvent partition coefficients and the liquid phase concentrations.

- These gas phase concentrations are passed to the gas phase transport solver. The gas phase solver keeps track of the chemical composition of each cell of gas as diffusion occurs away from the liquid surface and along the length of the nozzle to the combustion chamber. The boundary condition in this time step calculation at the surface of the liquid is that of constant concentration, using the values provided by the liquid solver.

- The amount of each species that diffuses away from the film surface after the previous time step is passed to the liquid phase chemistry solver for the next time step.

- These amounts are removed from the liquid cell. And the liquid chemistry solver and evaporation solver give the new concentrations after the time step.

- Some of the species are separated to the "'deposit"' phase. And those staying in the diesel phase are passed to the gas solver, and a new time step starts.

- When the time for a new injection arrived, the species in the "'diesel"' phase are replaced with the surrogate concentrations and washing models are used to give new concentrations of species in the "'diesel"' and the "'deposit"' phases. The cycle continues.

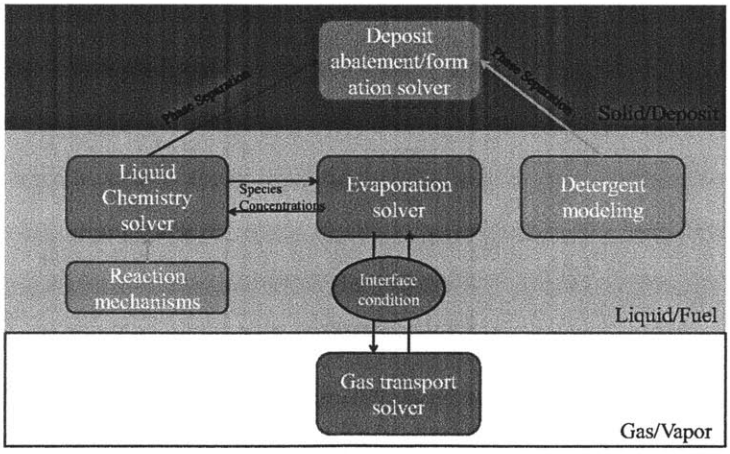

Figure 5-1: Coupled Solver diagram.

5.2 Deposit Formation

5.2.1 Deposit surrogate

It is not clear in the literature what groups in the reaction products are deposits. As a first step, an additional reaction and an additional species ("'deposit surrogate"') is added to the mechanisms to simulate the deposit formation. The artifical reaction is

$$2C_{16}H_{26}O_2 => C_{32}H_{52}O_4(Deposit) \tag{5.1}$$

The deposit mass (per unit area) accumulated in each engine cycle for an incubation time of 40 ms is shown in Fig. 5-2. The 40 ms time corresponds approximately to operation at 3000 rpm (it is an approximation because the injection duration was not accounted for.) All the deposit formed in the film is assumed to be transferred to the wall. For a 5 um initial fuel thickness, the deposit mass is $10^{-12}g/mm^2$.

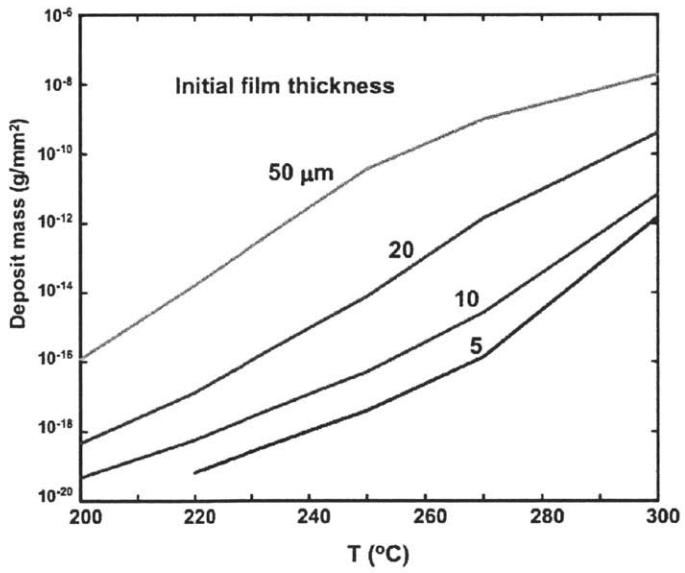

Figure 5-2: Deposit mass (per unit area) accumulated in each cycle for an incubation time of 40 ms, as a function of wall temperature and initial fuel film thickness.

To grasp the meaning of this value, if the deposit average density is assumed to be

2 g/cc, a deposit thickness of 5 um corresponds to a deposit mass of $10^{-5}g/mm^2$. Thus at formation of $10^{-12}g/mm^2$ per cycle, it would take 10^7 cycles to form. At 3000 rpm (1500 cycles/min.), the corresponding run time would be 100 hours. Notwithstanding that the formation rate may be different and the details of the chemistry model are not calibrated, the result is consistent with the experimental observation that deposit formation of the order of 5 um was observed in engine tests of 50-100 hours.

5.2.2 Phase Separation Models

Using a surrogate for deposit is straightforward, however, it doesn not provide any insights for the "'deposit"' and it is not easy to compare the model with the experiments. Here, a more natural model is developed for the "'deposit"'.

In chapter 4, when we calculate the solvation free energy, we used the Abraham model to determin the partition coefficient which is the ratio of concentrations of one species in the vapor phase and the liquid phase. Here, we used the same concept and defined two phases inside the liquid layer, the deposit phase and the diesel phase. The amount of each species entering the deposit phase is naturally given by the partition coefficient between deposit/diesel phases. Then the problems are what solvant shoud we choose for the deposit phase and how to calculate the partition coefficient.

The partitioning of a solute between two solvent phases is described by the partition coefficient K, which is the ratio of the solute concentration in each solvent phase at equilibrium (Eq. 5.2).

$$K = \frac{c_{s2}}{c_{s1}} \tag{5.2}$$

The Logarithm of K can be predicted by the Abraham model for solvent/solvent partitioning:

$$\log_{10} K = c + eE + sS + aA + bB + vV \tag{5.3}$$

This is similar to the Abraham model used in solving the solvation energy. But here, the solute parameter L is replaced with the solute parameter V, which is the McGowan's Volume [6] and the gas/solvent parameters (lower case letters) are replaced with solvent/solvent parameters which depend on the two solvents. Solvent/solvent

parameters are tabulated for many water/alkane pairs and some other pairs of solvents [7].

In our deposit formation case, the two solvant phases are 1) a mixture of hydrocarbons and 2) an insoluble deposit phase. The experimental data which match this two solvants haven't been done so we choose solvants that have been parameterized to reprent them. Phase 1 is hydrocarbon and phase 2 is consist of highly oxidized compounds that are very polar, we tried two approximations, first a decane/water pair and later switched to a more realistic octane/octanol pair to model the partitioning.

After we decide on a model for the partition coefficient, we need to calculate the amount separated into the deposit phase for each species. We denote the deposit phase as d, diesel phase as f, we have:

$$n_i^d = K_i^d * n_i^f * \frac{v_i^d}{v_i^f}$$

$$\frac{(N_i - n_i^d)}{\sum_i \nu_i (N_i - n_i^d)} = \frac{n_i^d}{K_i^d \sum_i \nu_i n_i^d} \tag{5.4}$$

We can then solve non-linear equation (Eq. 5.4) for each species.

However, when the number of species gets larger, this method is unstable because of the non-linearity. We can reformulate the equations:

$$N_i = n_i^d + n_i^f$$

$$K_i^d n_i^f = n_i^d \frac{V - V^d}{V^d}$$

$$N_i = n_i^d + n_i^d \frac{V - V^d}{K_i^d V^d}$$

$$n_i^d = \frac{N_i}{\left[1 + \frac{1}{K_i^d} \frac{V - V^d}{V^d}\right]} \tag{5.5}$$

$$V^d = \sum_i \nu_i n_i^d \tag{5.6}$$

Now, we only need to solve V^d, after we have V^d, from (Eq. 5.5) we can calculate n_i^d.

The integrated model was used to model lab experiment conditions which is shown in Table 5.1. The simulation results are compared with those from lab testing in

Heating Temperature	300 C
Tube length	76.2 mm (3 "')
Period of one complete cycle	125 ms
Fuel film thickness	15 um
Fuel pulse width	2 ms

Table 5.1: Condition for Modeling lab testing.

Chapter 6. The deposit accumulation per injection as a function of fuel injection frequency is shown in Fig. 5-3. A linear regression line is also shown on the plot. It can be seen that the deposit accumulation increases with lower injection frequencies. Compared with experimental data Fig. 6-18, we can see that although the simulation gives smaller accumulation rate, the quanlitative trend is very similar.

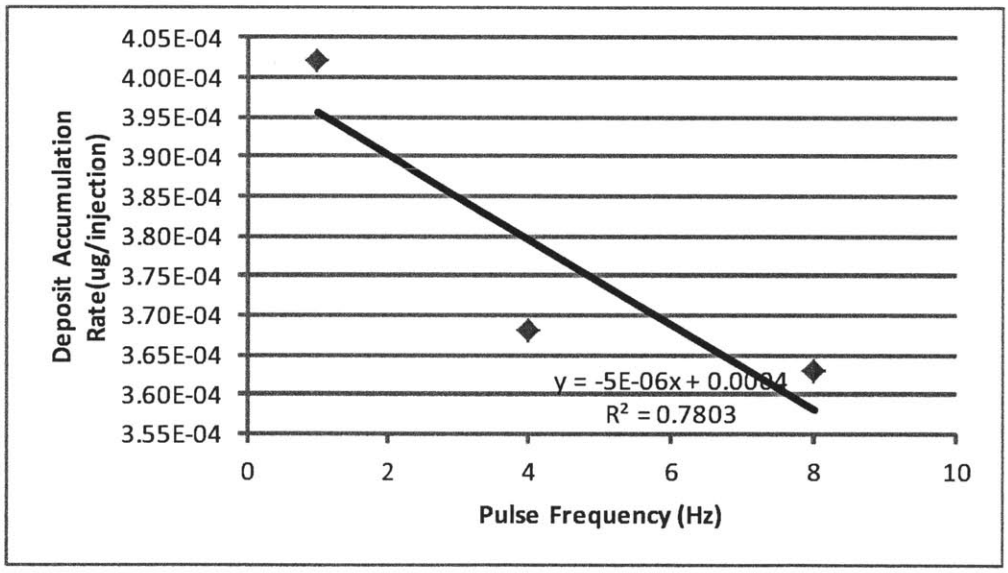

Figure 5-3: Deposit Accumulation as a function of fuel injection frequency.

The deposit accumulation rate as a function of temperature is shown in Fig. 5-4. A linear regression line is also shown on the plot. High temperature gives higher deposit formation. Compared with experimental data Fig. 6-13, we can see that although the simulation gives smaller accumulation rate, the quanlitative trend is very similar.

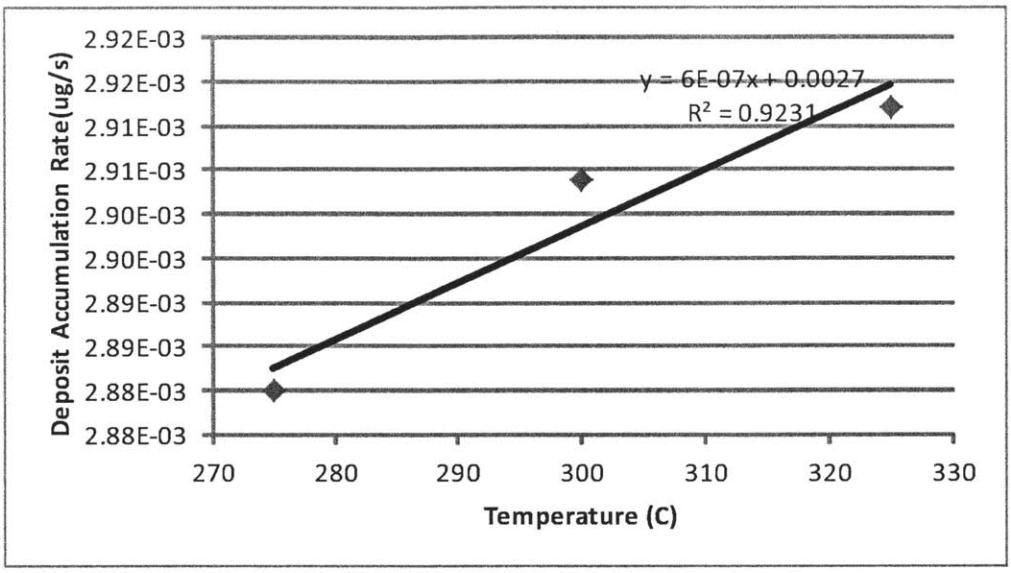

Figure 5-4: Deposit Accumulation as a function of heating Temperature.

And the deposit accumulation rate as a function of the film thickness is shown in Fig. 5-5. A linear regression line is also shown on the plot. We can see a thicker fuel film has a larger deposit accumulation.Compared with experimental data Fig. 6-15, we can see that although the simulation gives smaller accumulation rate, the quanlitative trend is very similar.

5.3 Modeling Detergent Action

A new detergent model was proposed by Jalan et al[4] which deal with the detergent as the same fashion as the deposit phase separation model. If detergent molecules are present, each species is separated to three phases: the deposit phase, the 'bound' phase (bound to a site on a surfactant molecule) and the 'free' phase:

$$(N_i - n_i^{deposit}) = n_i^{free} + n_i^{bound} \tag{5.7}$$

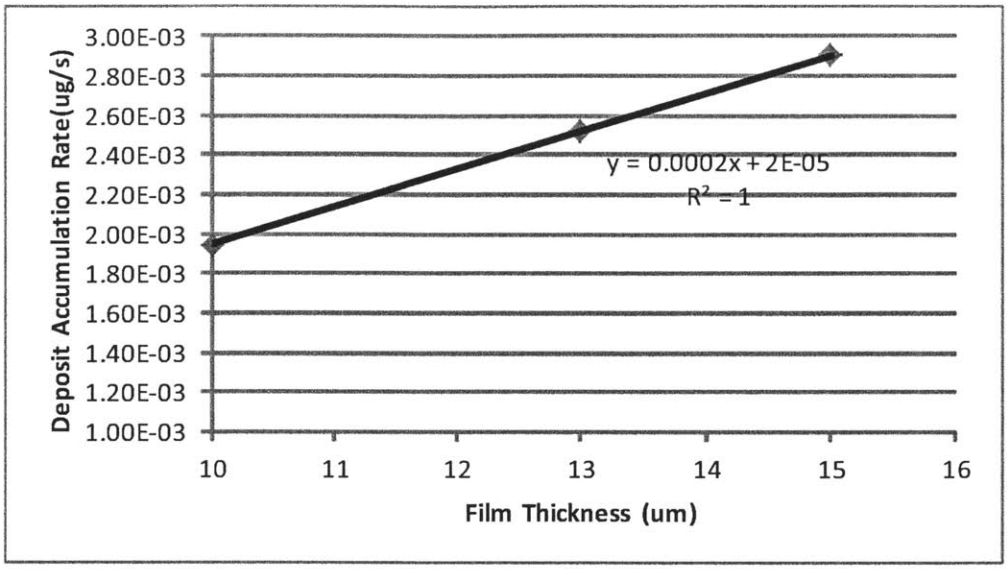

Figure 5-5: Deposit Accumulation as a function of film thickness.

The equilibrium concentration ratio predicted by the Abraham model is now between the deposit phase and the free diesel only and the bound species are in equilibrium with the free species and the free surfactant:

$$K_i^{dep} = \frac{c_i^{dep}}{c_i^{free}} \tag{5.8}$$

$$c_i^{bound} = K_i^{surf} c_i^{free} c_{surf}^{free} \tag{5.9}$$

where K_i^{surf} is the surfactant binding equilibrium constant for species i, and c_{surf}^{free} is the concentration of free surfactant. For evaluating the concentrations of free species, bound species, and free surfactant, all these share the same volume, that of the total diesel. Although a framework of detergent modeling is given here, the chemistry and the detailed modeling are left to future work.

Chapter 6

Deposit Formation Measurement

As stated in the first chapter, there are many reports on Engine Test results [todo cite]. However, Engine Tests are not only expensive but also difficult if we want to fix some control parameters such as Temperature or Pressure. Some authors did publish different bench scale designs [todo cite] to test the deposit formation but none of them embed enough physical and chemical processes such as washing and evaporation happened in real engines.

Our goal is to develop a bench scale test apparatus to emulate deposit formation in a controlled and accelerated manner while trying to cover essential physical/chemical processes in real engine environment. Data obtained with the apparatus will be used for validation of deposit formation model developed in the previous chapters. The apparatus is also designed to serve as a screening tool for preliminary evaluation of detergent candidates. In this chapter, an iteration of designs is introduced following by the test results.

6.1 Thin film reactor

6.1.1 Apparatus Design

A prototype thin film reactor was designed to see whether the deposit accumulation was observable, and to assess the magnitude and rate of this accumulation so that

future designs could be designed appropriately.

The thin film reactor design strategy was to confine the film in a cylindrical trough so that a well defined film thickness could be obtained from the trough diameter and the amount of fuel metered by a micro-pipette. The challenge was to get an approximately uniform fuel film. If a normal cylindrical hole was used to confine the film, the meniscus took up most of the liquid as shown in Fig.6-1. Hence, a film thickness could not be defined properly unless a large volume of liquid was added. Then the film would be unrealistically thick.

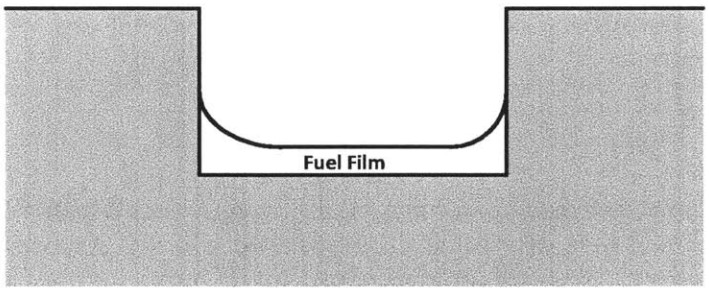

Figure 6-1: Cylindrical trough with vertical wall. Most liquid took up by the meniscus.

The problem to minimize meniscus effect could be solved with a simple design [cite todo]. As shown in Fig.6-2, a groove was cut to define the liquid film area, then the surface tension force was balanced by the normal reaction on the surface and a well defined film thickness could be produced.

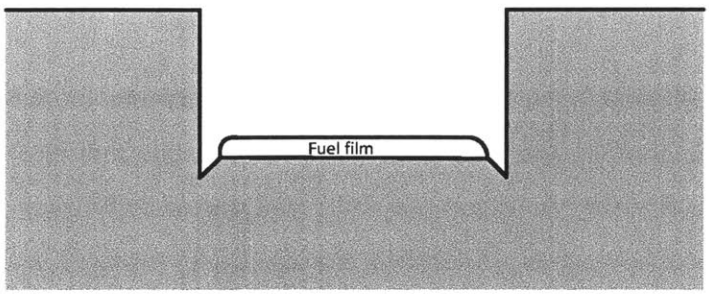

Figure 6-2: Cylindrical trough with groove defining the liquid film.

The block was manufactured with parameters shown in Table 6.1. The fuel used is commercial grade ultra low sulfur (15 ppm S) diesel fuel. The temperature was maintained by heating elements with feedback control and the scale used was Acculab Vicon microbalance with 0.1 mg resolution. The diameter of the circle is 2.27 cm and The mass of the fuel film is around 162 mg.

Parameters	Substrate	Temperature	Area	Volume	Thickness
Values	aluminum(6061-T6)	135 C	4.05 cm^2	200 μL	494 um

Table 6.1: Parameters for Film Reactor

The choice of temperature of 135 C in this first design is from testing experience rather than Engine environment. Test at 200 C had shown that visible smoke was coming out of the fuel film, and the film dried quickly (less than an hour). At lower temperatures, the fuel evaporation took very long (longer than 10 hours). The 135 C was chosen as the preliminary test point so that evaporation was reasonably fast (4-6 hours).

6.1.2 Testing Procedures

Three testing procedures are used to examine the deposit formation:

1. Dry Procedure. In this procedure, one unit of fuel was added onto the trough with a mirco-pipette (at 0.2 mm3 resolution) and was heated for enough time (6 hours) so that all the fuel evaporated. Then the substrate was weighted and another unit of fuel was added. The process was repeated to obtain the deposit accumulation history.

   Discoloring of the substrate was found after the drying of the first unit of fuel. The deposit accumulation history is shown in Fig. 6-3, You can see that the mass doesn't change after unit added, that's because the mass of the deposit was too small to be detected by the micro-balance (0.1 mg resolution). Data points at each x value were from repeat weighting of substrate.

   The data clearly show the increase of deposit with the repeated fuel units added. The quality of the data was not good enough to show whether there was any

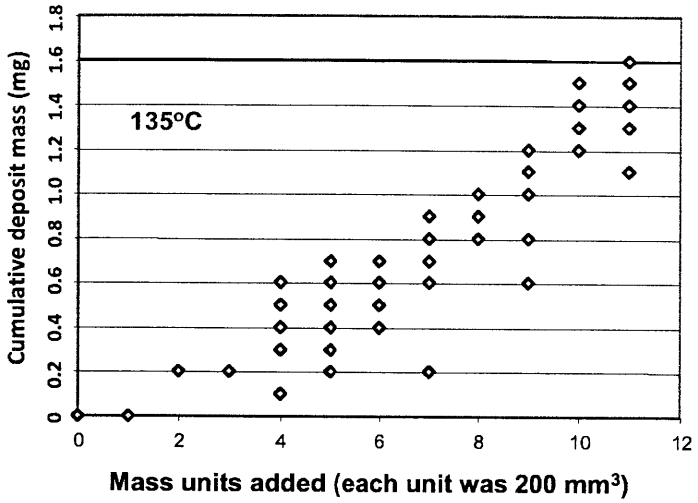

Figure 6-3: History of deposit accumulation at 135 C with the dry procedure.

non-linearity in the accumulation as a function of the mass of fuel units added. The slope of the accumulation history, on a mass basis, implies that at a fuel film thickness of 494 μm and at 135 C, 8×10^{-4} g of deposit is formed per g of fuel. In other words, a conversion rate of the fuel is around 8×10^{-4}.

2. Dry Wash Procedure. This procedure is almost the same as the dry procedure, except that the dried samples were rinsed with a volatile organic solvent (n-hexane; NBP = 69 C), air dried, and weighed. The purpose was to examine whether the deposit, when formed, was soluble in an organic solvent. The result is shown in Fig. 6-4.

3. Rinse procedure. This procedure was devised to partially emulate the deposit formation process in the injector nozzle: that some of the deposit precursors, formed in the engine shut off process and left in the liquid phase, is washed out by the injection process in the next engine start up. In this procedure, the liquid fuel film was allowed to hot soak for a period of time so that some of the liquid fuel remained in the end of the soak period. Then the sample was rinsed with a solvent (n-hexane) to remove the remaining liquid fuel, which carried some of the deposit precursors. The rinsed sample was allowed to air dry and weighed.

The procedure was repeated to assess the deposit accumulation history.

6.1.3 Testing Results

The results of deposit accumulation using the three procedures at 135 C are shown in Fig. 6-4. (The dry procedure was also tested at 200 C.) Because of the limited resolution of the micro-balance (0.1 mg), the substrates were repeatedly weighed to obtain a more accurate reading. The deposit accumulation from dry procedures at 135 C and 200 C were not materially different, in spite of the fact that at 200 C, the fuel film evaporated significantly faster (less than an hour) compared to at 135 C (4-6 hours). Thus the deposit conversion rate (mass of deposit as fraction of mass of fuel) in the dry process was not dependent on substrate temperature and evaporation time.

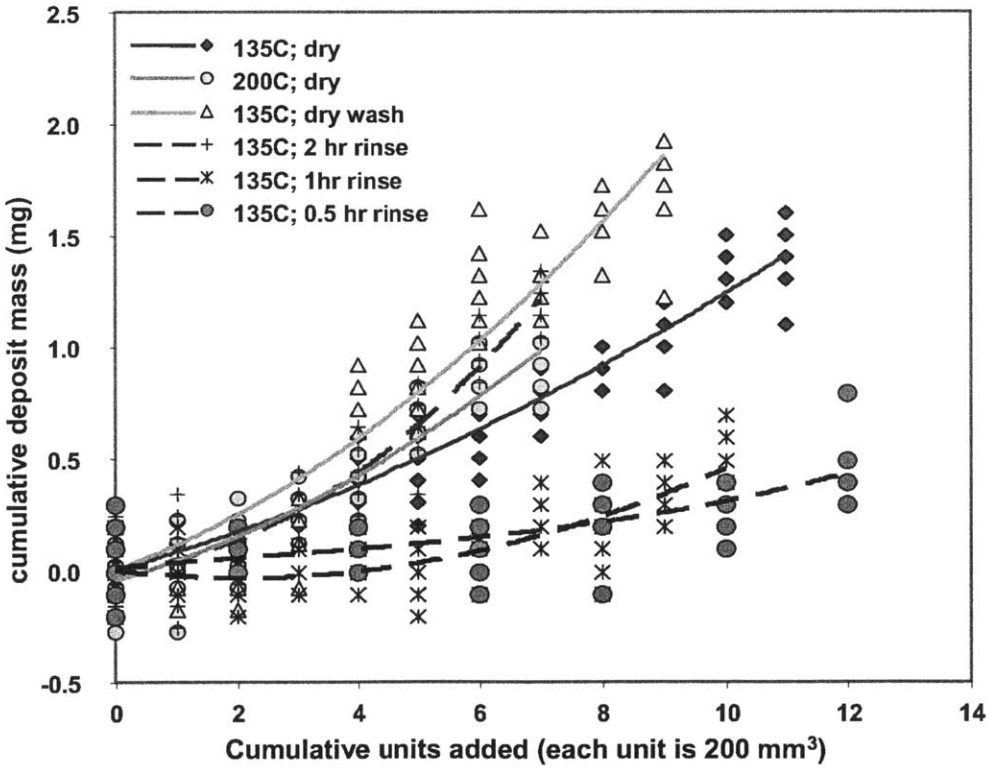

Figure 6-4: Cumulative deposit formation in fuel film reactor.

The deposit accumulation from the dry wash procedure was not significantly different from the dry procedure. (Although the dry wash procedure appeared to have a slightly higher yield, the data were not of sufficiently high quality to ascertain that.) Thus the deposit was not highly soluble in the n-hexane.

The deposit accumulation from the dry wash procedure with a two hour hot soak time was, within the limit of experimental error, the same as that from the dry procedure. Thus deposit was formed primarily in the first two hours of the soak time. The remaining fuel substances (unreacted or partially reacted hydrocarbons, including the deposit precursors) in the liquid fuel film either evaporated (in the dry procedure) or washed away by the solvent (in the rinse procedure). In either case, they did not substantially contribute to the deposit.

The deposit formations with the rinse procedure at 0.5 and 1 hour soak times were, however, substantially lower than the dry or rinse at 2 hour procedures. There were insufficient data to discern the difference in deposit accumulation rates between the 0.5 and 1 hour rinses. The data did support that higher washing frequency decreases the deposit conversion rate or deposit yield. The appearance of some the substrates at

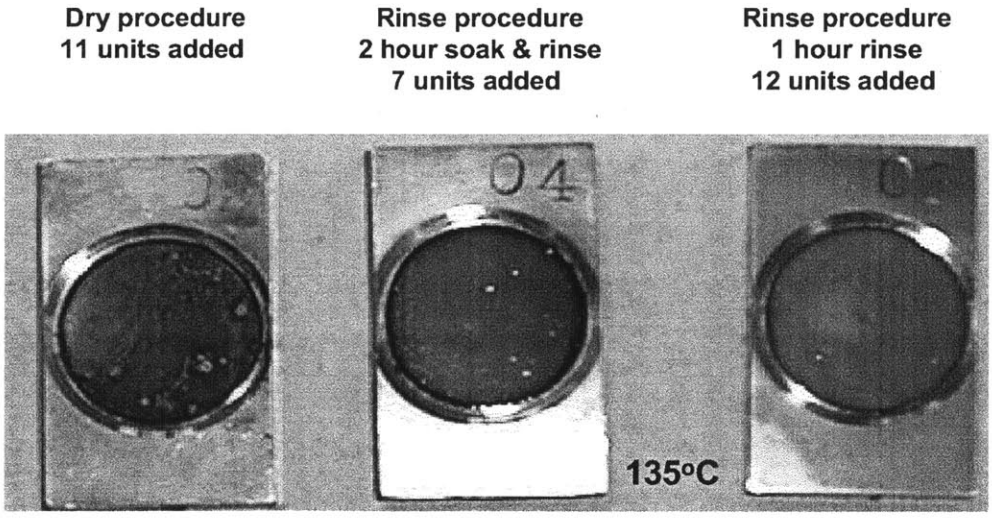

Figure 6-5: Appearance of substrates at the end of the film reactor testing.

the end of the tests are shown in Fig. 6-5. The brown deposit from the dry (after 11x 200 μL of fuel added) and from the 2 hour soak and rinse (after 7x200 μL fuel added) procedures had similar appearance. The deposit obtained from the rinse procedure with a 1 hour soak and rinse, however, appeared much lighter, although the total amount of fuel added to the substrate (12x200μL) was similar to the dry procedure and was substantially larger than the 2 hour soak and rinse procedure. Thus much of the potentially deposit forming fuel substance had been washed away in this case.

6.2 Hot Tube Film Reactor

The Thin Film Reactor (TFR) with the heat, rinse and weight procedure was easy to use, but it had shown several shortcomings:

- The temperature of the heated sample is limited to about 200 C because at higher temperatures, the fuel evaporated too fast (boiling) so that it is difficult to control the heating time.

- The rinse was done with n-hexane instead of with diesel fuel since it would be difficult to dry the sample with the latter.

- When testing fuels with additives, the results are not distinguishable with those without additives.

- The deposit produced from the thin film reactor does not have the same chemical composition as the one obtained in engine experiment. In specific, the deposit from engine testing has highly condensed structure and short-chain alkylaromatics while deposit from thin film reactor has low condensed structure and long chain aliphatics. This may due to the more severe oxidization in Engine testing.

To circumvent these operating difficulties, a new injector deposit simulation apparatus - Hot Tube Film Reactor (HTFR) had been designed and tested.

6.2.1 Apparatus Design

The intend of this design is to simulate the essential deposit formation processes in real engine, which include the emptying out of the fuel from the injection nozzle due to the fuel inertia at the end of the injection process, the evaporation of a thin fuel film and also the fuel washing effect on the deposit and precursors in the next injection.

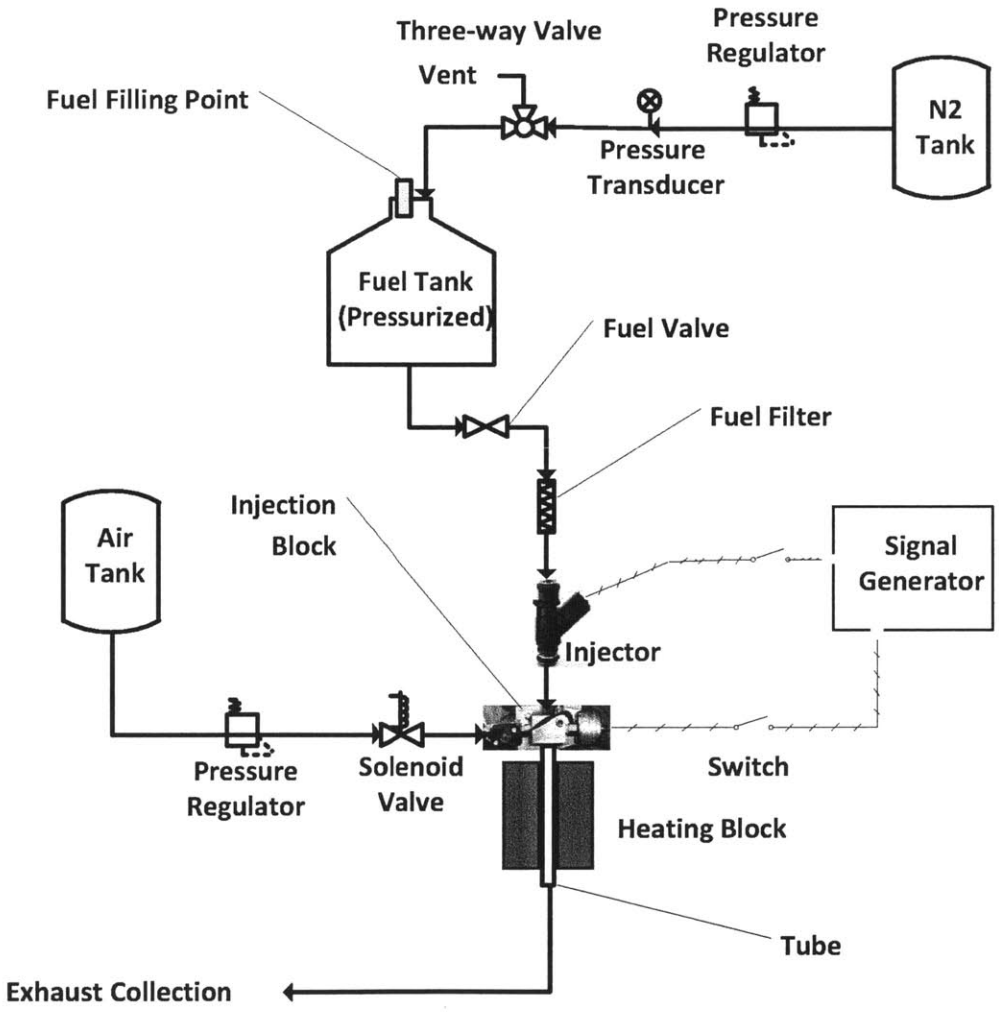

Figure 6-6: Diagram of Hot Tube Film Reactor (HTFR).

A solenoid valve and a flow restrictor is originally used to meter the amount of fuel per pulse. Because of the slow response time of the solenoid valve, the fuel delivered

is not repeatable for small amount of fuel. A commercial gasoline injector (for the Nissan MR18DE engine; used in the MY2006 Versa vehicle) is then used. The testing system is shown in Fig. 6-6. The system can be divided into 4 sub-systems: The Fuel line, Air line, signal line and Exhaust treatment system:

- Fuel line. The fuel tank is presurized using Nitrogen and the pressure is controled using a pressure regulator and transducer. This pressure P_{fuel} determins the amount of fuel coming out of the injector.

  The bottom of the fuel tank is connected to a commercial gasoline injector which is used to meter fuel into the injection block. The injection block is shown in Fig. 6-7 . Its upper part can fit in the injector while the lower part is connected with the steel tube. Inside the injection block, the fuel line meets with the air line, and eventually with the air pulse coming in, the fuel is blowed out of the injection block. The fuel then flows through the heated tube and gets dumped into the exhaust treatment system.

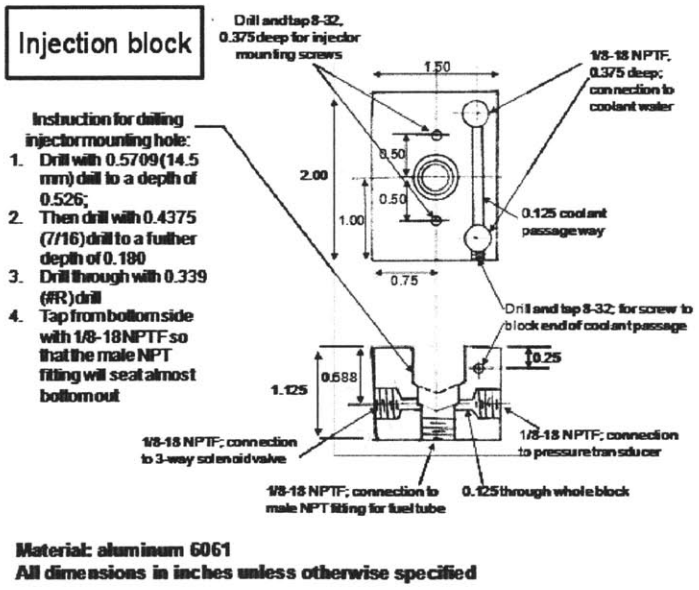

Figure 6-7: Design of injection block of HTFR.

- Air line. The air line is composed of an air tank, a pressure regulator and a

solenoid valve. The line serves two functions. First, it provides oxygen which could be dissovled into the fuel film. second, it pushes the fuel out of the injection block by pressure force.

- Signal line. The signal line is comprised of signal generators, switches and an oscilloscope. The signals control the injector and the solenoid valve at the left side of the injection block. The oscilloscope is used to read the air pressure as well as the fuel/air pulse widths.

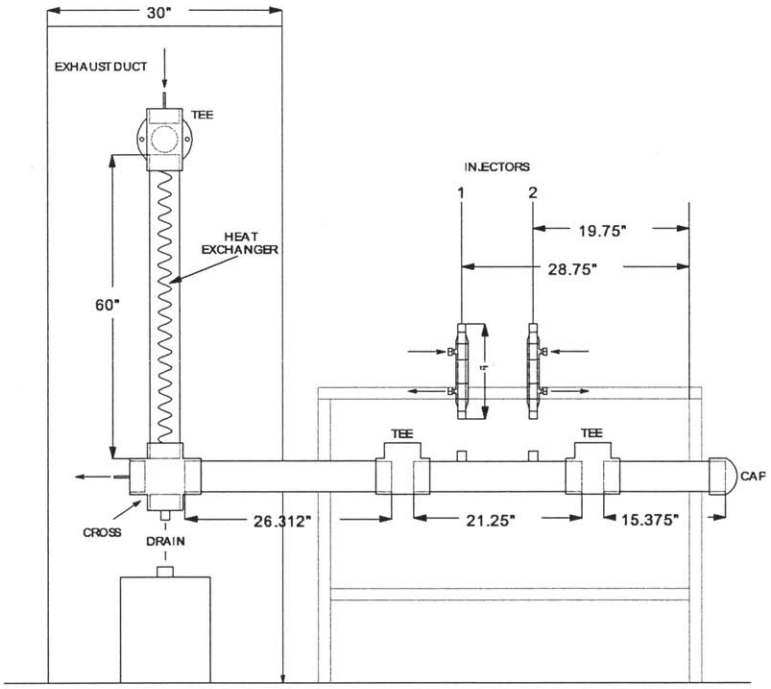

Figure 6-8: Design of exhaust system of HTFR.

- Exhaust treatment system. The system is shown in Fig. 6-8 which includes a heat exchanger, a exhaust duct and a tank collecting waste fuel. The heat exchanger is used to condense the fuel vapor in the mixture coming out of the heated tube. The exhaust duct is slightly titled to make sure the fuel drains into the waste tank.

A whole picture for the apparatus is shown in Fig. 6-9.

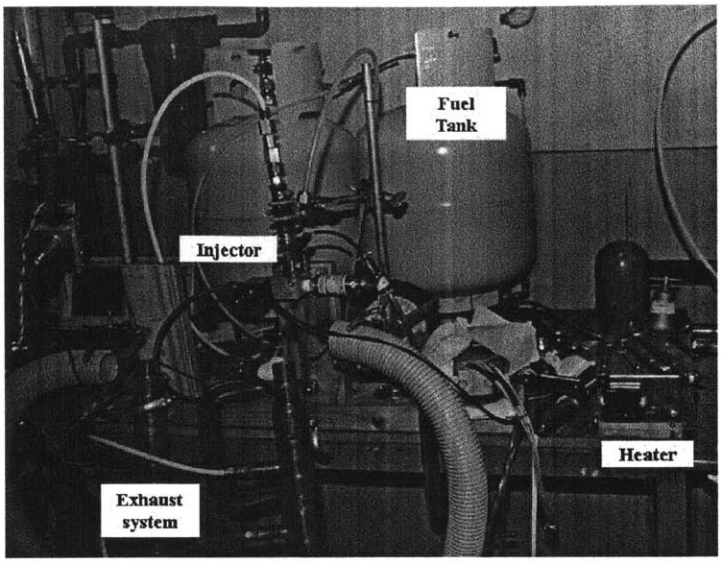

Figure 6-9: Picture of HTFR.

6.2.2 Testing Procedures

In Hot Tube Film Reactor, dry procedure was not used anymore since it was not what happened in the engine test. Instead, we will use the washing procedure most of the time. The following is what happened during one injection cycle with the signal pulses shown in Fig. 6-10.

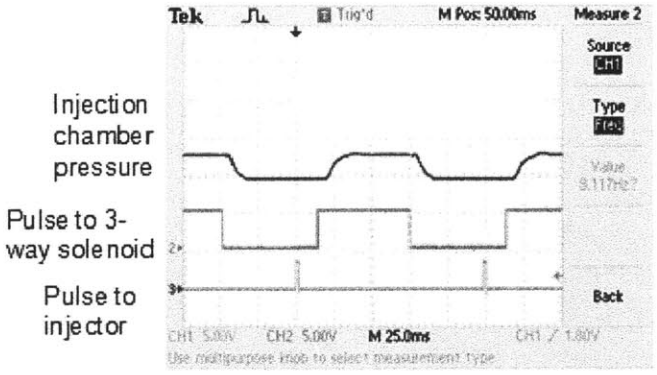

Figure 6-10: Timing of injection and air blow out pulses.

During the fuel pulse, fuel was injected into the hole inside injection block. Due

to the surface tension, the fuel sit on top of the tube. Then the air pulse came in, air blowed the fuel through the heated tube. After the air pulse, the fuel film left on the tube wall was heated and went through evaporation and reaction processes. And we had deposit formation on the wall. A new fuel pulse came in, fuel sit on top of the tube. With the next air pulse, fuel went through the tube, washing some of the deposit away while some fuel was again left inside the tube. The fresh film went through physical/chemical processes and we had new deposit formation. The total deposit included this new deposit and those which wasn't washed away. Finally, The cycle repeated.

Note that the above procedure is quite similar with the deposit formation process in real engine environment, as described in Chapter 3.

6.2.3 Testing Results

First, tests were conducted with Air and Nitrogen blowing out the fuel respectively. The results are shown in Fig. 6-11. We can see with more oxygen in Air, the deposit formation is enhanced significantly.

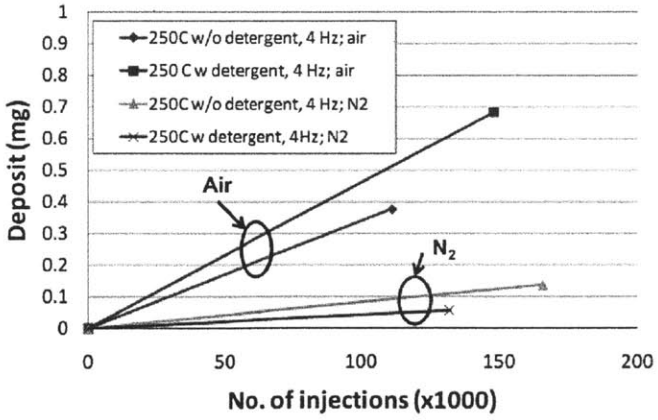

Figure 6-11: Deposit Accumulation in HTFR with Air and Nitrogen. Two fuels were Tested with each gas.

The deposit profiles of a special diesel under different temperatures are shown in

Fig. 6-12. The fuel pressure is 1.5 psi. There is only small amount of deposit when heating temperature is less than 250 C. The deposit accumulation rate as a function of temperature is shown in Fig. 6-13. A linear regression line is also shown on the plot. The perfect linear relationship may due to co-incidence since when temperature goes over the boiling point of all diesel components, there maybe no liquid inside the tube.

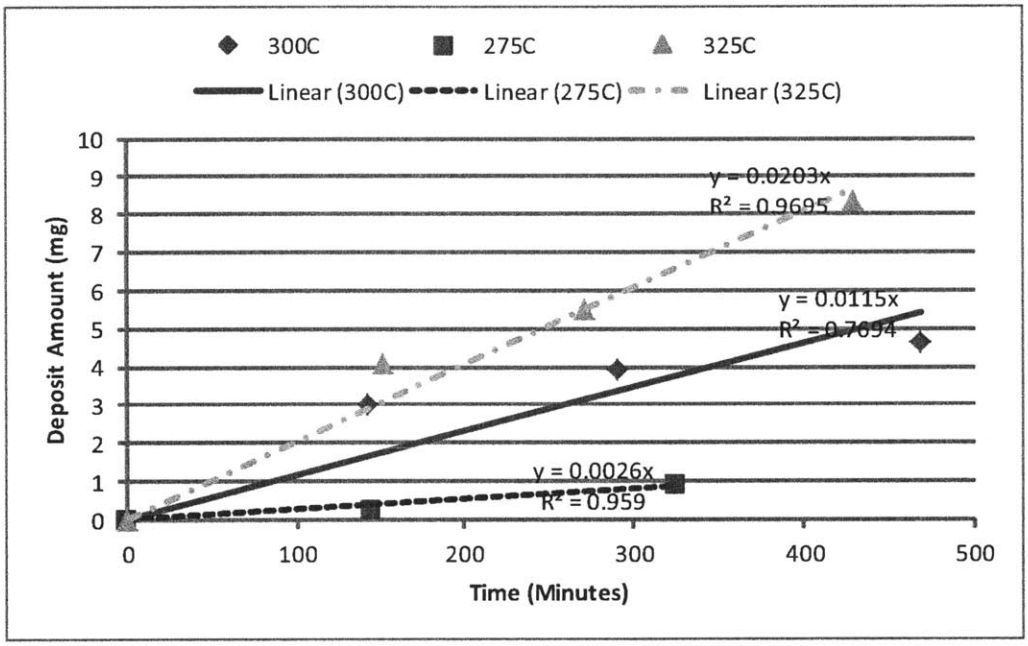

Figure 6-12: Deposit Profiles under different temperatures.

The deposit profiles of a special diesel under different air driven pressures are shown in Fig. 6-14. The fuel pressure is 1.5 psi and heating temperature is 300 C. We can see the larger air pressure, the smaller deposit accumulation. With a larger pressure, the flow inside the pipe has a higher velocity, but in the same time, the injection duration is shorter. Notice that in the laminar washing model, the flow velocity is not that important. Hence, if the air pressure only induces the amount of washing, higher pressure should have larger deposit accumulation rate thanks to the shorter injection duration, which is not correct with the measurement.

The main effect of high air pressure, however, is the resulting change of film

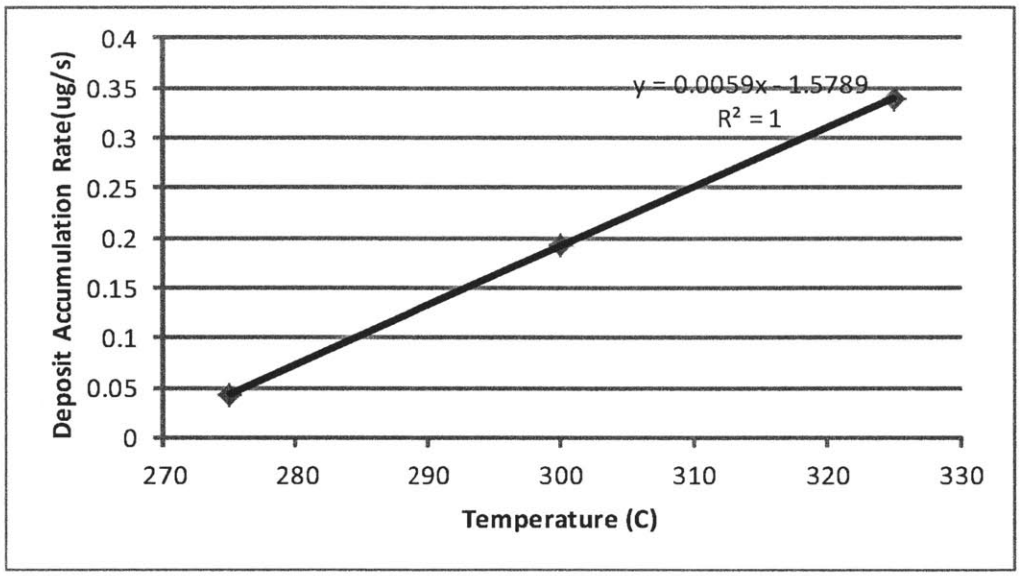

Figure 6-13: Deposit Accumulation as a function of heating Temperature.

Pressure (KPa)	Deposit accumulation rate (ug/s)	Film thickness(μm)
18.2	0.23	16.5
34.7	0.17	12.9
51.3	0.08	10.7

Table 6.2: Tube Film Thickness Measurement and deposit formation

thickness. Based on our film formation model, higher velocity has a thinner film thickness. The film thicknesses under different air pressures are also measured and shown in Table 6.2. And the deposit accumulation rate as a function of the film thickness is shown in Fig. 6-15. A linear regression line is also shown on the plot. We can see a thicker fuel film has a larger deposit accumulation.

The deposit profiles of a special diesel under different fuel injection pressures are shown in Fig. 6-16. The heating temperature is 300 C. The deposit accumulation rate as a function of fuel injection pressure is shown in Fig. 6-17. A linear regression line is also shown on the plot. It can be seen that the deposit accumulation dimishes with higher injection pressures. In our test design, higher injection pressure means more fuel is injected into the hole. In the subsequent air pulse, that means the injection

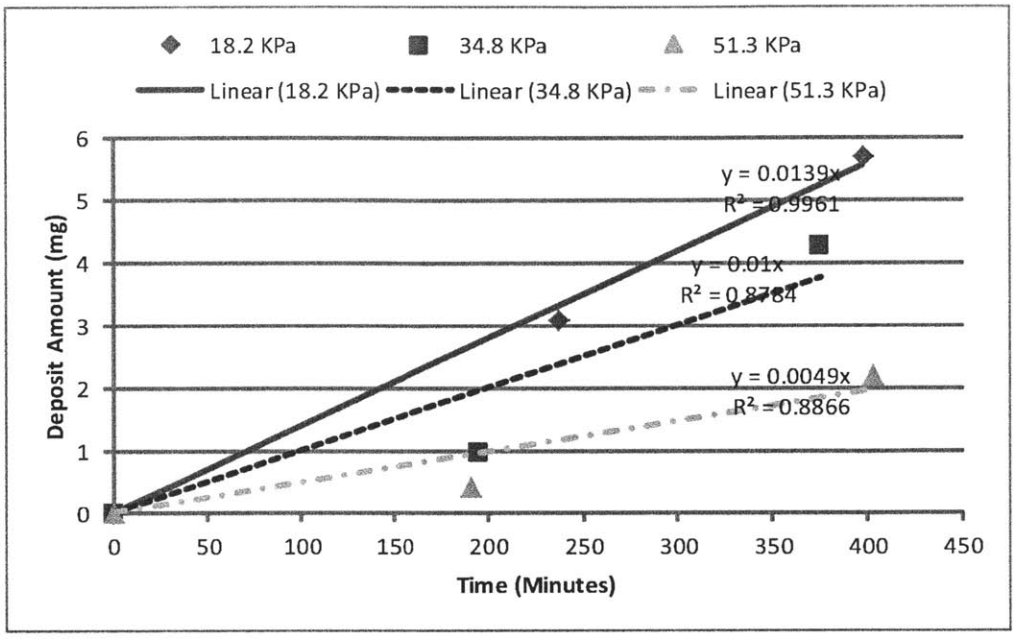

Figure 6-14: Deposit Profiles under different air pressures.

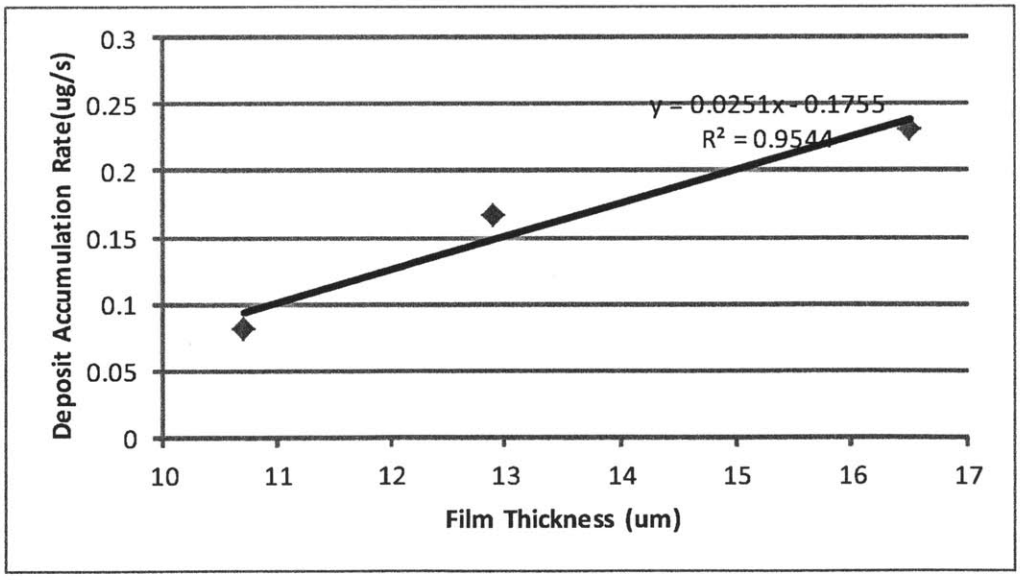

Figure 6-15: Deposit Accumulation as a function of film thickness.

interval gets longer. Hence, the washing effect again plays an critical role here.

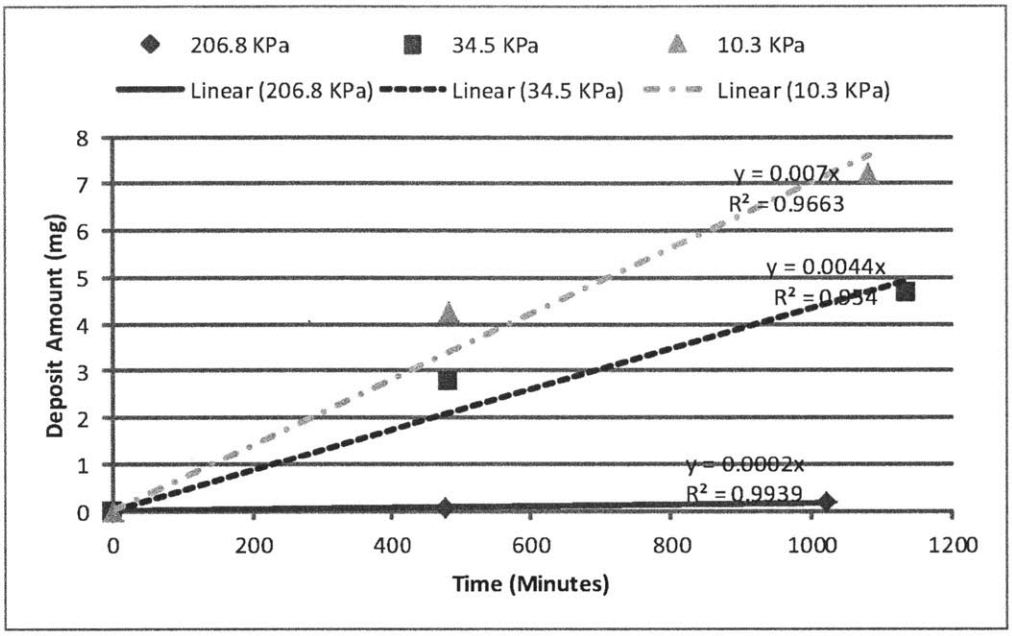

Figure 6-16: Deposit Profiles under different fuel injection pressures.

The deposit accumulation per injection as a function of fuel injection frequency is shown in Fig. 6-18. A linear regression line is also shown on the plot. It can be seen that the deposit accumulation increases with lower injection frequencies. In our test design, lower freqency means longer heating time in one injection.

The deposit profiles of a special diesel under different air pulse widths are shown in Fig. 6-19. We can see that neither longer or shorter air pulse width gives a higher deposit accumulation. To understand the reason behind this, the injected fuels under different air pulse widths are measured and shown in Fig. 6-20. We see an interesting behavior, the injected fuel gets flat after certain pulse width. The platueau is the amount of fuel in the hole before the air pulse. For even longer air pulse width, since all fuel were already blowed out, the air kept flowing through the fuel film and the film got thinner, and hence lower deposit accumulation rate. For the shorter air pulse width, not all the fuel sitting on the hole were blowing out. After some injections, the leftover fuel during each injection added up and the fuel would leak and flow

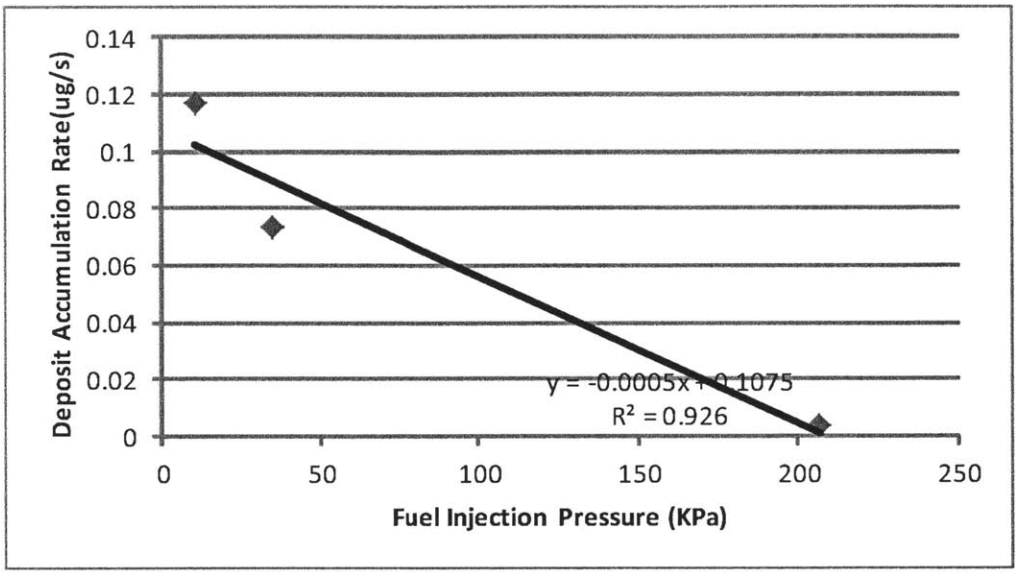

Figure 6-17: Deposit Accumulation as a function of fuel injection pressure.

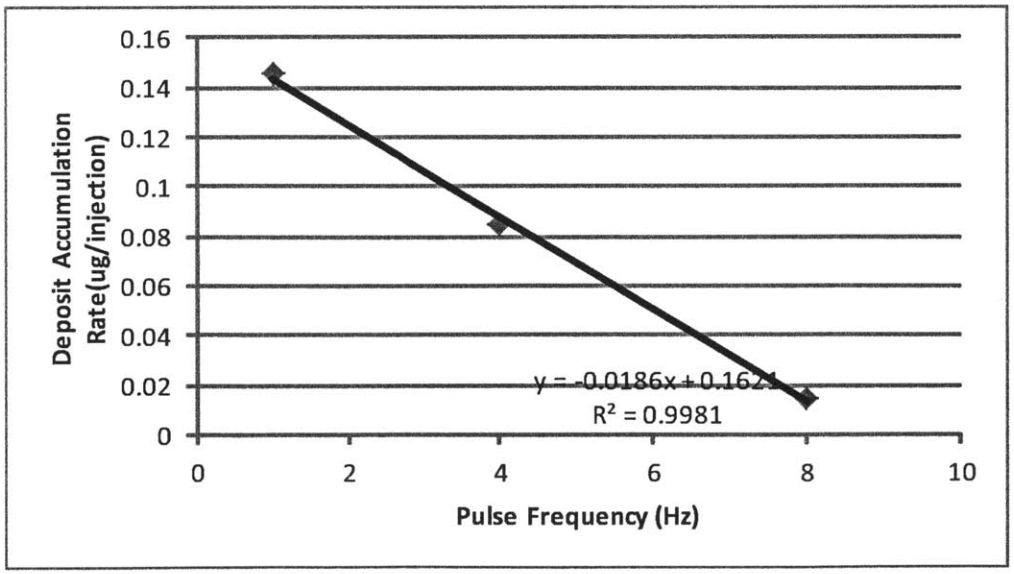

Figure 6-18: Deposit Accumulation as a function of fuel injection frequency.

through the tube. This continous fuel flow enhanced the washing effect and hence again smaller deposit accumulation rate.

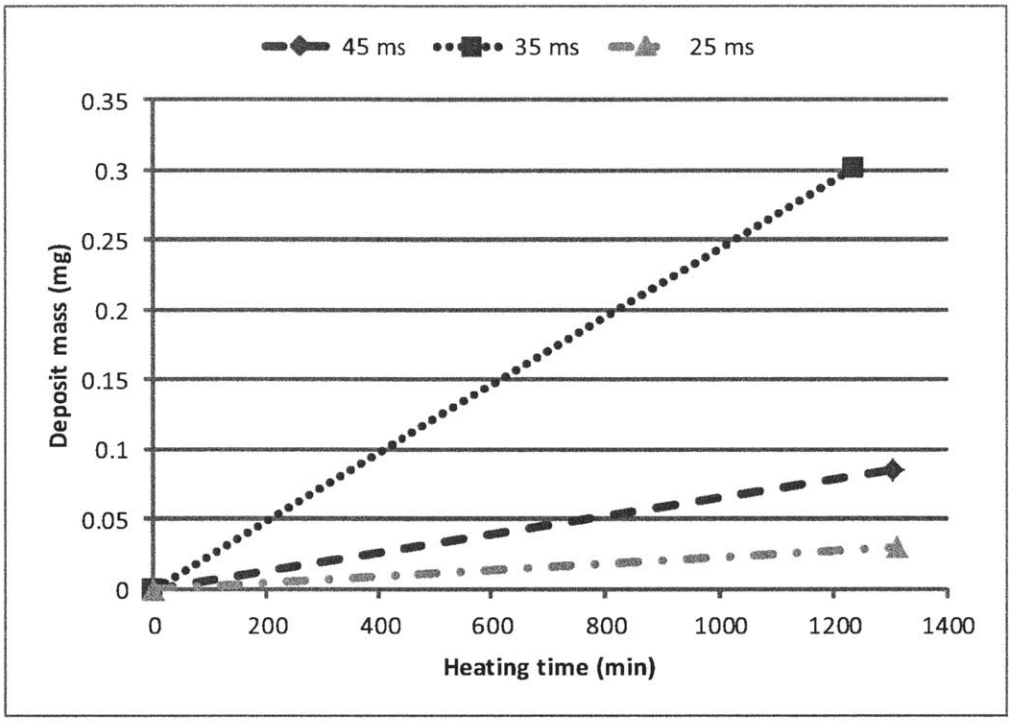

Figure 6-19: Deposit Profiles under different air pulse widths.

The air-fuel pulse gap is the amount of time between the end of fuel pulse and the start of air pulse. Generally speaking, this parameter should not have an effect to the final deposit formation since the heating time is same (from the end of air pulse to the start of air pulse). The deposit profiles of a special diesel under different pulse gaps are shown in Fig. 6-21. The fuel pressure is 1.5 psi and temperature is 275 C. We see that the shorter gap (30 ms) has a larger deposit formation rate, although at only a small enhancement. This may due to the design of the bench-scale apparatus. After the fuel pulse, the injected fuel will stay in the hole. Since the injection is not uni-directional. Fuel should everywhere inside the hole. When the gap is larger, those fuel on the side wall gets more time to flow back to the bottom hole. Then when the air pulse comes in, the larger gap has more fuel to blow out, i.e., longer

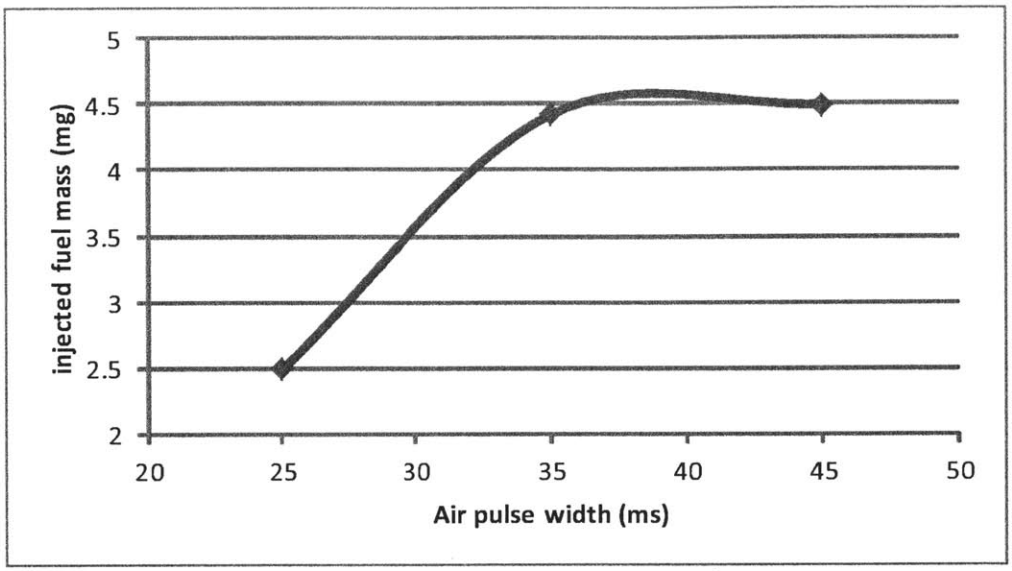

Figure 6-20: Injected fuel amount under different air pulse widths.

injection duration. Hence, with a little bit more washing effect, we see a smaller deposit accumulation rate with a longer pulse gap.

Zinc is known for acclerating the deposit formation process [cite todo]. The zinc compound we used is $Zn(C_{10}H_{19}O_2)_2$, its molecular weight is 407.89 g/mol. Its elemental composition is shown in Fig. 6-22. We tested the deposit formation with 3 ppm Zinc and without Zinc with two fuels: A commercial Diesel from US market and a special Diesel called PR49. The results are shown in Fig. 6-23. We can see zinc does promote the deposit formation in all cases.

6.3 Comparisons of Deposit Formation Rates

Let us review what we have achieved so far. Our goal is to understand the deposit formation inside diesel injector nozzles. To do that, we developed a software package to simulate the deposit formation rate, we also established a testing apparatus which can measure deposit formation rate. The question now is how the deposit formation rates relate to each other.

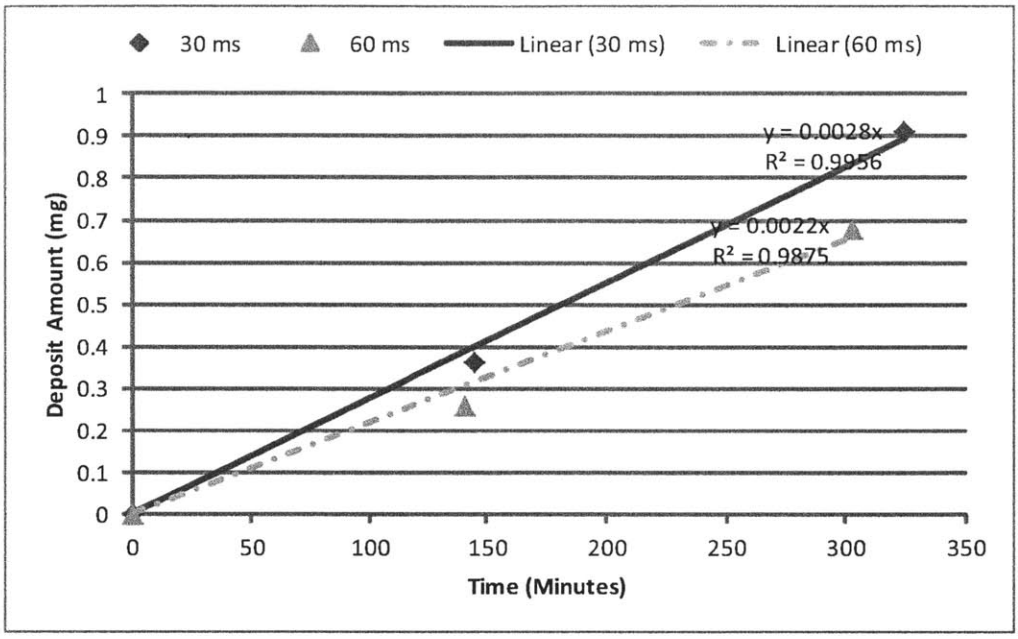

Figure 6-21: Deposit Profiles under different pulse gaps.

For injector nozzles, the deposit formation rate is around 10^{-12} g/mm2/cycle if we assume the deposit density is around $2000kg/m^3$ and the average deposit thickness is around 5 um. And if we simulate the formation in the software package with the engine nozzle geometry and conditions, the output is around $10^{-15}g/mm^2/cycle$. The model under-estimates the actual deposit formation.

For the lab tests, the deposit formation rate is around $10^{-11}g/mm^2/cycle$ if we assume 40 ms cycle length. Notice this rate is higher than that of engine injector nozzles, which is due to the smaller washing effect and thicker film thickness. This large deposit outcome in lab testing saves testing time and money. And the software gives a rate of $10^{-13}g/mm^2/cycle$ for the lab settings.

The modeling results consistantly under-estimate the experimental data. This is because all deposit are affected by the next injection (washing effect) in our current model which may not be true. Some of the deposit may go through secondary reactions or have reactions with the metal, hence some deposit will get "'sticky"' and stay on the surface after the injection. In other words, our current model over-estimate

Elemental composition

	number of atoms	mass fraction	atom fraction
C (carbon)	20	58.9%	31.7%
H (hydrogen)	38	9.39%	60.3%
O (oxygen)	4	15.7%	6.35%
Zn (zinc)	1	16%	1.59%

Zn(C10H19O2)2 WolframAlpha

Figure 6-22: Elemental composition of the zinc compound.

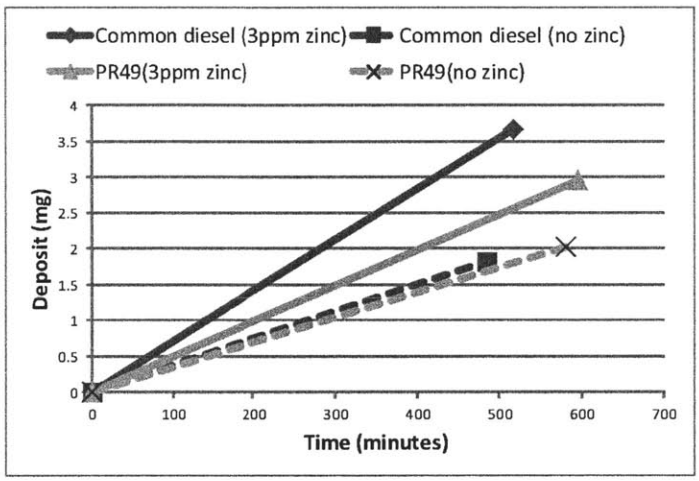

Figure 6-23: Deposit Accumulation in HTFR with and without Zinc. Two fuels were Tested in each case.

the washing effect and hence gives a smaller deposit outcome.

6.4 Detergency Testing

After serving the goal of validating model development, the next goal would be to serve the industry on detergency screening. Generally speaking, the detergents can prevent deposit formation in three ways:

- Keep Clean or dispersancy Action. In this mode, the detergent moleculars

attach to the dirt (deposit pre-cursors) surface and form micelles, hence prevent the further aggregation of dirt by steric exclusion as shown in Fig. 6-24 a.

- Clean up action. In this mode, the dirt is already aggregated on the wall. The detergent molecules attach themselves with the deposit and make it easy for the next injection to wash the deposit molecules away as shown in Fig. 6-24 b.
- Film formation action. In this mode, the detergent molecules are attached to the wall first. Then it is harder for deposit molecules to be attached on the wall as shown in Fig. 6-24 c.

We will focus the first two effects which are mainly used in the oil industry. The goal is to develop testing protocols so that the bench-scale apparatus could be used to complement the engine testing.

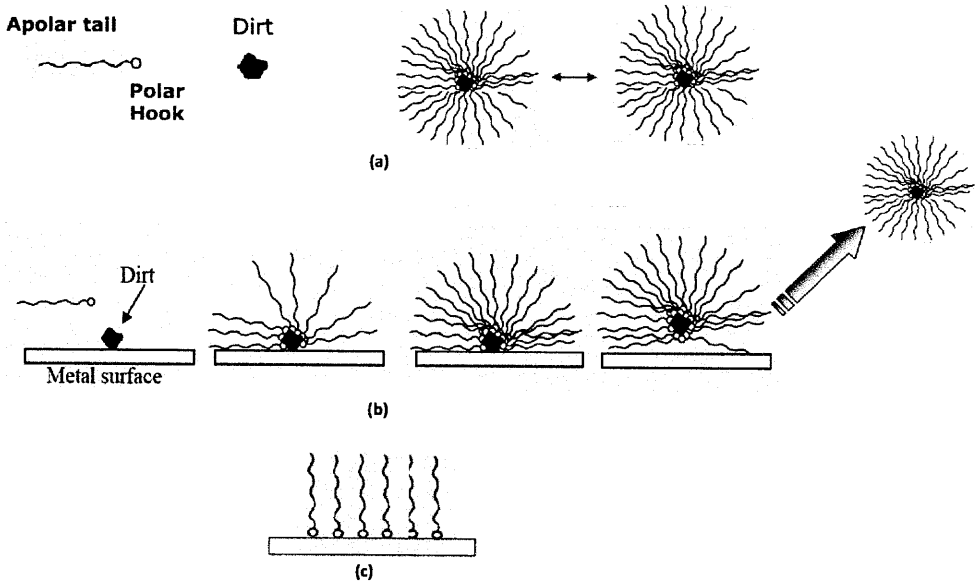

Figure 6-24: Detergent modes of actions.

6.4.1 Keep-Clean Test

In keep-clean tests, different fuels are tested using a clean tube and the tube mass are recorded with the heating time passed. Fig. 6-25 shows a testing result with nine

Heating Temperature	250 C
Tube length	50 mm (2 "')
Period of one complete cycle	125 ms
Fuel tank pressure	20 psi (137.9 kPa)
Fuel pulse width	2 ms
Air drive pressure differential	7.2 psi (49.6 kPa)
Air pulse width	50 ms
Pulse Gap	33 ms

Table 6.3: Condition for trial keep clean testing.

different fuels under condition in Table 6.3. The test took a long time and the results were not distingiushable nor repeatable. Part of the reason is the small amount of deposit differences (level of 0.01 mg) which exceed the precision of the balance.

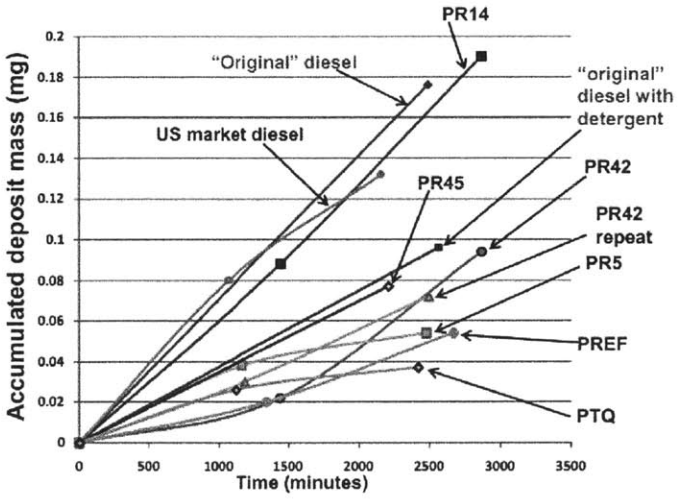

Figure 6-25: Deposit accumulation using the bench scale heated fuel tube apparatus.

A new testing protocol is developed to address the problems and is shown in Table 6.4. The testing result for different fuels without Zinc contamination is shown in Fig. 6-26. There is substantial difference in the deposit formation between different fuels and fuels with different detergents. Comparing the data of Fig. 6-26 to those of Fig. 6-25, the deposit accumulation rate has been enhanced by about an order of magnitude with the elevated temperature and decrease of washing. The results are in good match with those from Engine testing which are not shown here.

Heating Temperature	300 C
Tube length	76.2 mm (3 "')
Period of one complete cycle	125 ms
Fuel tank pressure	1.5 psi (10.3 kPa)
Fuel pulse width	2 ms
Amount of fuel injected per injection (from calibration)	0.534 mg
Air drive pressure differential	7.2 psi (49.6 kPa)
Air pulse width	40 ms
Pulse Gap	33 ms

Table 6.4: A Keep Clean testing protocol.

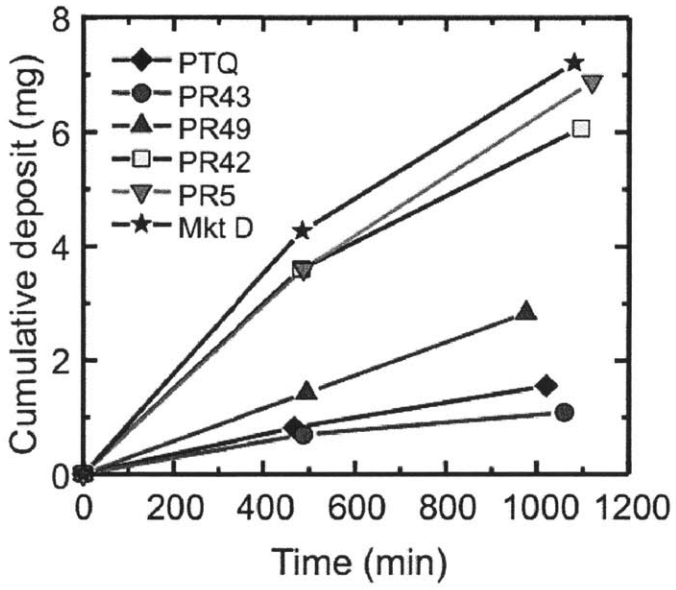

Figure 6-26: Deposit formation with the keep clean protocol to enhance deposit formation; no zinc has been used in this set of data.

The keep clean protocol is further used to test different fuels with Zinc contamination. The result is shown in Fig. 6-27. When the 3 ppm Zinc is added to the fuel, the fuels without detergent (the market diesel and the PTQ fuel) show remarkable increase in the deposit formation rate. The fuels with detergents (the remaining fuels) show some or no increase in the formation rate. Again, the results are in good match with those from Engine testing which are not shown here.

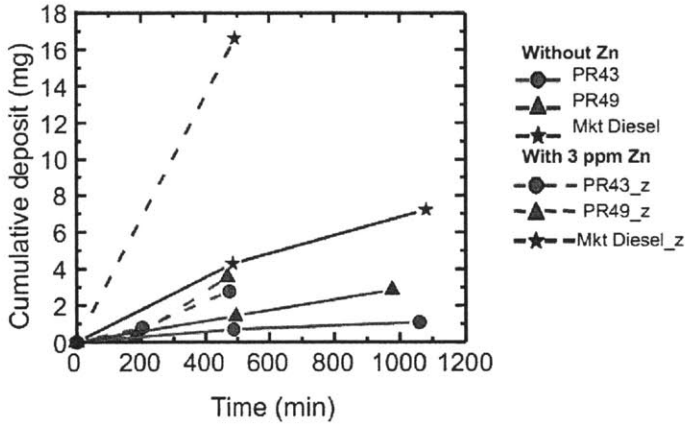

Figure 6-27: Deposit formation with the keep clean protocol to enhance deposit formation; 3 ppm zinc has been used in this set of data.

6.4.2 Clean-Up Test

The clean-up ability of detergent fuel is then assessed. To assess the clean-up effect, a fixed amount of deposit in the tube using a regular diesel without detergent and with the 3 ppm Zinc is accumulated using the protocol in keep-clean testing. Then different test fuel with the detergent is applied and the new rate of accumulation is measured.

After a lot of testing, the clean-up testing protocol is summarized in Table 6.5. And the result using the protocol is shown in Fig. 6-28 for 4 different fuels:

- Diesel fuel with additive PR49 (a proprietory detergent) without Zinc

Heating Temperature	300 C
Tube length	76.2 mm (3 "')
Period of one complete cycle	125 ms
Fuel tank pressure	16 psi (110.3 kPa)
Fuel pulse width	2 ms
Amount of fuel injected per injection (from calibration)	2.63 mg
Air drive pressure differential	7.2 psi (49.6 kPa)
Air pulse width	40 ms
Pulse Gap	33 ms

Table 6.5: A Clean-up testing protocol.

- Diesel fuel with additive PR49 as well as 3 ppm Zinc
- Diesel fuel with additive PR55 (another proprietory detergent) without Zinc
- Diesel fuel with additive PR55 with 3 ppm Zinc

The results show that the PR55 additive is not effective for clean-up while the PR49 without zinc gives pretty good negative deposit accumulation rate. However, When zinc is added to the PR49, the accumulation rate is approximately zero - the clean up action balances the new deposit formation. These general results are in consistant with those from Engine testing which are not shown here.

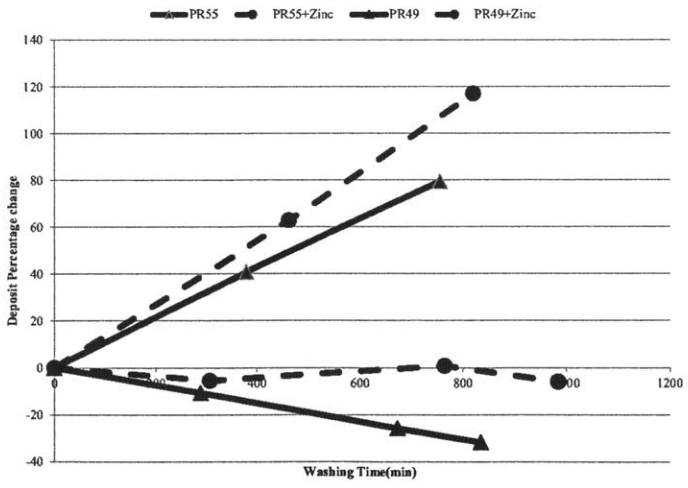

Figure 6-28: Deposit formation with the clean up protocol.

But the sudden deposit decrease which is observed in engine testing (shown in Fig. 6-29) is not presented in the bench scale testing. This doesn not mean the testing is not accurate, instead, the result is the consequence of the design decision. In our bench scale test design, we avoided high pressure for easier safty considerations. Let us compare the wall shear stress in the lab test and the engine nozzles.

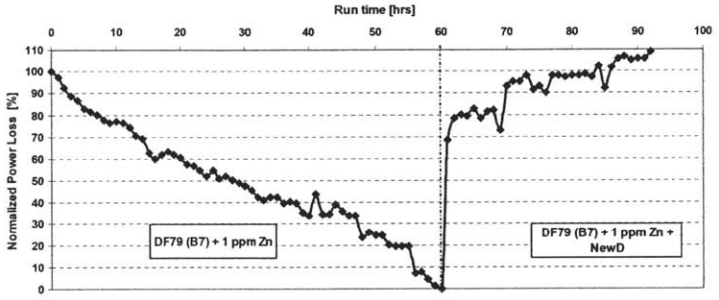

Figure 6-29: Normalised power loss- DW10 clean up performance of new diesel detergent technology at treat rate which is typical for premium diesel fuel.

In lab test, since it is a laminar pipe flow. We have an equation for the wall shear stress:

$$\tau_w = -\frac{\Delta P D}{4L} \tag{6.1}$$

Using our lab testing conditions, the wall shear stress is around 400 Pa. The wall shear stress is more complicated in the engine nozzles, nevertheless, we can use the law of the wall. The logarithmic law of the wall (shown in Equation 6.2) is a self similar solution for the mean velocity parallel to the wall in turblent pipe flows. It is an approximation which is accurate enough for our purposes here.

$$\frac{u}{u^*} = \frac{1}{k} \ln \frac{y u^*}{\nu} + 5.0 u^* = \sqrt{\frac{\tau_w}{\rho}} \tag{6.2}$$

where k is Von Karman constant (0.41) and y is the distance from the wall. We assume the centerline velocity is 500 m/s, then we can solve the equation and get

$u^* = 20.16$, then we have:

$$\tau_w = \rho u^{*2} = 3.25 \times 10^5 Pa \tag{6.3}$$

Now the shear strength of common metals is in the order of 100 MPa [2]. However, for the polymers (like PBT, PC, POM etc.), their strength is in the order of 0.05 MPa which is smaller than the wall shear stress inside the nozzle. Hence, if the detergent makes polymer structure inside the deposit, the flow in nozzle is able to wash them away, while the flow in the tube is not "'strong"' enough.

Chapter 7

Conclusion

Deposit formation inside diesel injector nozzles is an important consideration for the development of new generation FIE with high efficiency nozzles. While traditional research focuses are on Engine testing and quanlitative deposit formation mechanisms, this work is on the development of quantitative modeling and bench-scale testing of deposit formation. There are three major contributions of this work:

- A new mechanism of deposit formation is proposed which correcly identifies the heavy deposit formation in the outer half of nozzle close to the combustion chamber end.
- The hot tube apparatus is established as a bench scale lab apparatus which simulates film formation, evaporation and washing in the deposit formation process.
- The integrated deposit formation model combines physical processes (film formation, evaporation and washing) with liquid chemistry to calculate the deposit formation rate quantitatively.

From this study, the following conclusions could be made:

1. A bench scale deposit formation testing apparatus is established. It can be used to simulate the essential processes in deposit formation such as film formation, evaporation and washing. The apparatus offers additional flexibility that is

complementary to engine testing since control parameters such as temperature and washing could be adjusted easily.

2. Protocols for testing keep-clean and clean-up detergency effects are proposed. Benchmark tests are done using fuels with different detergents and the ranking results are in agreement with those from engine testing. Compared to engine testing, the apparatus and protocols require less testing time and lower testing cost.

3. An integrated quantitative model for the deposit formation is developed. It includes detailed modeling for film formation, evaporation and washing. Using reaction mechanism generator (RMG) software, detailed chemistry of liquid phase reactions are implemented. The modeling results under-estimate the lab test experimental data because the current model doesn't include secondary oxidization and reactions with metals.

4. The effects of important parameters such as heating temperature, heating time and washing intensity are studied using both lab scale testing and the integrated model. Although the computed and observed deposit formation rates are not the same, the trends are matched which supports the quantitative model.

Although a significant amount of insight has been gleaned into the nature of deposit formation within diesel injector nozzles, only the tip of the iceberg has so far been studied. For example, the micoscopic properties of the deposit needs to be studied. This includes not only the components or elements, but also the physical and chemical properties. We can also extend our chemistry models to include secondary oxidizaiton and bio-fuel reaction mechanisms.

Our bench scale testing apparatus also opens a new world for the deposit study, for example, the following questions could be asked:

- What's the effect of the metals? Is there any difference if we use Aluminium tube, Zinc tube other than the steel tube?

- What's the effect of the viscosity of fuel? We now know thin film gives small deposit. Could we tune the viscosity somehow to avoid the deposit?

- How about the roughness of tube to the deposit formation? We can coat small blocks on the inner side of the tube and examine the deposit accumulation. More recently, super-hydrophobic surfaces are getting more and more attention, could we use that to derease the deposit formation?

All these questions have practical implications and could be answered with our lab testing apparatus.

Appendix A

Injector Components

The specifications of the injector components were based on a modern common rail diesel injector (Siemens DW10 prototype injector). The dimensions and component masses are shown in Fig. A-1 and A-2. The details of the needle closing geometry are shown in Fig. A-3.

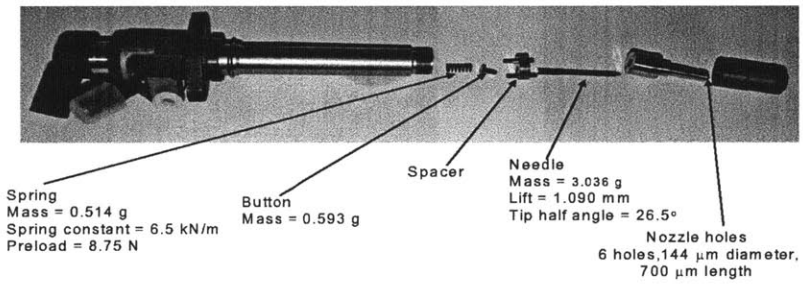

Figure A-1: Siemens DW10 injector components.

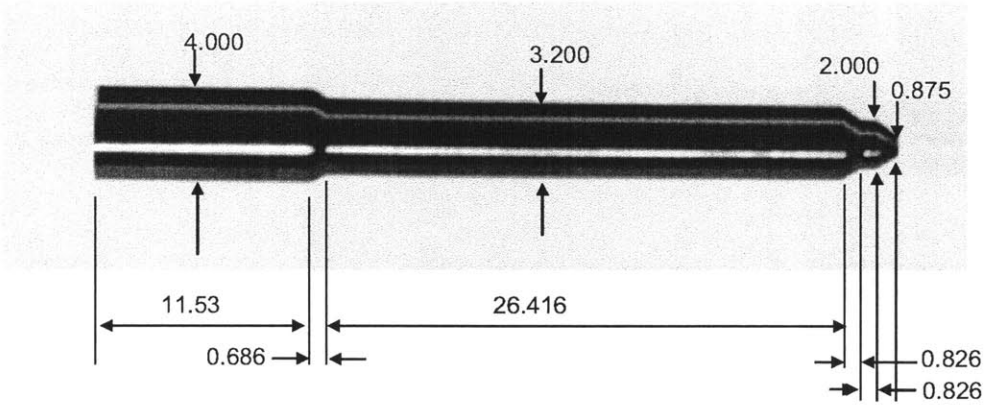

Figure A-2: Dimension of needle; all values in mm.

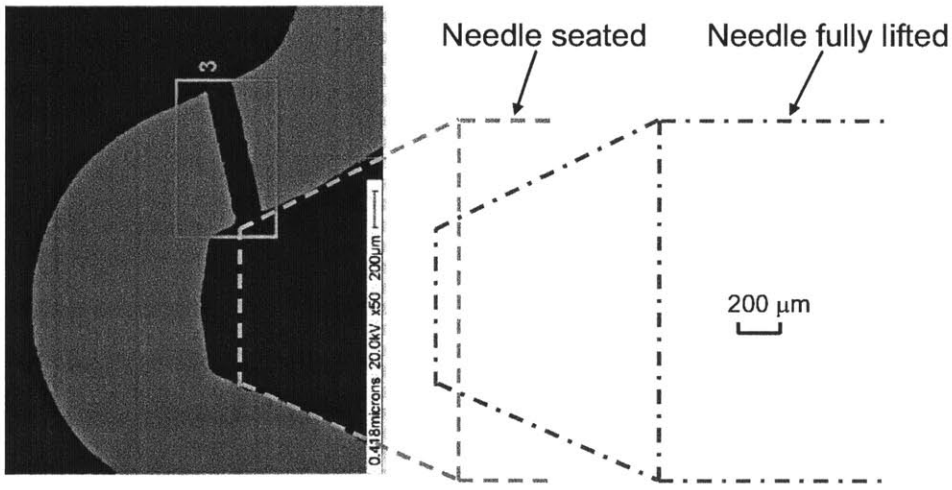

Figure A-3: Superposition of needle on cut-out section of injector nozzle; needle at seated and fully lifted positions.

Appendix B

Diesel Fuel Properties

The properties of a typical diesel fuel, from which the fuel surrogate is developed, are shown in Fig. B-1. It consists of only saturates and aromatics. The saturates comprise mostly paraffins. The aromatics are mostly alkyl benzenes and naphthenbenzenes at almost the same amount of each, with a slightly larger amount of the alkyl benzenes.

Density at 15°C	g/cm3	0.8309
Nitrogen	ppm wt	1.5
Sulfur	Mg/kg	26.4
Distillation D86	-	
IBP	°C	178.0
5%v	°C	211.5
10%v	°C	225.5
50%v	°C	279.5
90%v	°C	339.0
FBP	°C	368.0
Cetane index (4V)	-	58.0
Aromatics (HPLC)	-	
Monoaromatics	wt%	21.0
Diaromatics	wt%	3.4
Triaromatics	wt%	0.3
Total Aromatics	wt%	24.7
Saturates	wt%	**77.4**
Saturates (0 rings)	vol%	53.4
Saturates (1 rings)	vol%	21.4
Saturates (2 ring)	vol%	16.1
Saturates (3rings)	vol%	7.5
Saturates (4 rings)	vol%	1.7
Aromatics	wt%	**22.6**
Alkyl benzenes	vol%	36.4
Naphthenbenzenes	vol%	30.8
Dinaphthenbenzenes	vol%	12.0
Naphthalenes	vol%	9.6
Acenaphthenes	vol%	5.1
Fluorenes	vol%	2.7
Pyrenes	vol%	1.3
Crysenes	vol%	0.0
Phenanthrenes	vol%	0.1
Naphthene-phenanthrenes	vol%	0.0
Aromatic Thiophenes	vol%	2.2
Unidentified Aromatics	vol%	0.1

Figure B-1: Properties of a typical diesel fuel.

Bibliography

[1] Standard test method for thermal oxidation stability of aviation turbine fuels (jftot procedure).

[2] *Handbook of Chemistry and Physics.* CRC, 2011.

[3] P. Aleiferis A. Birgel, N. Ladommatos, S. Zlch, N. Milovanovic, V. Lafon, A. Orlovic, P. Lacey, and P. Richards. Deposit formation in the holes of diesel injector nozzles: A critical review. *SAE 2008-01-2383.*

[4] W.H. Green A. Jalan, R.H. West. Capturing solvent effects in automatic mechanism generation. In *International Conference on Chemical Kinetics*, 2011.

[5] N. S. Mera M. Pourkashanian D. B. Ingham A. S. Wade, A. G. Kyne and S. Whittaker. Genetic-algorithm optimization of a chemistry mechanism for oxidation of liquid hydrocarbons. *AIAA JOURNAL*, 43:2259, 2005.

[6] M. Abraham and J. McGowan. The use of characteristic volumes to measure cavity terms in reversed phase liquid chromatography. *Chromatographia*, 23:243–246, 1987. 10.1007/BF02311772.

[7] Michael H. Abraham, Adam Ibrahim, and Andreas M. Zissimos. Determination of sets of solute descriptors from chromatographic measurements. *Journal of Chromatography A*, 1037(1-2):29 – 47, 2004. ¡ce:title¿Estimation of Physicochemical Properties by Chromatographic and Electrophoretic Techniques¡/ce:title¿.

[8] Herbert M. Scull Jr. Allen A. Aradi, William J. Colucci and Martin J. Openshaw. A study of fuel additives for direct injection gasoline (dig) injector deposit control. *SAE 2000-01-2020.*

[9] Pavlos Aleiferis Andreas Birgel, Nicos Ladommatos, Nebojsa Milovanovic, Paul Lacey, and Paul Richards. Investigations on deposit formation in the holes of diesel injector nozzles. *SAE 2011-01-1924.*

[10] YUSMADY BIN MOHAMED ARIFIN. *Diesel and Bio-diesel fuel deposits on a hot wall surface.* PhD thesis, GUNMA UNIVERSITY, 2009.

[11] Pascale Aussillous and David Quere. Quick deposition of a fluid on the wall of a tube. *Physics of Fluids*, 12(10):2367–2371, 2000.

[12] J Barker, P Richards, C Snape, and W Meredith. Diesel injector deposits an issue that has evolved with engine technology. *SAE 2011-01-1923.*

[13] Jim Barker, G John Langley, and Paul Richards. Insights into deposit formation in high pressure diesel fuel injection equipment. *SAE 2010-01-2243.*

[14] Rubin Battino, Timothy R. Rettich, and Toshihiro Tominaga. The solubility of oxygen and ozone in liquids. *Journal of Physical and Chemical Reference Data*, 12(2):163–178, 1983.

[15] Rubin Battino, Timothy R. Rettich, and Toshihiro Tominaga. The solubility of nitrogen and air in liquids. *Journal of Physical and Chemical Reference Data*, 13(2):563–600, 1984.

[16] W Bergwerk. Flow pattern in diesel nozzle spray holes. *ARCHIVE: Proceedings of the Institution of Mechanical Engineers 1847-1982 (vols 1-196)*, 173(1959):655–660, June 1959.

[17] F. P. Bretherton. The motion of long bubbles in tubes. *Journal of Fluid Mechanics*, 10:166, 1961.

[18] Linda J. Broadbelt and Jim Pfaendtner. Lexicography of kinetic modeling of complex reaction networks. *AIChE Journal*, 51(8):2112–2121, 2005.

[19] Patrick Gastaldi Lysiane Grosjean Franck Levy Alexandre Michel Bruno Argueyrolles, Stephan Dehoux and Daniel Passerel. Influence of injector nozzle design and cavitation on coking phenomenon. *SAE 2007-01-1896.*

[20] Robert Bunnell. *Unsteady, Viscous, Cavitating Simulation of Injector Internal Flows.* PhD thesis, Purdue University, 1999.

[21] Roger Busch. Advanced diesel common rail injection system for future emission legislation. In *10th Diesel Emission Reduction Conference*, 2004.

[22] J. L. DUDA C. C. JERRY WANG and E. E. KLAUS. A kinetic model of lubricant deposit formation under thin film conditions. *Tribology Transactions*, 37:168–174, 1994.

[23] Rinaldo Caprotti, Angela Breakspear, Olaf Graupner, Thomas Klaua, and Oliver Kohnen. Diesel injector deposits potential in future fueling systems. *SAE 2006-01-3359.*

[24] Rinaldo Caprotti, Angela Breakspear, Thomas Klaua, Peter Weiland, Olaf Graupner, and Martin Bittner. Rme behaviour in current and future diesel fuel fies. *SAE 2007-01-3982.*

[25] Philip P. Mulard ELF Research Center; Philip N. China. Development of a diesel fuel screening test for injector nozzle coking. *SAE 922184.*

[26] Thomas Welton Christian Reichardt. *Solvents and Solvent Effects in Organic Chemistry.* Wiley-VCH, 2011.

[27] Steven H. Collicott and Haiyun Li. True-scale true-pressure internal flow visualization for diesel injectors. *SAE 2006-01-0890.*

[28] Yeon-Talk Kim Collins, R.W. Ellipsometry for thin film and surface analysis. *Analytical Chemistry*, 62, 1990.

[29] E. L. Cussler. *Diffusion: Mass Transfer in Fluid Systems.* Cambridge University Press, 1997.

[30] U.S. Department of Energy Energy Information Administration. International energy annual 2003.

[31] Theodore L. Bergman Adrienne S. Lavine Frank P. Incropera, David P. Dewitt. *Fundamentals of Heat and Mass Transfer.* John Wiley & Sons, 2007.

[32] O. Chiavola G. Chiatti and F. Palmieri. Flow features in reduced dwell time diesel injector. *SAE 2008-01-0927.*

[33] W. H. Green, P. I. Barton, B. Bhattacharjee, D. M. Matheu, D. A. Schwer, J. Song, R. Sumathi, H.-H. Carstensen, A. M. Dean, and J. M. Grenda. Computer construction of detailed chemical kinetic models for gas-phase reactors. *Industrial & Engineering Chemistry Research*, 40(23):5362–5370, 2001.

[34] Marcel Gutman, Leonid Tartakovsky, Yoseph Kirzhner, and Yoram Zvirin. Development of a screening test for evaluating detergent/dispersant additives to diesel fuels. *SAE 961184.*

[35] Robert N. Hazlett. *Thermal oxidation stability of aviation turbine fuels.* ASTM, 1991.

[36] Sheldon Herbstman and Kashmir Virk. Use of dispersants/detergents in diesel injector keep clean and clean up studies. *SAE 912330.*

[37] John B. Heywood. *Internal Combustion Engine Fundamentals.* McGraw-Hill, Inc., New York, 1988.

[38] Patrick Biller Gordon E. Andrews Seyed Hadavi Hu Li, Amanda Lea-Langton and Alex Charlton. Effect of multifunctional fuel additive package on fuel injector deposit, combustion and emissions using pure rape seed oil for a di diesel. *SAE 2009-01-2642.*

[39] F. Dryer C. Law D. Friend C. Hergart R. McDavid A. Patel C. Mueller H. Pitsch J. Farrell, N. Cernansky. Development of an experimental database and kinetic models for surrogate diesel fuels. *SAE 2007-01-0201.*

[40] J. Yu C.D. Wijaya G. Stephanopoulos W.H. Green J. Song, S. Raman. Rmg: the next generation of automatic chemical reaction mechanism generator. In *Proceedings AIChE Annual Meeting*, 2003.

[41] Amrit Jalan, Robert W. Ashcraft, Richard H. West, and William H. Green. Predicting solvation energies for kinetic modeling. *Annu. Rep. Prog. Chem., Sect. C: Phys. Chem.*, 106:211–258, 2010.

[42] R. K. Jensen, S. Korcek, and M. Zinbo. Formation, isomerization, and cyclization reactions of hydroperoxyalkyl radicals in hexadecane autoxidation at 160-190.degree.c. *Journal of the American Chemical Society*, 114(20):7742–7748, 1992.

[43] Stephen R. Daniel Jonathan H. Worstell and Greg Frauenhoff. Deposit formation in liquid fuels 3. the effect of selected nitrogen on diesel fuel. *FUEL*, 60, 1981.

[44] Marion Geduldig Jrg Ullmann, Rinaldo Caprotti Heinz Stutzenberger, and Graham Balfour. Investigation into the formation and prevention of internal diesel injector deposits. *SAE 2008-01-0926.*

[45] V. R. KATTA, E. G. JONES, and W. M. ROQUEMORE. Modeling of deposition process in liquid fuels. *Combustion Science and Technology*, 139(1):75–111, 1998.

[46] Magdi K. Khair. Dieselnet technology guide, 2011.

[47] Masao Kinoshita, Akinori Saito, Souichi Matsushita, Hitoshi Shibata, and Yutaka Niwa. A method for suppressing formation of deposits on fuel injector for direct injection gasoline engine. *SAE 1999-01-3656.*

[48] Tony Kitchen. A technical overview of common rail diesel fuel systems. Technical report, AK Training.

[49] Levich B. Landau L.D. Dragging of a liquid by a moving plate. *Acta Physicochim*, 17:42–54, 1942.

[50] Angela Leedham, Rinaldo Caprotti, Olaf Graupner, and Thomas Klaua. Impact of fuel additives on diesel injector deposits. *SAE 2004-01-2935.*

[51] G. Lepperhoff and M. Houben. Mechanisms of deposit formation in internal combustion engines and heat exchangers. *SAE Technical Paper 931032*, 1993.

[52] R. Leuthel, M. Pfitzner, and M. Frobenius. Numerical study of thermal-fluid-interaction in a diesel fuel injector. *SAE 2008-01-2760.*

[53] Souichi Matsushita Hitoshi Shibata Masao Kinoshita, Akinori Saito and Yutaka Niwa. Study of deposit formation mechanism on gasoline injection nozzle. *JSAE Review*, 19:351–371, 1998.

[54] Christina Mintz, Katherine Burton, WilliamE. Acree, and MichaelH. Abraham. Enthalpy of solvation correlations for gaseous solutes dissolved in linear alkanes (c5c16) based on the abraham model. *QSAR & Combinatorial Science*, 27(2):179–186, 2008.

[55] Zachary J. West Nicholas J. Kuprowicz, Steven Zabarnick and Jamie S. Ervin. Use of measured species class concentrations with chemical kinetic modeling for the prediction of autoxidation and deposition of jet fuels. *Energy & Fuels*, 21:530–544, 2007.

[56] T. Klaua O. Graupner, R. Caprotti, and A. Breakspear. Injector deposit test for modern diesel engines. *TAE Int. Coll. Fuels 2005*, 2005.

[57] Ruveyda Cetiner Dania A. Fonseca Maria Sobkowiak Sharon Falcone-Miller Bruce G. Miller Parvana Aksoy, Omer Gul and Bruce Beaver. Insight into the mechanisms of middle distillate fuel oxidative degradation. part 2: On the relationship between jet fuel thermal oxidative deposit, soluble macromolecular oxidatively reactive species, and smoke point. *Energy & Fuels*, 23:20472051, 2009.

[58] Jean Marc Kientz Nebojsa Milovanovic Christian Gris Paul Lacey, Sandro Gail. Internal fuel injector deposits. *SAE 2011-01-1925.*

[59] Jim Pfaendtner and Linda J. Broadbelt. Mechanistic modeling of lubricant degradation. 2. the autoxidation of decane and octane. *Industrial & Engineering Chemistry Research*, 47(9):2897–2904, 2008.

[60] James A. Platts, Darko Butina, Michael H. Abraham, and Anne Hersey. Estimation of molecular linear free energy relation descriptors using a group contribution approach. *Journal of Chemical Information and Computer Sciences*, 39(5):835–845, 1999.

[61] S.E. Prickett and M.L. Mavrovouniotis. Construction of complex reaction systemsii. molecule manipulation and reaction application algorithms. *Computers & Chemical Engineering*, 21(11):1237 – 1254, 1997.

[62] David Qur. Fluid coating on a fiber. *Annual Review of Fluid Mechanics*, 31(1):347–384, 1999.

[63] G. Lepperhoff R. Caprotti, W. J. Fowler and M. Houben. Diesel additive technology effects on injector hole erosion/corrosion, injector fouling and particulate traps. *SAE 932739.*

[64] W.H. Green R. H. West, A. Jalan. Building kinetic models for the liquid phase: Hydrocarbon auto-oxidation. In *the AIChE Annual Meeting*, 2010.

[65] Paul Rawson. Evaluation of a jet fuel thermal stability rig. Technical report, Platforms Sciences Laboratory, 2004.

[66] Konrad Reif, editor. *Bosch Automotive Handbook.* Robert Bosch GmbH, 2011.

[67] Mark Brewer Renate Uitz and Rod Williams. Impact of fame quality on injector nozzle fouling in a common rail diesel engine. *SAE 2009-01-2640.*

[68] YinChun Wang Wai Cheng William Green Richard West, Amrit Jalan. Deposit formation in diesel injector nozzles.

[69] Nadia Bhatti Rinaldo Caprotti and Graham Balfour. Deposit control in modern diesel fuel injection systems. *SAE 2010-01-2250.*

[70] Alexander Sappok. *The Nature of Lubricant-Derived Ash-Related Emissions and Their Impact on Diesel Aftertreatment System Performance.* PhD thesis, MIT, 2009.

[71] Steven J. Dell Julie M. Galante-Fox-Alexander M. Kulinowski Scott D. Schwab, Joshua J. Bennett and Keith T. Miller. Internal injector deposits in high-pressure common rail diesel engines. *SAE 2010-01-2242.*

[72] Sandeep D. Sovani. *High Pressure Gas-Liquid Flow inside an effervescent Diesel Injector and its effect on spray characteristics.* PhD thesis, Purdue University, 2001.

[73] Jens Tang, Stefan Pischinger, Matthias Lamping, Thomas Krfer, Marek Tatur, and Dean Tomazic. Coking phenomena in nozzle orifices of di-diesel engines. *SAE 2009-01-0837.*

[74] G. Taylor. Deposition of a viscous uid on the wall of a tube. *Journal of Fluid Mechanics*, 10:161, 1961.

[75] Takeshi Ohmori Tomohiko Furuhata and Masataka Arai. Evaporation deposits of diesel and bio-diesel fuels on a hot surface. *SAE 2011-01-1933.*

[76] Kevin M. Van Geem, Marie-Francoise Reyniers, Guy B. Marin, Jing Song, William H. Green, and David M. Matheu. Automatic reaction network generation using rmg for steam cracking of n-hexane. *AIChE Journal*, 52(2):718–730, 2006.

[77] Ramya Venkataraman. *SOLID DEPOSIT FORMATION FROM THE PYROLYTIC AND OXIDATIVE DEGRADATION OF JET FUEL AND DIESEL FUEL.* PhD thesis, Pennsylvania State University, 2007.

[78] Richard West Amrit Jalan YinChun Wang Wai Cheng, William Green. Modeling fuel detergency behavior in diesel injectors. Technical report, MIT, 2009.

[79] Orian Welling. Thin film reactor testing for characterization of diesel fuel deposit formation. *Bachelor Thesis*, 2009.

[80] Steven Zabarnick. Chemical kinetic modeling of jet fuel autoxidation and antioxidant chemistry. *Industrial & Engineering Chemistry Research*, 32(6):1012–1017, 1993.